U.S. Department of Energy
Energy Efficiency and Renewable Energy
Bringing you a prosperous future where energy is clean, abundant, reliable, and affordable

Industrial Technologies Program
Industrial Materials for the Future

Final Technical Report

Compressive Creep and Thermophysical Performance of Refractory Materials

June 2006

Principal Investigators:

Dr. M. K. Ferber
Dr. A. A. Wereszczak
Dr. J. G. Hemrick
Oak Ridge National Laboratory

ORNL
OAK RIDGE NATIONAL LABORATORY

Managed by
UT-Battelle, LLC

ORNL/TM-2005/134

DOCUMENT AVAILABILITY

Reports produced after January 1, 1996, are generally available free via the U.S. Department of Energy (DOE) Information Bridge.

Web site http://www.osti.gov/bridge

Reports produced before January 1, 1996, may be purchased by members of the public from the following source.

National Technical Information Service
5285 Port Royal Road
Springfield, VA 22161
Telephone 703-605-6000 (1-800-553-6847)
TDD 703-487-4639
Fax 703-605-6900
E-mail info@ntis.fedworld.gov
Web site http://www.ntis.gov/support/ordernowabout.htm

Reports are available to DOE employees, DOE contractors, Energy Technology Data Exchange (ETDE) representatives, and International Nuclear Information System (INIS) representatives from the following source.

Office of Scientific and Technical Information
P.O. Box 62
Oak Ridge, TN 37831
Telephone 865-576-8401
Fax 865-576-5728
E-mail reports@adonis.osti.gov
Web site http://www.osti.gov/contact.html

FINAL TECHNICAL REPORT

Project Title: Compressive Creep and Thermophysical Performance of Refractory Materials

Contract No.: DE-AC05-00OR22725

Project Period: April 1997–June 2000

PI(s): Dr. M. K. Ferber
(865) 576-0818
ferbermk@ornl.gov

Dr. A. A. Wereszczak
(865) 576-1169
wereszczakaa@ornl.gov

Dr. J. G. Hemrick
(865) 574-7601
hemrickjg@ornl.gov

Recipient: Oak Ridge National Laboratory (ORNL)
Bethel Valley Road
P. O. Box 2008
Oak Ridge, TN 37831

Subcontractor University of Missouri–Rolla
Department of Materials Science Engineering
222 McNutt Circle
1870 Miner Circle
Rolla, MO 65409

ORNL/TM-2005/134

Compressive Creep and Thermophysical Performance of Refractory Materials

Dr. M. K. Ferber, Dr. A. A. Wereszczak, Dr. J. G. Hemrick
Oak Ridge National Laboratory

June 2006

Prepared by
OAK RIDGE NATIONAL LABORATORY
P.O. Box 2008
Oak Ridge, Tennessee 37831-6283
managed by
UT-Battelle, LLC
for the
U.S. DEPARTMENT OF ENERGY
under contract DE-AC05-00OR22725

Acknowledgments, Disclaimer, and Proprietary Data Notice

Acknowledgments

This report is based upon work supported by the U.S. Department of Energy, Office of Energy Efficiency and Renewable Energy, Industrial Technologies Program, Industrial Materials for the Future, under Contract No. DE-AC05-00OR22725. The authors are also indebted to the following individuals for supplying the mullite refractories: Paul Hutchinson (DSF Refractories & Minerals), Michael Nelson (Corhart Refractories), Larry Stover (Minteq International), D. J. Thomas, (VGT-DYKO Industrial Ceramics), Jim Houp (National Refractories & Minerals), and Don McIntyre (NARCO); the guidance provided by the Glass Industry Advisory Committee, which comprises the following individuals: Larry Kotacska (Corning), Al Poolos (Owens-Brockway), Randy Sturtz (Owens-Corning), Warren Curtis (PPG), Jim Shell (Techneglas), Mike Nelson (Corhart), Steve Winder (UKSS/Monofrax), John Tracey/Dilip (Patel VRD-Americas), and Bob Moore (University of Missouri-Rolla); ORNL/HTML machinists L. O'Rourke, T. Jenkins, and R. Parten for the specimen preparation; and Peter Angelini, ORNL, for project guidance and review.

Oak Ridge National Laboratory is operated by UT-Battelle, LLC, for the U.S. Department of Energy under contract DE-AC05-00OR22725.

Disclaimer

This report was prepared as an account of work sponsored by an agency of the United States Government. Neither the United States Government nor any agency thereof, nor any of their employees, makes any warranty, express or implied, or assumes any legal liability or responsibility for the accuracy, completeness, or usefulness of any information, apparatus, product, or process disclosed, or represents that its use would not infringe privately owned rights. Reference herein to any specific commercial product, process, or service by trade name, trademark, manufacturer, or otherwise, does not necessarily constitute or imply its endorsement, recommendation, or favoring by the United States Government or any agency thereof. The views and opinions of authors expressed herein do not necessarily state or reflect those of the United States Government or any agency thereof.

Proprietary Data Notice

If there is any patentable material or protected data in the report, the recipient, consistent with the data protection provisions of the award, must mark the appropriate block in Section K of the DOE F 241.3, clearly specify it here, and identify them on appropriate pages of the report. Other than patentable material or protected data, reports must not contain any proprietary data (limited rights data), classified information, information subject to export control classification, or other information not subject to release. Protected data are specific technical data, first produced in the performance of the award, which is protected from public release for a period of time by the terms of the award agreement. Reports delivered without such notice may be deemed to have been furnished with unlimited rights, and the Government assumes no liability for the disclosure, reproduction, or use of such reports.

Contents

List of Figures

List of Tables

Abbreviations and Acronyms

AIM	Advanced Industrial Materials
ASTM	American Society for Testing and Materials
AZS	aluminum-zirconium silicate
CL	cathodoluminescent imaging
DOE	U.S. Department of Energy
EDS	energy-dispersive X-ray spectroscopy
LVDT	linear variable differential transducer
ITP	Industrial Technology Program
NBA	Norton-Bailey Arrhenius
OIT	Office of Industrial Technologies
ORNL	Oak Ridge National Laboratory
RL	reflected light microscopy
SEM	scanning electron microscopy
TPS	transient plane source
XRD	X-ray diffraction
XRF	X-ray fluorescence

1. Executive Summary

1.1 Research and Development

Over the last 10 years, the U.S. Department of Energy Office of Industrial Technology, through the Industrial Materials for the Future activity, has funded a number of projects at industry, university, and national laboratory sites to increase the energy efficiency of energy-consuming industries, including glass, steel, pulp and paper, and chemical. In the case of the glass industry, using valid engineering creep data to optimize furnace superstructure design is a means to achieve these goals. The objective of the ORNL project described in this report was to facilitate that endeavor by conducting creep testing and analysis on refractories of interest to glass manufacturers at representative service temperatures, enabling the availability of new and improved refractories by suppliers, and generating creep data on "equivalent" refractories that furnace designers can use for optimizing the design of their superstructures or for predicting their long-term structural integrity. The choice of refractories evaluated in the project was based on the advice of technical experts from the glass manufacturing industry, refractory suppliers, and academia. Although the results cited in this report are specific to refractories for glass applications, the techniques developed in this project are applicable to refractories used in all industrial applications.

The creep and corrosion behaviors of several refractories, including six types of conventional silica, ten types of mullite, two types of fusion-cast alumina, and fused spinel were measured. The data generated for the silica refractories served as a baseline. The mullite refractories were examined because they are used in borosilicate glass furnace crowns and superstructures and in sidewall applications. Additionally, despite their high cost (≈$500/ft^3) they are cheaper than other refractories such as chrome alumina (≈ $3000/ft^3) or fusion-cast alumina (≈ $900/ft^3), which are used as replacements for traditional silica refractories in harsh oxy-fuel environments. Fusion-cast alumina refractories, which are a popular choice for crowns and sidewalls in oxy-fueled glass furnaces, were selected for this study because of their homogeneity, low porosity, high refractoriness, low levels of glassy phase, and good spall resistance. Although more expensive, the fused spinel offers improved creep and corrosion resistances.

Compressive creep testing was performed at 1300 to 1650^{o}C and at static stresses between 0.2 and 0.6 MPa on a pneumatically controlled compressive creep frame in an electrically heated furnace. The phase content, microstructure, and secondary phase composition of the refractories were characterized before and after their creep testing in an attempt to correlate the creep responses with any observed changes. Corrosion resistance of each of the refractories was also examined. Lastly, the effect of temperature and time (in the absence of stress) on the dimensional stability of the materials was examined.

In the case of the silica refractories, the compressive creep rates of all six brands could not be represented as a function of temperature and compressive stress by using the conventionally used Norton-Bailey Arrhenius (NBA) creep equation. Concurrently active mechanisms other than creep resulted in larger or oppositely anticipated dimensional changes than those produced by creep; this effect limited the ability to identify or interpret the less-active creep mechanism in them. The change in dimensions of the compressively crept specimens indicated that their size (both diameter and length) increased (by 0.35 to 1.0%) as a consequence of the creep test conditions. The cause of the volume expansion was not identified; however, because of the absence of quartz, it can be concluded that the expansion was not due to quartz (a relatively high-density phase) converting to tridymite or cristobalite (lower-density phases). The secondary phase constituents remained constant in all brands

when they were tested at 1550°C. A fraction of these phases visibly evolved in the specimens at 1600°C. This phenomenon was quite severe at 1650°C. The density changes in the crept specimens (a net effect of the volume expansion and loss in secondary phase mass) ranged from a decrease of 1.6 to 3.9% with a subtle trend of greater density decreases at higher test temperatures. The density decreases among the six brands were statistically equivalent within the data scatter. The corrosion resistances of the six silicas were statistically equivalent when they were exposed to sodium carbonate at 1400°C (2550°F) for 24 h. The amount of recession increased linearly with temperature between 1250 and 1450°C for the Gen-Sil silica.

Creep rates for three brands of the mullite refractories were on the order of 10^{-11} s^{-1} at the lower test temperature and 10^{-10} s^{-1} at the higher test temperature. Creep rates for four of the brands ranged from 10^{-10} s^{-1} at the lower test temperature and to 10^{-9} s^{-1} at the higher test temperature. The remaining three brands exhibited creep rates ranging from 10^{-9} s^{-1} to 10^{-8} s^{-1} and exhibited low stress exponents (< 0.5) and changes in chemistry or in microstructure due to the creep-testing conditions. Several of the mullite refractories exhibited a creep stress exponent approximately equal to unity, suggesting that creep was controlled by diffusion. One of mullite refractories had a stress exponent of 2.4, indicating that the rate-controlling mechanism may be grain boundary creep. The creep mechanism for the remaining mullite materials, which had stress exponents much less that unity, was attributed to a non-steady-state condition existing during the entire extent of testing. This condition is a consequence of contraction or time-hardening effects occurring during testing and of the samples never reaching a state of equilibrium. Those brands possessing high levels of matrix porosity all showed compaction of the microstructure during creep testing, which was ultimately responsible for their poorer creep resistance. One of the mullite refractories was found to be composed of andalusite grains containing free quartz, which was converted to cristobalite during firing. Further, the andalusite grains were fully converted to mullite during creep testing, and the amount of glassy phase increased. These events in combination may lead to the brand's poor creep resistance.

Activation energies for the various mullite refractory brands ranged from 50 to 223 kcal/mol. Although no direct correlation between the magnitude of the activation energy and the amount of creep exhibited by a particular brand could be drawn from the data, it is known that materials possessing a high activation energy will have greater sensitivity to temperature than those possessing a lower activation energy. Also, the values for many of the calculated activation energies correspond to the activation energy of vitreous silica. This finding indicates that the glassy phases in these brands affect the overall creep behavior of the material.

The distinction of a brand being fused-grained or non-fused-grained mullite did not appear to have a bearing on the creep resistance of the individual brands.

Eight of the ten mullite refractory brands showed less than a 0.2% change in mass and less than a 0.6% change in volume after thermal aging in the absence of an applied load. The two exceptions exhibited extraneous amounts of change (≈8.5%) in both mass and volume due to thermal exposure. All samples showed less than a 0.5% change in bulk density. The corrosion rates of the ten mullite brands could not be determined through the use of ASTM C987, but it was determined visually that only minimal amounts of recession occurred because of exposure as defined by the ASTM lid test.

Fused-cast alumina refractories from Corhart and Monofrax were examined. Both the density and porosity of the as-cast refractory blocks were highly consistent. The phase profiles for the α- to β-alumina ratios also showed similar trends to those seen in the density/porosity profiles. X-ray diffraction (XRD) showed that both brands consisted of only peaks identifiable as corundum (PDF# 10-0173) or sodium aluminum oxide (PDF# 31-1263). Closer examination of the XRD patterns showed that there were some differences in ratios of α- to β-alumina between the two brands and

between the bulk and columnar microstructures. The microstructures of the two brands of refractory were also comparable with a columnar region existing in the outer 1 to 1 ½ in. of the blocks and then transitioning to a more equiaxed structure of α-alumina grains embedded in a β-alumina matrix toward the center of the block. Average grain sizes were found to be on the order of 172 μm and 82 μm for the Corhart bulk and columnar regions, respectively. Average grain sizes were found to be on the order of 231 μm and 79 μm for the Monofrax bulk and columnar regions, respectively.

Both columnar orientations show much less accumulated strain than the bulk samples under similar stresses because the elongated needle-like grains, which are oriented perpendicular to the direction of the applied compressive load, inhibit creep in the transverse columnar samples. In the longitudinal columnar case, it is expected that the unrecoverable expansion effect plays a role in the reduced strain accumulation. The columnar samples at 1650°C showed less accumulated strain than the bulk sample under similar stress, but the behavior between the bulk and columnar samples was more similar. Both microstructures showed traditional creep behavior under 1.0 MPa of stress and much larger amounts of accumulated strain than the bulk samples at 0.6 and 0.8 MPa.

The three bulk 1650°C/1.0 MPa samples all had similar creep rates, with the Corhart material on the order of 5×10^{-6} h^{-1} and the Monofrax material on the order of 6×10^{-6} h^{-1}. The columnar structures at 1650°C/1.0 MPa had a lower creep rate, on the order of 4.25 to 4.50 $\times 10^{-6}$ h^{-1}. Creep rates for the other samples were not obtainable because nontraditional creep behavior occurred. Stress exponents and activation energies could not be calculated from the data because steady-state creep rates were only obtained at one stress and temperature.

Unrecoverable expansion was seen in all materials and was thought to be connected to the nontraditional creep behavior seen in the compressive creep testing at temperatures and loads up to 1650°C and 0.8 MPa. As the temperature increased, the amount of unrecoverable expansion occurring over a given time interval also increased. The occurrence of the unrecoverable expansion was thought to be caused by thermal expansion hysteresis due to microstresses or microcracking. Because of that behavior, the generated creep curves could not be represented by the empirical NBA creep equation. Instead, an empirical fit utilizing an exponential expansion series with multiple time constants was used to represent the behavior exhibited by the fusion-cast alumina refractories. The same exponential fit used to model the raw creep curves was also utilized to describe this composite behavior.

Several samples were analyzed after being crept, and results were compared with those previously obtained from virgin samples. Analysis included thermal conductivity, optical microscopy, and scanning electron microscopy/energy-dispersive X-ray spectroscopy (SEM/EDS) chemical analysis. The thermal conductivity values for the Monofrax post-creep cores were similar to those obtained earlier from the virgin cores, which had thermal conductivities in the range of 5.9 W/mK. The value obtained from the Corhart post-creep core was significantly lower than the average value of 6.61 W/mK found earlier for the Corhart bulk material. Initial optical microscopy and SEM/EDS analyses were performed on Corhart and Monofrax bulk samples exposed to 1550°C and 1.0 MPa. This work was conducted to determine whether any changes in the microstructure or chemistry could be detected at that intermediate condition. No discernible deformation and only slight chemical changes were seen in the samples. Subsequent optical microscopy and SEM/EDS analyses were performed on Corhart and Monofrax bulk samples exposed to the extreme conditions (1650°C and 1.0 MPa). The structure of the Corhart sample was found to resemble the virgin structure; the Monofrax crept structure displayed a smaller α-alumina grain size and a tighter α-alumina grain structure with more equiaxed angular grains than in the virgin structure. More severe chemical changes were also seen between the virgin and crept samples.

The fused spinel materials had negligible creep rates up to 1650°C at 8.5MPa of stress. The bonded spinel, surprisingly, crept substantially compared to the fused material. However, this must be compared with other common crown materials; the total creep of the bonded material is less than 0.5% over 100 h at 1550°C and 0.3 MPa which are fairly standard temperature and pressure for testing refractory materials The creep of silica materials is approximately 0.4% over 100 h at 1450°C and 0.3 MPa. The spinel materials did not react with soda in the exposure tests. There was some limited reaction with silica and calcia from the gasifier atmosphere. Thermal conductivity was determined by laser flash and was found to decrease as temperature increases from 14 (100°C) to 8 (700°C) W/mK for the fused spinel and 9.5 (100°C) to 4 (1300°C) for the bonded spinel. A model of the glass tank crown was developed that takes into account nonlinear changes in the refractory material due to time, temperature, and corrosion.

1.2 Technology Transfer

The results of this project have established hardware and a test methodology that can be used by the refractories community to evaluate the creep and aging behaviors of most refractory materials. Of particular merit is the development of specialized extensometry, which offers extremely high resolution required for the measurement of small deformations. The project staff made presentations at national meetings and published results in industry technical journals.

1.3 Commercialization

The data generated in this project were provided to participating refractory manufacturers and are available from those manufacturers to any users of these types of refractories. It has been confirmed with industrial partners involved in this project that creep data and other thermomechanical property information generated as part of this project was used in analysis of glass furnaces currently in service and for the planning and design of refractory systems for future furnace constructions. The data has not only been used by glass companies in their analysis and planning of furnace systems, but by refractory companies and industrial consultants as well. The information generated was said to be “invaluable” by one industrial participant and more data of similar scope is felt to be of general interest to the industry as a whole.

1.4 Recommendations

Technical efforts should be undertaken to measure and model the composite effects of unrecoverable expansion (aging behavior) and creep response. Given that these processes may be highly nonlinear, the traditional equations, which assume that steady-state deformation rates are dominant, are not appropriate. New models must be derived from basic theoretical principles that can describe the nonlinear, transient, nonsteady equilibrium behavior observed in this work. Creep testing needs to include simultaneous measurement of specimen elongation/contraction occurring in the absence of an applied stress. Such testing could be conducted using a system consisting of furnace of sufficient size to accommodate multiple mechanical load trains. During testing one load train would be used to monitor elongation/contraction in the absence of any appreciable stress. The stress range employed with the other load stations must be large enough to promote significant and measurable changes in the deformation response. It is recommended that the stress range cover at least one order of magnitude (e.g., 5 to 50 MPa). Testing times must also be much longer (> 1000 h) to ensure that representative deformation data are generated. A second approach for distinguishing creep from aging effects is to use the stress relaxation technique for measuring creep response. Because this method is able to generate an entire creep-rate vs stress curve in a matter of a few hours, one could use it to

measure creep behavior at periodic intervals during a standard aging test. Thus a single sample could be used to assess both aging and creep behavior.

To facilitate technology transfer and commercialization, software tools should be developed which allow users to readily link the key properties to finite element codes used in furnace construction. This software would allow one to quickly assess the effects of specific materials upon long-term thermal and structural reliability. It should also include a routine that allows the user to optimize performance of a given material by changing the material properties; these altered properties would serve as new targets for those involved in materials development.

Any follow-on effort must also address new materials.

2. Introduction

Furnace designers and refractory engineers recognize that optimized furnace superstructure design and refractory selection are needed as glass production furnaces are continually striving toward greater output and efficiencies. Harsher operating conditions test refractories to the limit, while changing production technology (such as the conversion to oxy-fuel from traditional air-fuel firing) can alter the way the materials perform [1–3]. Refractories for both oxy- and air-fuel fired furnace superstructures (see Fig. 1) are subjected to high temperatures that may cause them to creep excessively or subside during service if the refractory material is not creep resistant, or if it is subjected to high stress, or both. Furnace designers can ensure that superstructure structural integrity is maintained if the creep behavior of the refractory material is well understood and well represented by appropriate engineering creep models.

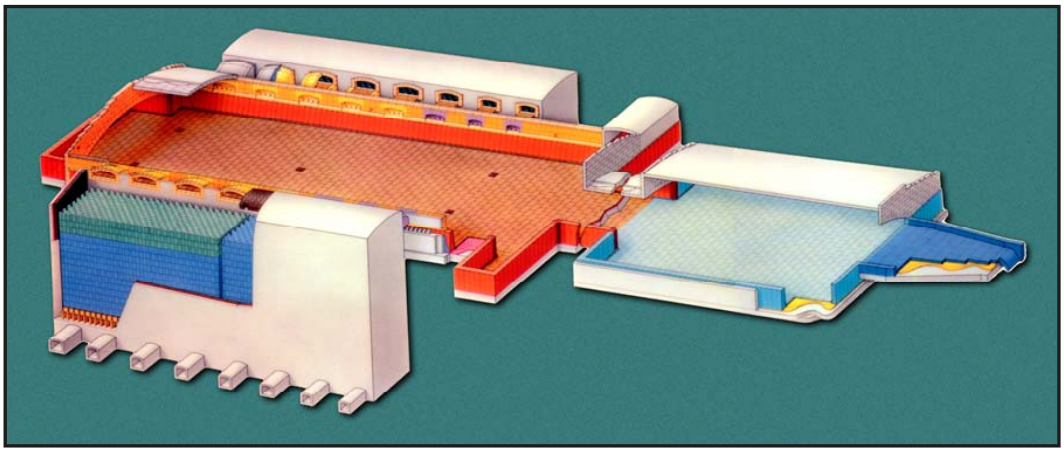

Fig. 1. Superstructure refractories in glass production furnaces.

Several issues limit the abilities of furnace designers to (1) choose the optimum refractory for their applications, (2) optimize the engineering design, or (3) predict the service mechanical integrity of their furnace superstructures. Published engineering creep data are essentially nonexistent for almost all commercially available refractories used for glass furnace superstructures. The limited data that do exist are supplied by the various refractory suppliers. Unfortunately, the suppliers generally have different ways of conducting their mechanical testing, and they interpret and report their data differently. This inconsistency makes it hard for furnace designers to draw fair comparisons between competing grades of candidate refractories. Furthermore, the refractory suppliers' data are often not available in a form that can be readily used for furnace design or for the prediction and design of long-term structural integrity of furnace superstructures.

As a consequence, the U.S. Department of Energy (DOE) Industrial Technology Program (ITP) Glass Industry of the Future sponsored research and development at industry, university, and national laboratory sites with the intent to help domestic glass manufacturers improve their energy and operating efficiencies. The optimization of furnace superstructure design using valid engineering creep data is a means to achieving these ITP goals. The present project at Oak Ridge National Laboratory (ORNL) aided in this endeavor by conducting creep testing and analysis on refractories of interest to glass manufacturers at representative service temperatures, enabling the availability of new and improved refractories by refractories suppliers and by generating creep data on equivalent refractories that furnace designers could use for optimizing the design of their superstructures or for predicting their long-term structural integrity. Similar refractory creep-testing projects have been

conducted at ORNL [4–6], so many of the unique experimental nuances and difficulties associated with the high-temperature creep testing of refractories have been encountered and overcome.

3. Background

The ITP program has recognized that a reduction in overall domestic energy consumption will occur if the primary energy-consuming industries improve their own energy efficiencies [7]. Recognizing this need, the glass industry is currently converting older, conventional air-fuel-fired furnaces to oxy-fuel firing, or in the case of new construction, is building new oxy-fuel-fired furnaces instead. This has caused oxy-fuel technology to become one of the fastest growing technologies in the glass industry because it promises pollution abatement, increased glass-pull effectiveness, capital cost savings, and increased energy efficiency. For example, a recent study [8] has shown that approximately $202M in energy savings per year in 2005 and a $445M per year savings by 2020 could be expected with the conversion of air/fuel to oxy-fuel–fired glass manufacturing furnaces. These results, which reflect energy savings of 2.8 and 14.2 TBtu/year, respectively, are based on the projection that 61% and 100% furnace conversions will occur by the years 2005 and 2020, respectively.

Unfortunately, the new internal furnace environment produced by oxy-fuel firing creates many problems with refractory life not previously encountered with conventional firing. These problems include increased potential for corrosion and "rat holing" along with deterioration of traditionally used conventional silica crown refractories. Additionally, due to a significant increase in the concentration of volatiles in the furnace, the refractories can experience a more intense alkali attack as water vapor reacts with alkali to form hydroxide vapors. Therefore, alternatives to silica must be considered for refractory superstructure applications, and data must be obtained to predict the performance of the refractories in service. Furthermore, the cost of the alternate refractories must be balanced with their effects on furnace life and glass quality while also considering the comparative performance of the other refractories in the furnace and overall furnace life.

Given the need for data on alternative refractories, the first objective of this project was to identify superstructure refractory categories of greatest interest to the glass manufacturing industry via a survey. To achieve this, the advice of project participants and technical experts from the glass manufacturing industry, refractory suppliers, and academia was first sought to organize a list of distinct refractory categories to include in the survey (Table 1).

The mechanical deformation of thirteen different candidate refractory categories was determined to be of possible interest to the flat, fiber, container, and specialty glass manufacturers (Table 2). A list of the categories was then forwarded to nine refractory suppliers (Table 1), and company representatives were asked to indicate if any of their marketed refractory brands belonged to those categories. From their input, anywhere between four to ten competing or "equivalent" brands were identified per category.

A survey consisting of the thirteen categories (and subcategory brands) was then forwarded to a furnace or refractory specialist at more than thirty domestic glass manufacturers (Table 1). The person taking the survey was asked to rank each refractory category as "high," "middle," or "low" priority in terms of their desire to have access to engineering creep data for that particular refractory category. To quantify the results of the survey, a score of ten, five, and zero points was respectively given to a "high," "middle," and "low" priority. The total points were summed and then used to rank and compare the interest among the thirteen categories.

Eight categories received relatively high total scoring (> 100 points) while the remaining five received little priority (< 100 points) (Table 2). Creep data for fusion-cast alumina was of greatest interest to the most respondents followed in descending order by creep data for conventional silica,

Table 1. Project and survey participants

Subject matter experts		
P. Antimarino, Harbison-Walker	M. Nelson, Corhart	S. Winder, UKSS
R. Antram, NARCO	J. Petreanu, Owens-Corning	J. Wosinski, Corning
W. Curtis, PPG	P. Ross, Glass Industry Consulting	
R. Moore, University of Missouri-Rolla	J. Shell, Techneglas	
Refractory suppliers		
A. P. Green	Harbison-Walker	NARCO
Corhart/SEPR	Monofrax	VGT-DYKO
DSF	National	Zedmark
Survey recipients		
AFG Industries	Glenshaw	Philips Lighting
Anchor Glass	Guardian Industries	Pilkington
Ball-Foster Glass	Holophane	Pittsburgh Corning
Cardinal FG	Kimble Glass	PPG
Carr-Lowrey	Knauf Fiber Glass	PQ Corporation
CertainTeed	Lancaster Glass	Schuller International
Corning	Leone	St. George Crystal
Corning Glass - RBMG	Libbey	Techneglas
Ford	Osram Sylvania	Thomson Consumer Electronics
Gallo Glass	Owens-Brockway	Vetrotex
General Electric Lighting	Owens-Corning	Wheaton

fusion-cast AZS, fused-grain mullite, bonded AZS, andalusite, fused silica, and bonded zircon. The relatively high interest in creep data for fusion-cast alumina and AZS is indicative of the glass industry's desire to convert to oxy-fuel firing and of the belief that these refractory categories may be attractive alternatives to traditionally used (but perhaps unsuitable) conventional silica refractories. The availability of creep data for mullite, spinel, or-containing, and 5–15% chromium-containing refractories received little interest from the respondents.

Table 2. Ranking of refractory categories whose creep data are desired. The top eight ranked categories were creep tested at ORNL.

Ranking	Refractory category
1	Fusion-cast alumina
2	Conventional silica
3	Fusion-cast AZS
4	Fused-grain mullite
5	Bonded AZS
6	Andalusite
7	Fused silica
8	Bonded zircon
9	MgO
10	Spinel
11	50–80% Chrome
12	≈ 30% Chrome
13	5–15% Chrome

Creep testing was initiated in 1998. In addition to creep testing, the brand in each category was characterized by analyzing its (1) grain size and grain size distribution, (2) before- and after-testing microstructure using catholuminescence, (3) before- and after-testing phase content using X-ray diffraction (XRD), (4) before- and after-testing density, and (5) corrosion resistance [9]. The results from efforts (1)–(4) were used to explain any observed differences among the measured creep responses of the refractories, while the results from effort (5) were used to assess their corrosion responses. When the program was completed in 2000, the creep and corrosion behaviors of six types of conventional silica, ten types of mullite, and two types of fusion-cast alumina had been examined. This report summarizes the key findings obtained from the studies and provides recommendations for follow-on research. Detailed results are provided elsewhere [10–13].

4. Materials and Experimental Procedures

4.1 Materials

Six conventional silica refractories were analyzed in the present study (see Table 3). All brands were "Type A" [14] conventional silicas except SI96AU (a Type B silica refractory); namely, their flux factors (alumina content plus twice the alkali content) were less than 0.50%. The chosen refractories provided a comparison between similar Type A silicas at well as comparison between Type A and Type B silicas. According to the published Teltech Report *Crown Refractories for Glass Manufacturing with Oxy-Fuel Combustion* [1], Type B conventional silica is not recommended for crowns; however, its mechanical performance at representative furnace crown temperatures and stresses were characterized for the sake of comparison. The major secondary-phase constituent in all six brands was calcia (CaO), with additional reported constituents consisting of alumina (Al_2O_3), iron oxide (Fe_2O_3), magnesia (MgO), titania (TiO_2), sodium oxide (Na_2O), and potassium oxide (K_2O). The amounts of these secondary phase constituents were semiquantitatively measured by the authors using SEM/EDS and are presented and described in later sections.

Table 3. Silica refractories tested in the present study and their manufacturers

Refractory Brand Name	Manufacturer
Gen-Sil	A. P. Green
SI96AU	VGT-DYKO
Stella GGS	NARCO
Vega	Harbison-Walker
Vega H	Harbison-Walker
Unnamed developmental brand	Harbison-Walker

Ten mullite refractories were analyzed in the present study (see Table 4). Seven of the materials were fused-grained and three were not (although one non-fused-grain material did contain a small amount of fine fused mullite grains). Many of the manufacturers listed have merged or changed names since program initiation.

Table 4. Mullite refractories tested in the present study and their manufacturers

Brand Name	Type	Manufacturer
BP mullite	fused-grained	Corhart
DURITAL S75	non-fused-grained	NARCO
Frimul F	fused-grained	DSF
GEM	fused-grained	NARCO
HF 17	fused-grained	DSF
MU75AF	fused-grained	VGT-DYKO
SL75AD	non-fused-grained	VGT-DYKO
UFALA UCR	non-fused-grained	Harbison-Walker
ZED FMC	fused-grained	Minteq
ZED FM	fused-grained	Minteq

Two brands of M-type fusion-cast alumina refractories (Corhart Refractories of Louisville, Kentucky, and Monofrax Inc. of Falconer, New York) were examined. All specimens were fabricated from regular fusion-cast alumina blocks of approximate dimensions $0.60 \times 0.50 \times 0.30$ m ($24 \times 20 \times 12$ in.). Key findings are summarized below.

Two types of spinel were examined: fusion cast and reaction bonded. In the case of the fusion cast material, specimens having both columnar and equiaxed grains were examined.

4.2 Creep Testing

The testing frame used for the compressive creep testing consisted of a large clamshell furnace that used resistance heating, a contacting extensometer that was used to measure axial dimension changes, and silicon carbide push rods that transferred the applied compressive load from an actuator to the test specimen (see Figs. 2 and 3).

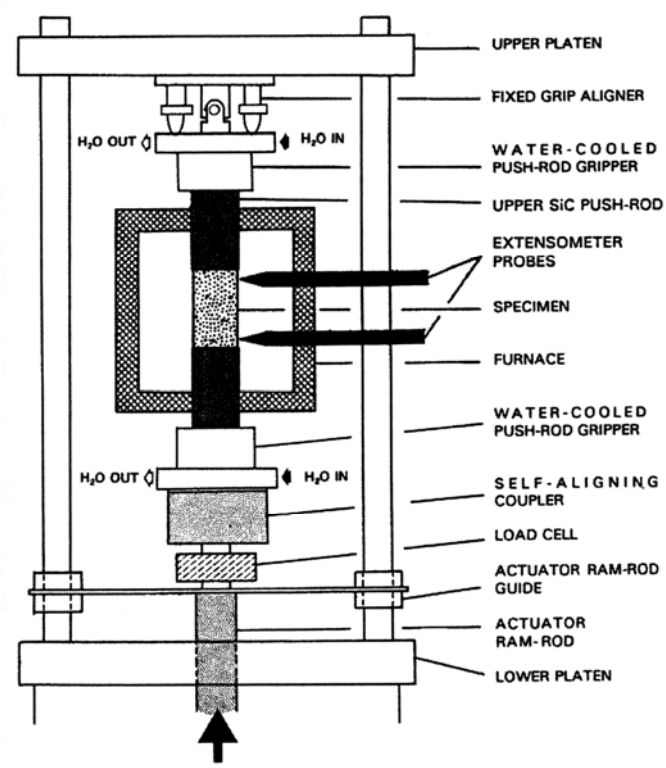

Fig. 2. Schematic of creep frame and supporting instruments.

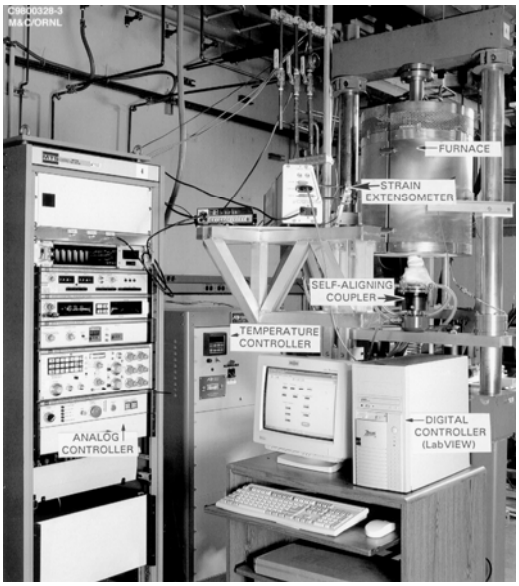

Fig. 3. Primary components of creep frame.

Creep tests were accomplished by using either digitally controlled pneumatic power (by LabVIEW™ software, National Instruments, Austin, Texas) or hydraulic power controlled by an analog controller. The latter feature provides both static (creep) and dynamic loading. The test specimen was heated with a high-temperature furnace capable of 1800°C. Within ASTM guidelines, temperature fluctuations were approximately ± 2°C and load fluctuations were less than 1% of the test load. The specimen was compressed by two long push rods (each 0.3 m long) with the unheated ends connecting to water-cooled anvils. The upper compression anvil was fixed to an upper platen by a universal joint and was leveled by four turnbuckles. The lower compression anvil rests on a self-aligning coupler that plays an important role in maintaining load-train stability and uniform compression to the specimen. Details of the compressive creep testing system are given elsewhere [10].

The generated creep strain was measured by a scissors-type mechanical extensometer, a schematic of which is shown in Fig. 4. The extensometer employs a capacitance sensor whose gap was conditioned, calibrated, and measured as a function of time. The lever-arm assembly was made from a continuous rod of silicon carbide. The probes monitored creep deformation of the specimen continuously in real time with a capacitive transducer attached to the cool end of the extension rod. Concurrently, a laser-based scanner was used to measure the movement of two fiducial flags attached to the ends of the extension rods for verification. The extensometer provided an accuracy and resolution of about 5 μm, which is equivalent to the sensitivity yielded by conventional strain gages. Strain measurements with the transducer and the laser system were in good agreement.

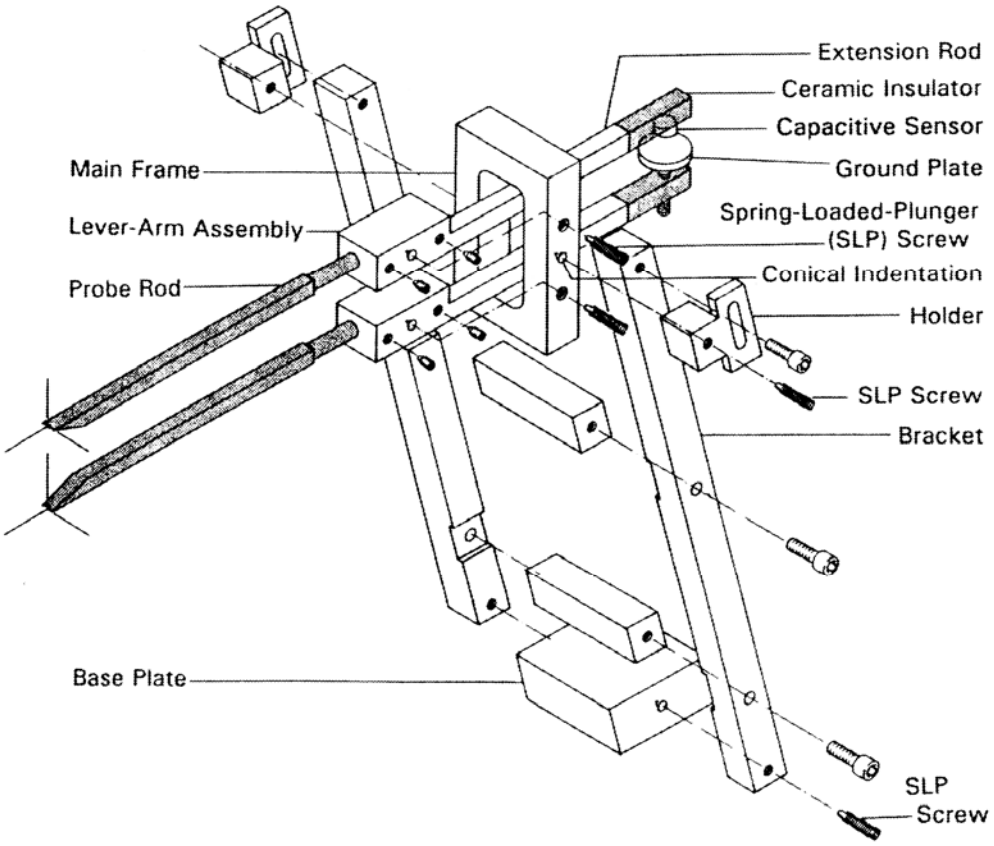

Fig. 4. Schematic of creep frame extensometer.

Extensometry methods other than the capacitance contacting extensometers used in this study are often used for the measurement of refractory creep; however, the capacitance contacting extensometer circumvents problems that other techniques inherently possess. The deformation of refractories is frequently measured continuously during compressive creep testing using two (sometimes more) linear variable differential transducers (LVDTs) whose mutual displacements coincide with the continuous position of the specimen ends. The creep results generated from this technique are accurate only as long as the accumulated measured deformation coincides with the actual specimen heights measured before and after testing. Deformation and/or translation of the load train during the creep testing of the specimen, reaction of the specimen ends with the fixturing, and "bedding-down" of the specimen all have been shown to cause a lack of correlation between the measured deformation during testing and the change in pre- and post-test specimen height. If any of these events occurs then the measured contraction during testing is not solely due to creep. Consequently, caution must be exercised when interpreting deformation data generated by the LVDT technique because it will only be representative creep data if the experimenter verified and correlated pre- and post-test specimen height with the accumulated measured deformation. The advantage of the contacting extensometers used in the present study is that their accurate operation is independent of any rigid body motion or deformation of the test hardware, specimen (e.g., "end-crushing"), and push rods.

4.3 Specimen Preparation

In the case of the silica and mullite refractories, cylindrical creep test specimens having dimensions shown in Fig. 5 were core-drilled from the supplied conventional bricks in the manner illustrated in Fig. 6. The primary axis of the machined cylinder-shaped specimens was oriented parallel to the pressing direction. Although not verified in the present study, the measured creep deformation was assumed to be isotropic, so specimens were not machined from the bricks in different orientations. After core drilling, the specimen ends were ground parallel to within 0.013 mm (0.001 in.). All specimens were dried in an oven at 300°C (570°F) for 4 h after they were core drilled and before they were creep tested.

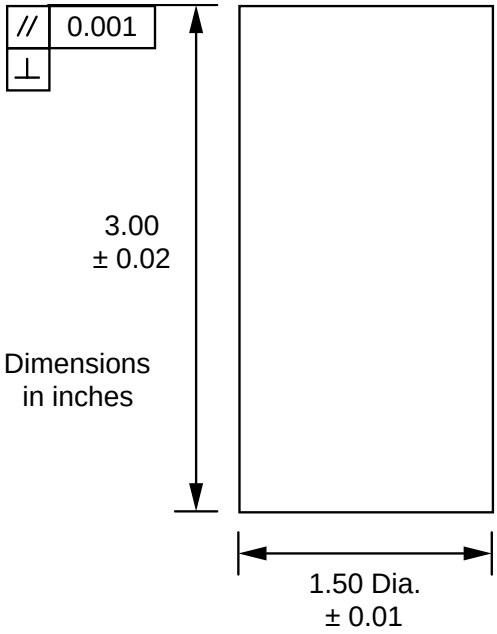

Fig. 5. Dimensions of core-drilled test specimens.

Using an appropriate aspect ratio of compression test specimens is an important consideration. A specimen aspect ratio of 2.6 or greater is recommended for compressive strength tests so that the friction effects between the specimen ends and loading ram are small compared to the axially applied compressive stresses [15]. However, in the present study (aspect ratio = 2.0), the applied axial compressive stresses during creep testing were already low (i.e., much less than the refractories' compressive strengths). Consequently, the stresses and strains due to such friction were likely negligible, so adherence to the height/diameter ratio of 2.6 or greater was deemed unnecessary.

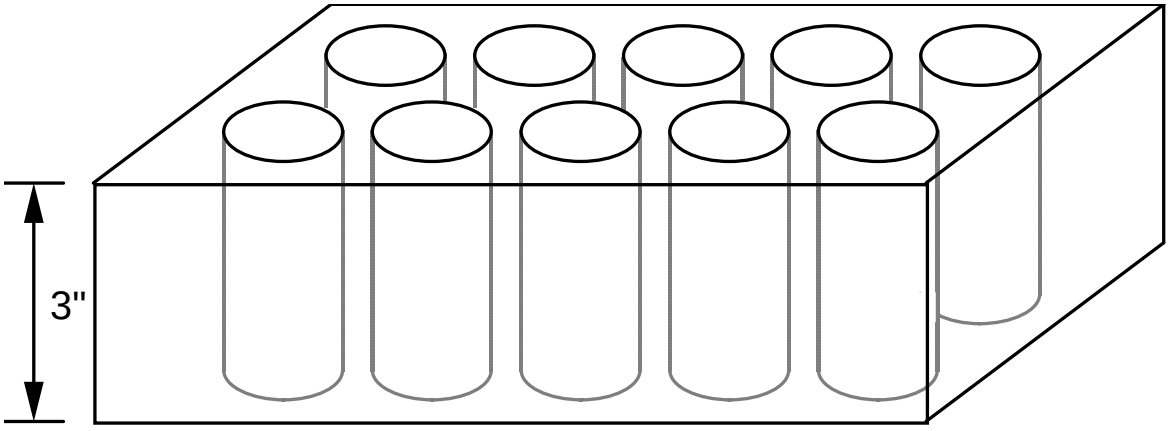

Fig. 6. Schematic of how specimens were core-drilled from as-received bricks.

In the case of the fusion-cast alumina, large blocks of approximate dimensions 0.60 × 0.50 × 0.30 m (24 × 20 × 12 in.) were prepared by both Corhart Refractories and Monofrax Inc., using their normal processing conditions. These blocks were sectioned in half with one half being shipped to ORNL and one half being retained by the preparing company. Cores of 19 mm (0.75 in.) diameter were drilled from whole regular cast blocks at three locations prior to being sectioned. Location one was in the center of the bottom of the block in the positive *y*-direction (designated *y*-core). Locations two and

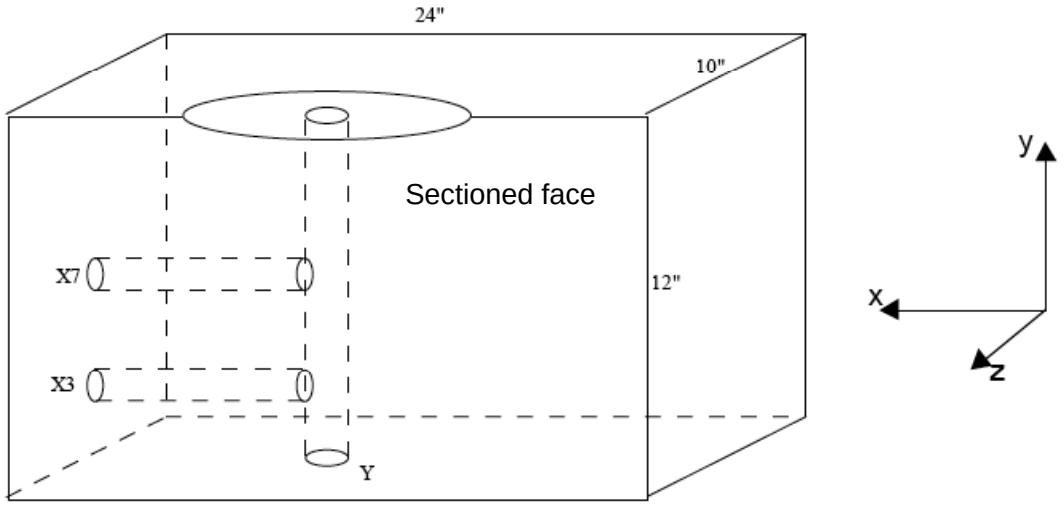

Fig. 7. Refractory block core-drill locations for physical and chemical analysis.

three were in the side of the block at 76 mm (3 in.) and 178 mm (7 in.) from the base in the *y*-direction with the cores taken in the *x*-direction (designated *x*3-core and *x*7-core, respectively). Core locations and orientations are shown in Fig. 7. Individual cores were then sectioned into 25-mm (1-in.) pieces for density/porosity and X-ray fluorescence (XRF) analysis. The coordinate system used in Fig. 7, which is a nontraditional left-handed coordinate system, was chosen to comply with sample orientations utilized by Monofrax Inc. for its physical and chemical analysis techniques.

The regular cast blocks were further sectioned as shown in Fig. 8 to obtain creep specimens that were representative of the interior bulk region of each cast block. The individual bulk creep specimens were 38 mm (1.5 in.) in diameter and 76 mm (3 in.) in length. A specially cast block of M-type fusion-cast alumina was also prepared at Monofrax Inc. by incorporating an increased cooling rate. The block possessed a columnar zone of ≈ 50 mm (2-in.) thickness (as opposed to a columnar zone of ≈ 25 mm (1 in.) thickness on the regular cast blocks). A $0.30 \times 0.20 \times 0.05$ m ($12 \times 8 \times 2$ in.) slab was cut from the exterior of the block and was shipped to ORNL. Monofrax retained the remainder of the block. The entire 50-mm cross section contained the characteristic columnar zone microstructure. Creep specimens were sectioned such that the orientation of the columnar structure was oriented in both a longitudinal direction [dimensions: 38 mm (1.5 in.) diameter, 50 mm (2 in.) length] and transverse direction [(38 mm diameter (1.5 in.), 70 mm (2.75 in.) length] with respect to the length of the cylinder.

Cylindrical specimens [dimensions: 13 mm (0.5 in.) diameter, 38 mm (1.5 in.) length] for thermal expansion and elastic modulus determination were also taken from the sectioned regular cast Monofrax and Corhart blocks at locations between the creep specimens. Equivalent specimens were taken from the specially cast Monofrax block possessing the columnar structure. Similar to that of the creep specimens, the columnar structure in the specimens was oriented in both the longitudinal and transverse directions with respect to the length of the cylinders.

The cylindrical specimens were encased in a fine-grained H-type (100% β-alumina) fusion-cast alumina shell (shown in Fig. 9) to inhibit soda evolution from the test specimens into the furnace atmosphere during testing. Attempts were made to ensure that a gap existed between the sample and H-shell during testing, but that was not always the case.

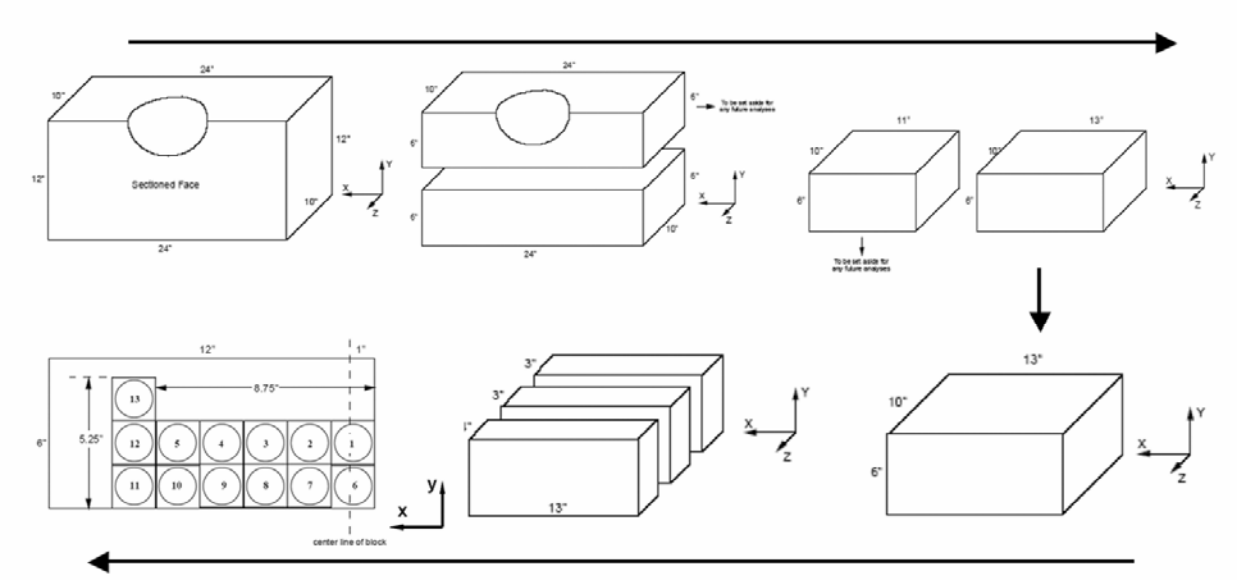

Fig. 8. Schematic representation of the sectioning plan used to fabricate creep specimens from the bulk region of the refractory blocks.

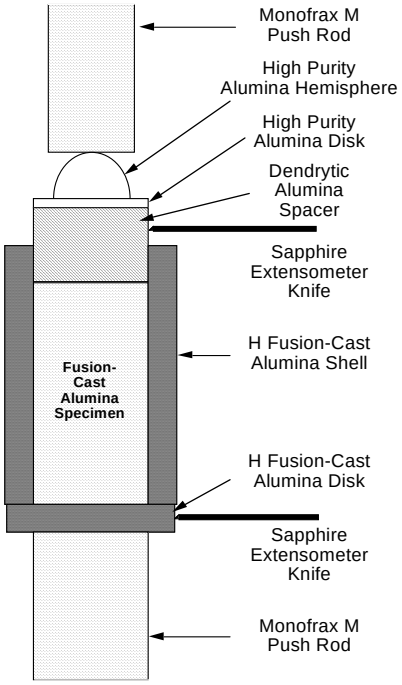

Fig. 9. Creep specimen assembly H-shell arrangement required for the creep testing of the fusion-cast alumina.

4.4 Creep Testing and Data Interpretation

Tables 5, 6, and 7 describe the creep test matrices for the silica, mullite, and fusion-cast alumina refractories, respectively. A typical stress-temperature-time history is provided in Fig. 10. All specimens were preloaded in compression to approximately 0.04 MPa (≈6 psi) during furnace heat-up to keep all the load train components and the specimen in continuous contact. The specimens were then heated from room temperature up to the test temperature in 4 h. Each of the specimens was soaked at temperature for 25 h prior to the application of the first stress.

Most creep analyses for long-term applications (i.e., where steady-state creep accumulation dominates the accumulation of strain, not the amount of primary creep) involve the determination of a steady-state or minimum creep rate and its examination as a function of applied stress and temperature. The steady-state or minimum compressive creep rate ($d\varepsilon/dt_{min}$) can be related to the applied compressive stress and temperature by using an empirical Arrhenius power law or the familiar Norton-Bailey creep equation [16]

$$d\varepsilon/dt_{min} = A\,\sigma^{n}\exp(-Q/RT), \quad (1)$$

where A is a constant, σ is the applied stress, n is the stress exponent, Q is the activation energy, R is the universal gas constant, and T is the absolute temperature. Multilinear regression may be performed to determine the constants A, n, and Q for each material. By performing the analysis in this manner, it is implied that the same dominant (or rate-controlling) creep mechanism is active at all temperatures and stresses. The validity of this assumption is assessed by the goodness-of-fit of this equation to the experimental data and the reasonableness of the obtained values for n and Q.

Table 5. Creep test matrix for the silica refractories (stress, MPa)[a]

Refractory	1550°C (2820°F)	1600°C (2910°F)	1650°C (3000°F)
Gen-Sil	0.2, 0.4, 0.6	0.2, 0.4, 0.6	0.2, 0.4, 0.6
SI96AU	0.2, 0.4, 0.6	0.2, 0.4, 0.6	*b*
Stella GGS	0.2, 0.4, 0.6	0.2, 0.4, 0.6	0.2, 0.4, 0.6
Vega	0.2, 0.4, 0.6	0.2, 0.4, 0.6	0.2, 0.4, 0.6
Vega H	0.2, 0.4, 0.6	0.2, 0.4, 0.6	0.2, 0.4, 0.6
Unnamed development brand	0.2, 0.4, 0.6	0.2, 0.4, 0.6	0.2, 0.4, 0.6

[a]0.2 MPa = 29.0 psi, 0.4 MPa = 58.0 psi, 0.6 MPa = 87 psi.

[b]Material exhibited excessive creep deformation at 1600°C, so its testing at 1650°C was omitted.

Table 6. Creep test matrix for the mullite refractories (stress, MPa)[a]

Refractory	1300°C (2370°F)	1375°C (2500°F)	1450°C (2640°F)
BP mullite		0.4, 0.6	0.4, 0.6
DURITAL S75	0.2, 0.4, 0.6		0.2, 0.4, 0.6
Frimul F		0.4, 0.6	0.4 & 0.6
GEM	0.2, 0.4, 0.6		0.2, 0.4, 0.6
HF 17		0.4, 0.6	0.4, 0.6
MU75AF		0.4, 0.6	0.4, 0.6
SL75AD		0.4, 0.6	0.4, 0.6
UFALA UCR		0.4, 0.6	0.4, 0.6
ZED FMC		0.4, 0.6	0.4, 0.6
ZED FM		0.4, 0.6	0.4, 0.6

[a]0.2 MPa = 29.0 psi, 0.4 MPa = 58.0 psi, 0.6 MPa = 87 psi.

Table 7. Creep-test matrix for the fusion-cast alumina refractories (stress, MPa)[a]

Refractory	1450°C (2640°F)	1550°C (2820°F)	1650°C (3000°F)
Corhart Jargal M cast block, regular bulk	0.6, 0.8, 1.0	0.6, 0.8, 1.0	0.6, 0.8, 1.0
Monofrax M cast block, regular bulk	0.6, 0.8, 1.0	0.6, 0.8, 1.0	0.6, 0.8, 1.0
Monofrax M cast block, special longitudinal columnar	0.6		1.0
Monofrax M cast block, special transverse columnar	0.6		1.0

[a]0.6 MPa = 87.0 psi, 0.8 MPa = 116 psi, 1.0 MPa = 145 psi.

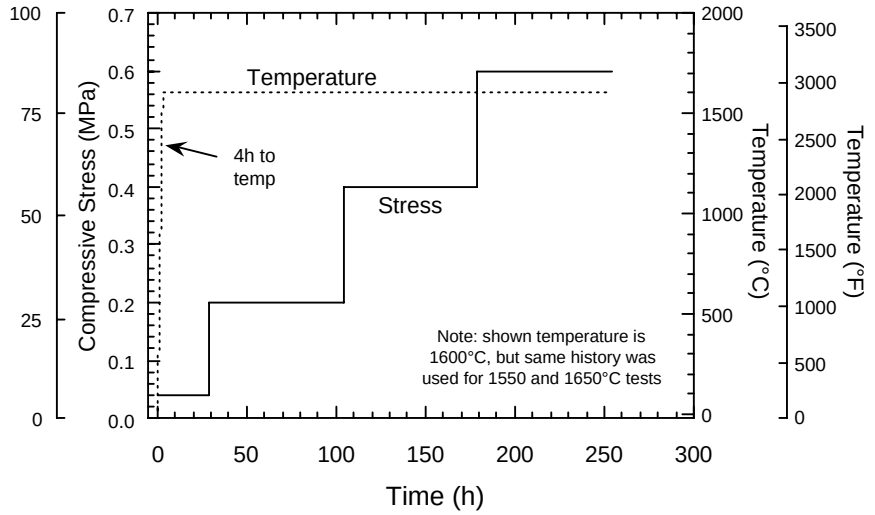

Fig. 10. Example of temperature and stress history used in the creep testing.

4.5 Microstructural Characterization

The microstructures of the various refractories were examined using reflected light (RL) imaging, cathodoluminescent (CL) imaging, and SEM. In the case of RL and CL, disks for examination were sectioned from both as-received and crept specimens Disks were cut from the top of each as-received specimen as shown in Fig. 11(a); disks were sectioned from crept specimens in their centers as shown in Fig. 11(b). The disk sections were cleaned and dried and were then impregnated with a low-viscosity resin to fill the pores. The impregnated specimens were mounted on Co-Cast mounting media. Cured sections were ground with diamond wheels down to 600 grit and then were finally polished with diamond paste and lapping oil. RL and CL microscopy were utilized for the characterization. A cold-cathode CL microscopy system (Model Mk4, Cambridge Imaging

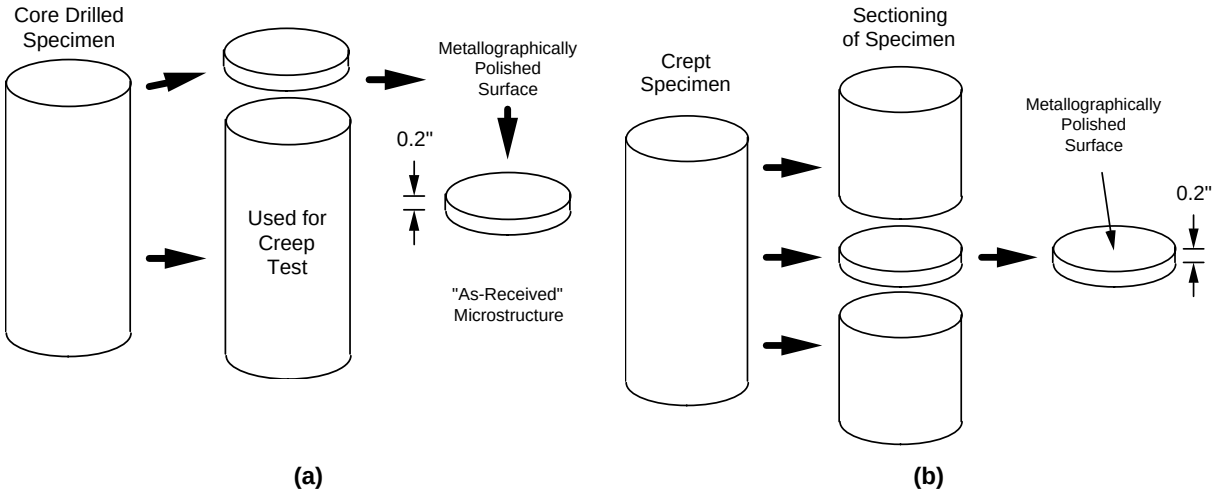

Fig. 11. Schematic describing how disk sections were machined from core-drilled specimens for (a) as-received and (b) post-test RL and CL imaging.

Labophot-Pol with a Nikon UFX-DX photomicrographic system) was used for these microstructural analyses. The CL microscopy characterization technique has been described in detail by Karakus and Moore [17] and is briefly described here. The CL imaging system utilizes an energetic electron beam that is produced from a cold cathode ray tube. The electron beam is trained on the surface of uncovered polished or unpolished specimens in a low vacuum environment. As a result of the electron beam-solid specimen interaction, minerals or phases in the specimen produce characteristic colored light known as "cathodoluminescent" emission. The CL technique is unique and provides microstructural information that often cannot be obtained by any other technique. The CL microscopy system can provide an immediate assessment of the phases in refractory materials through the identification of characteristic CL color and crystal habits that minerals exhibit. The CL microscopy system can also be used in conjunction with RL and SEM for elemental analysis of individual phases.

Certain minerals produce a characteristic CL color. For example, corundum (α-Al_2O_3) is characterized by a characteristic bright red CL color while spinel ($MgAl_2O_4$) produces a characteristic green color. These CL emissions are due to "activator" elements present in trace amounts in these mineral structures; Cr^{3+} in corundum produces a characteristic CL emission at approximately 694 nm, and tetrahedrally coordinated Mn^{2+} in spinel produces a CL emission at approximately 520 nm. Activator elements related to CL emission centers in these minerals often require low voltages ($\approx$ 8 kV) for excitation.

Important for the materials analyzed in this study are the CL behaviors of mullite, alumina, and silica grains along with that of the glassy matrix phase. Regular mullite grains do not produce bright CL but rather exhibit a dull response. Contrary to this, fused mullite grains produce intense dark blue or violet CL. Secondary mullite bonds between primary fused mullite grains can produce intense violet reddish CL, distinguishing them from primary mullite. Fused alumina grains exhibit very bright violet blue CL, while tabular alumina grains appear as an intense violet. Andalusite grains give off dark reddish CL and zirconia, a blue-white CL.

4.6 Supplemental Analysis

The bulk densities of various core-drilled specimens were measured prior to creep testing. Masses were measured on a balance that had a resolution of ± 0.0005 g. The masses were then divided by the respective specimens' volumes (diameters and lengths measured with calipers having a resolution of ± 0.005 mm) to calculate density.

Room-temperature thermal conductivity of the "as-received" bricks was measured by a transient plane source (TPS) technique in the "hot-disk" arrangement [18]. In this arrangement, a Kapton TPS element was used as both a heat source and a temperature sensor to measure the time required to conduct a known amount of heat across a prescribed distance of sample. Measurements were taken in the "standard method" by sandwiching the Kapton element between two identical cylindrical creep specimens and passing 1 W of power through the sample for 20 s. Five measurements were taken on each specimen type with 15 min. or longer between measurements. The specimen configuration along with the sensor itself is shown in Fig. 12.

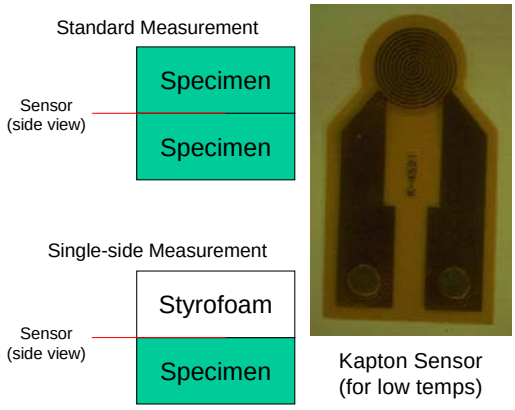

Fig. 12. Schematic of transient plane source direct thermal conductivity method experimental set-up and picture of Kapton sensor.

The phase content of the materials in their as-received state was characterized and was compared with that after creep testing at 1450°C. Specimen preparation involved grinding the refractory to approximately 325 mesh in an agate mortar and pestle. XRD was performed with all ten mullite materials in a Scintag 2000 diffractometer. The samples were scanned at a rate of 1°/min with Cu-K_a radiation (l = 1.54059 Å), and a step size of 0.02° over a scan range of 10 to 120° two-theta.

In the case of the fusion-cast alumina, thermal diffusivity was also measured from room temperature up to 1400°C (2552°F) by the laser flash method [19]. In the laser flash method, a cylinder of the bulk refractory [13-mm (0.5-in.) diam., 32 mm (1.25-in.) length] was sectioned into small disks [2 mm (0.08 in.) thick], and the disks were subjected to a high-intensity, short-duration thermal pulse through their thicknesses. The temperature resulting at the rear face of each specimen, due to the pulse, was recorded and was used to calculate the time required to raise the rear face temperature a certain percentage of its maximum value. Thermal conductivity values were then calculated:

$$\lambda = \rho \, \alpha \, C_p, \tag{2}$$

where λ is the thermal conductivity, ρ is the density, and C_p is the heat capacity. The latter parameter was measured by calorimetery at ORNL and Monofrax, Inc., in New York.

To examine dimensional stability due entirely to only exposure at temperature, specimens from each refractory were subjected to aging at times and temperatures that were equivalent to those applied to the creep specimens. Two methods were used for measuring these aging characteristics. The first involved heating the specimen at temperature for a prescribed number of hours and then cooling the furnace to room temperature. The specimen was then weighed, and its dimensions were measured before it was put back in the furnace for subsequent reheating. The mass, dimensions (volume), and density of the specimens were thus determined as a function of cumulative time and temperature.

The second method involved measuring the real-time specimen displacement at temperature using a dual-rod LVDT system (Fig. 13). The specimen was supported by a high-purity alumina disk resting on a fixed SiC push rod while the test assembly was supported by the body of the furnace. The test assembly for monitoring the linear dimensional changes consisted of two sapphire rods in contact with individual LVDTs. One sapphire rod and LVDT pair was used to monitor changes in the test

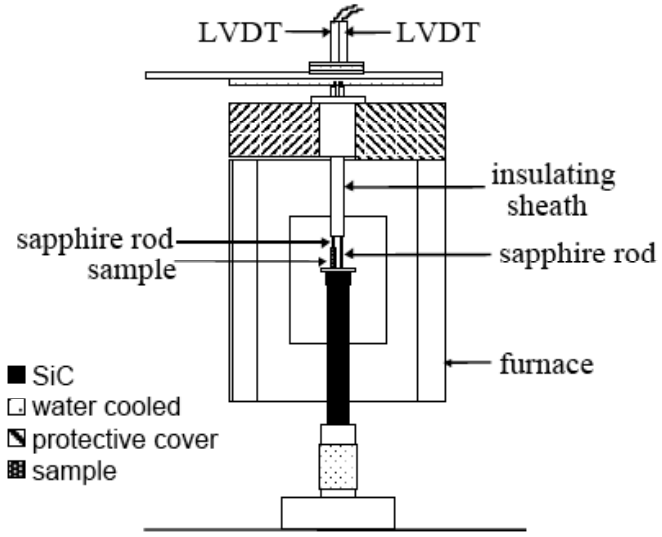

Fig. 13. Schematic of dual-rod LVDT system used to measure thermal expansion.

sample (designated LVDT-1) while the other rod and LVDT were placed in contact with the high-purity alumina disk supporting the test specimen (designated LVDT-2). The difference between these readings was used to calculate the dimensional changes of the specimen [13].

The ASTM lid test was used to evaluate the corrosion of the various refractories [9]. A refractory specimen ($2.5 \times 2.5 \times 1$ cm) sectioned from the as-received bricks was placed over a small alumina crucible containing 12.5 g of sodium carbonate. The crucible and refractory specimen "lid" were then placed in a secondary alumina container and isothermally exposed at 1400°C for 24 h. After exposure, samples were removed and were examined for recession.

5. Results and Discussion

5.1 Silica Refractories

A major finding from the compressive creep tests of the silica refractories was that concurrently active mechanisms, other than creep, resulted in positive dimensional changes. Specifically, as shown in Fig. 14, some specimens exhibited axial expansion during creep testing even though an axial compressive load was applied. This peculiarity is a consequence of the bulk expansion that these refractories exhibited. This effect limited the ability to identify or interpret the lesser-active creep mechanism in these silica refractories. Consequently, the compressive creep rates of all six brands were not able to be represented as a function of temperature and compressive stress using the conventionally used NBA creep equation (i.e., the Arrhenius power-law creep model).

The change in dimensions of the compressively crept specimens indicated that their size (both diameter and length) had actually increased as a consequence of the employed creep test conditions (see Table 8). This expansion phenomenon greatly complicates creep analysis in which Eq. (1) is used and likely invalidates its use. All six brands showed this expansion effect. The increases in diameter and length of the creep specimens were between 0.35 and 1.0%.

Table 8. Dimensional changes of crept specimens. A negative value constitutes contraction and a positive value represents expansion.

Length change (%)	Gen-Sil	SI96AU	Stella GGS	Vega	Vega H	H-W Dev. Brand
1550°C						
Diameter	1.0	0.65	0.45	−0.08	0.49	0.38
Length	0.55	0.55	0.36	0.94	0.42	0.41
1600°C						
Diameter	1.0	9.12	0.42	0.24	0.46	0.38
Length	0.52	−24.0	0.70	0.35	0.47	0.49
1650°C						
Diameter	0.50		0.71	0.50	0.53	0.50
Length			0.47	0.71	0.59	0.46

Consistent with bulk changes exhibited by the creep specimens, the unstressed or “aged” silica refractory specimens from all six materials also exhibited loss of mass, dimensional increases, and density decreases between 1550 and 1650°C (see Table 9). The mass losses of the six brands at 1550 and 1600°C were equivalent; however, some silica brands lost more mass than others at 1650°C: Harbison-Walker’s developmental brand lost approximately 0.1% of its mass; SI96AU lost ≈ 0.2%, Vega H lost ≈ 0.3%, Gen-Sil lost ≈ 0.5%, Vega lost ≈ 1.0%; and Stella GGS lost ≈ 1.5%. Most of the mass loss occurred in less than 25 h for all six brands.

The dimensional increases of the silica specimens were a function of temperature, as illustrated in Fig. 15. Additionally, some brands expanded more than others. Each of the specimens expanded isotropically in each of three directions (within statistical confidence). The ranges of expansion were ≈ 1–2.5% at 1550°C, ≈ 2.25–3.75% at 1600°C, and ≈ 3.5–6% at 1650°C. Harbison-Walker’s developmental brand expanded the least amount at all three temperatures, followed by Gen-Sil. The ascending order of expansion for the other four brands varied with temperature. Stella GGS expanded

Table 9. Density changes of crept specimens. A negative value constitutes a decrease in density and a positive value represents an increase.

	Gen-Sil	SI96AU	Stella GGS	Vega	Vega H	H-W Dev. Brand
After 1550°C creep testing						
Density (g/cc)	1.75	1.80	1.81	1.73	1.83	1.90
Change (%)	−1.8	−2.6	−1.9	−3.2	−2.8	−1.6
After 1600°C creep testing						
Density (g/cc)	1.73		1.79	1.76	1.82	1.90
Change (%)	−2.7		−2.0	−1.8	−1.9	−2.2
After 1650°C creep testing						
Density (g/cc)	1.72		1.79	1.74	1.80	1.88
Change (%)	−3.0		−2.2	−3.1	−3.9	−3.0

the most at 1550°C (≈ 2.5%), SI96AU expanded the most at 1600°C (≈ 3.75%), and Vega expanded the most at 1650°C (≈ 6%). Dimensional increases in these aged specimens were greater than axial expansion of the crept silica specimens at the same temperatures, indicating that there may have been a specimen-size effect. The change in the as-received assemblage of tridymite, amorphous silicate, Ca-silicate, and cristobalite to the crept microstructure consisting entirely of cristobalite likely caused the observed volume expansion. The same phenomenon appeared to have occurred in the aged specimens. Temperature is the activator of this phenomenon; the application of stress is not a prerequisite for it.

Based upon the data given in Fig. 15 it is reasonable to assume that the deformation rate measured during the application of a compressive stress was composed of two parts: (1) specimen contraction arising from creep-related processes (a function of time, stress, and temperature) and (2) specimen elongation arising from the change in the phase assemblage (a function of time and temperature only). One can therefore estimate the contribution arising from creep alone by subtracting the rate of elongation occurring at zero stress from the rates measured under a fixed stress. To this end, the curves in Fig. 15 were subsequently used to calculate the linear expansion rates occurring at 250 h for the 1600 and 1650°C aging tests. The calculated rates were then subtracted from the rates measured under an applied stress at comparable times.

For the 1600 and 1650°C aging tests the stress of 0.6 MPa was used because the total time at temperature was comparable to that used to calculate the zero-stress expansion rate:

- Gen-Sil: $d\varepsilon/dt_{min}$ (1/s) = 3.6×10^{20} σ exp[-25 (kcal/mole)/RT]
- SI96AU: $d\varepsilon/dt_{min}$ (1/s) = 4.2×10^{44} σ exp[-44 (kcal/mole)/RT]
- Stella GGS: $d\varepsilon/dt_{min}$ (1/s) = 5.5×10^{14} σ exp[-20 (kcal/mole)/RT]
- Vega: $d\varepsilon/dt_{min}$ (1/s) = 1.9×10^{12} σ exp[-18 (kcal/mole)/RT]
- Vega H: $d\varepsilon/dt_{min}$ (1/s) = 1.4×10^{13} σ exp[-18 (kcal/mole)/RT]

XRD results showed that all six as-received silica refractories consisted of cristobalite (PDF# 39-1425) and tridymite (PDF# 18-1170). Even though a calcium silicate was present in the grain boundaries (as detected by SEM/EDS), its concentration was sufficiently small that XRD did not

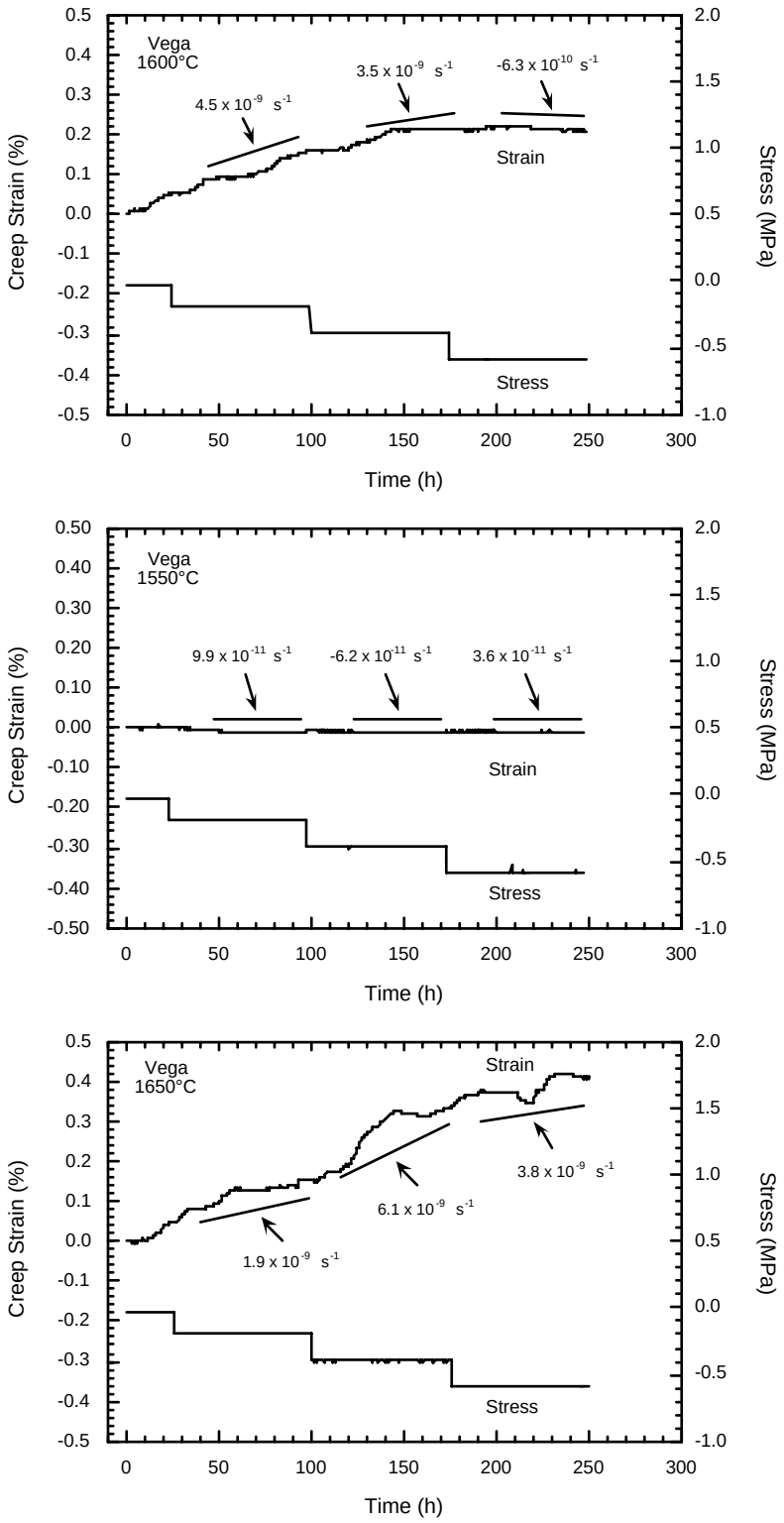

Fig. 14. Creep behavior of Vega as a function of temperature.

identify it. It was qualitatively determined that Gen-Sil had the highest tridymite content and that SI96AU had the highest cristobalite content. Very small amounts of quartz were detected only in SI96AU and Vega.

Based on the density differences in the silica minerals (quartz = 2.64 g/cc, tridymite = 2.26 g/cc, cristobalite = 2.32 g/cc), it takes the conversion of approximately 6.5% of residual quartz to tridymite or cristobalite to cause a bulk expansion of 1%. Because no quartz was detected in four of the conventional silicas, and because its concentration was minute in SI96AU and Vega, the phase-change phenomenon could not have caused the volume expansion that these materials exhibited as a consequence of the creep testing. Subsequent creep testing changed the phase content in the six silica refractories in that all the tridymite in the silica refractories was converted to cristobalite. The stable silica phase above 1470°C (2680°F) is cristobalite, so the XRD results are not surprising.

The microstructures of the six silica refractories changed as a consequence of the applied test conditions. The changes in as-received to crept microstructures in the six materials had commonality and are shown schematically in Fig. 16. The as-received silica microstructures of the six materials typically consisted of cristobalite aggregates or "islands" in a matrix or "sea" or of prismatic tridymite (approximately 10 to 20 µm in size near the cristobalite islands, 20 to 80 µm farther away from them), calcium silicate crystals, and an amorphous silicate. The structure of the cristobalite in the islands often resembled fish scales. The individual cristobalite grains comprising the cristobalite islands had a

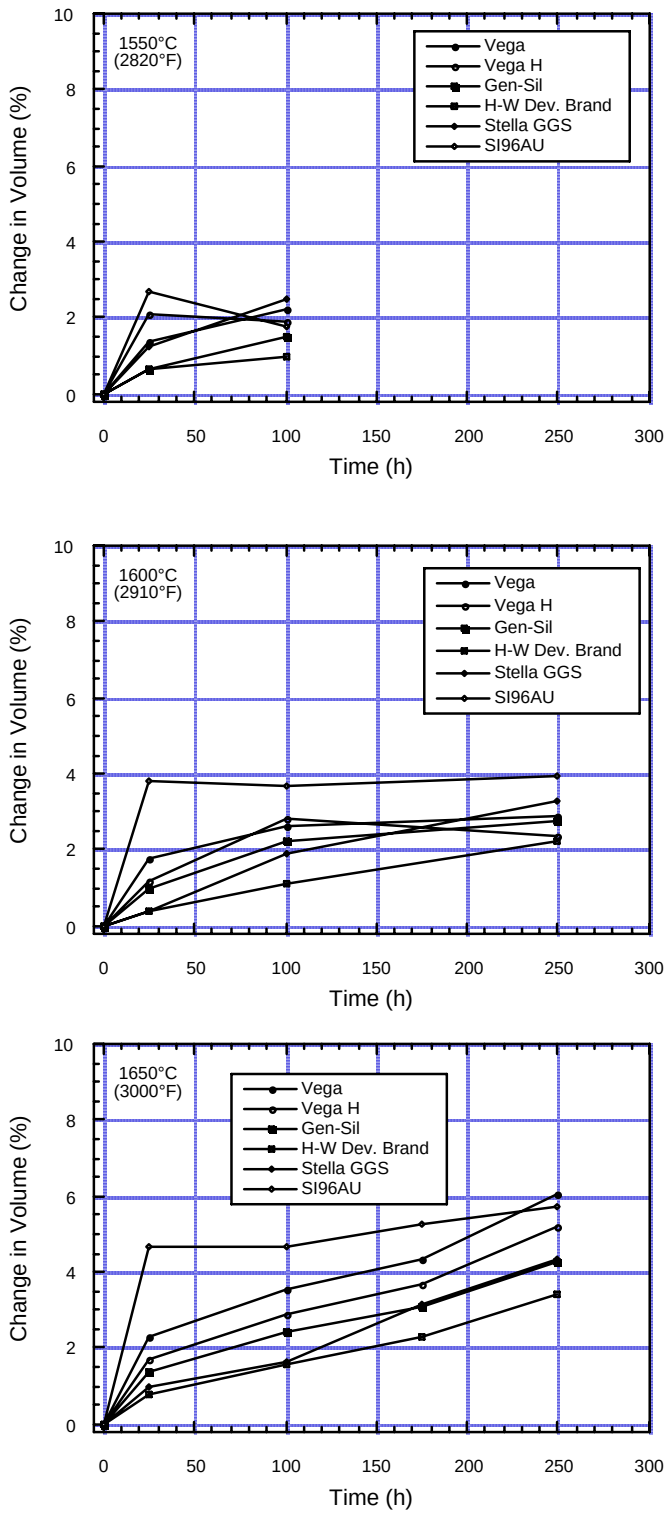

Fig. 15. Change in volume of "aged" specimens as a function of time and temperature.

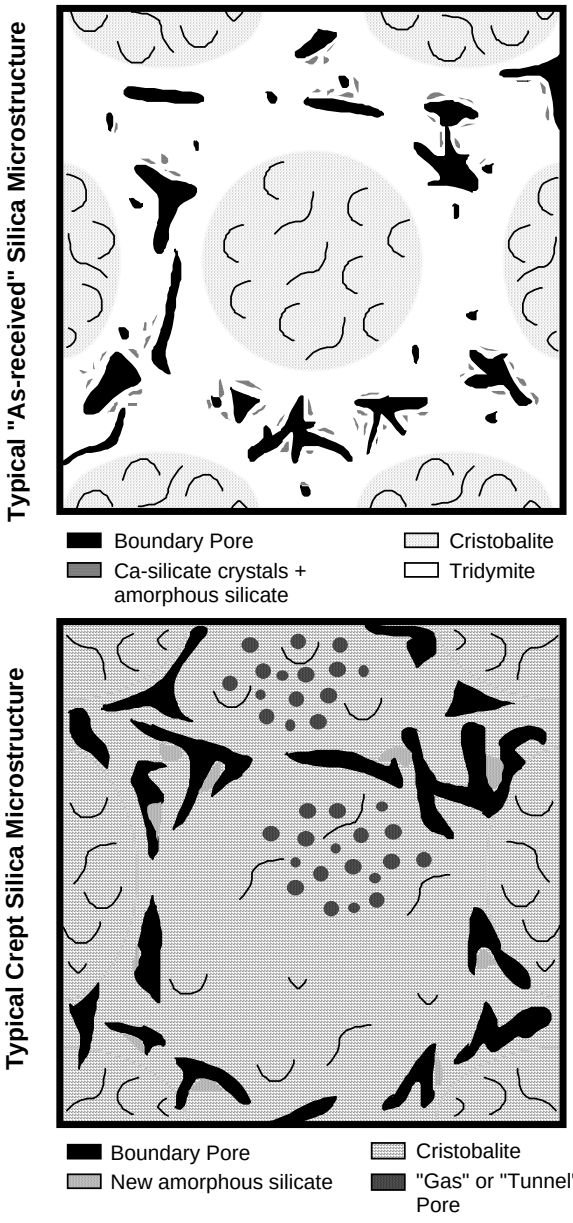

Fig. 16. Schematic of the change in microstructure from the as-received material state to that after creep or high-temperature exposure.

rather uniform size distribution, 5 to 10 μm across; the size of the cristobalite islands ranged from approximately 40 μm to more than 1 mm.

During creep testing at 1550, 1600, and 1650°C, the tridymite converted to cristobalite, and a new amorphous silicate (formed between the new and growing cristobalite islands). Additionally, many of the crept cristobalite microstructures contained pores that resembled tunnels. They appeared to be avenues for vaporization, but their structure was not examined, so their cause is not known.

RL and CL imaging supplemented one another well to explore these microstructural changes. Examples of the RL images of the as-received and crept microstructures are shown for the Vega refractory in Fig. 17. Pores, tridymite, and Ca-silicate were consistently observed in the as-received microstructures of each refractory. Changes in the microstructure arising from creep testing included the formation of larger pores, larger cristobalite islands, the new amorphous silicate, and the creation of gaseous pores. The bulk expansion of the crept specimens may be explained by the destruction of original tridymite bonds and the enlargement of pores and of the cristobalite islands.

CL imaging (Fig. 18) provided an interesting and different perspective into how the microstructures changed as a consequence of the creep testing. The CL imaging revealed the tridymite in the as-received state better than the RL imaging, and it provided new insights into how the cristobalite islands changed or grew.

Specifically, the cores of most of the cristobalite aggregates in these specimens exhibited a light blue color while their outer zones or rims were dark blue. The light blue core represents the original fish-scale cristobalite island. The core or center of the islands after creep testing was relatively free of impurity phases, resulting in the light blue CL color. During the creep testing, the tridymite converted to cristobalite or added to the size of existing cristobalite islands. Additionally, the original calcium and amorphous silicates (containing transition metals and alkalis) formed a liquid phase during creep testing that either diffused into the enlarging cristobalite islands or was present during their growth. This outer zone or rim was characterized by dark blue CL. The Ca-silicate phase luminesced bluish-white and locally bright yellow, with some of its crystals being as small as 15 μm, in the as-received microstructures. However, during creep testing, iron impurities in the original amorphous silicate combined with the Ca-silicate phase to form a new amorphous silicate that because of the presence of the iron, did not produce CL color.

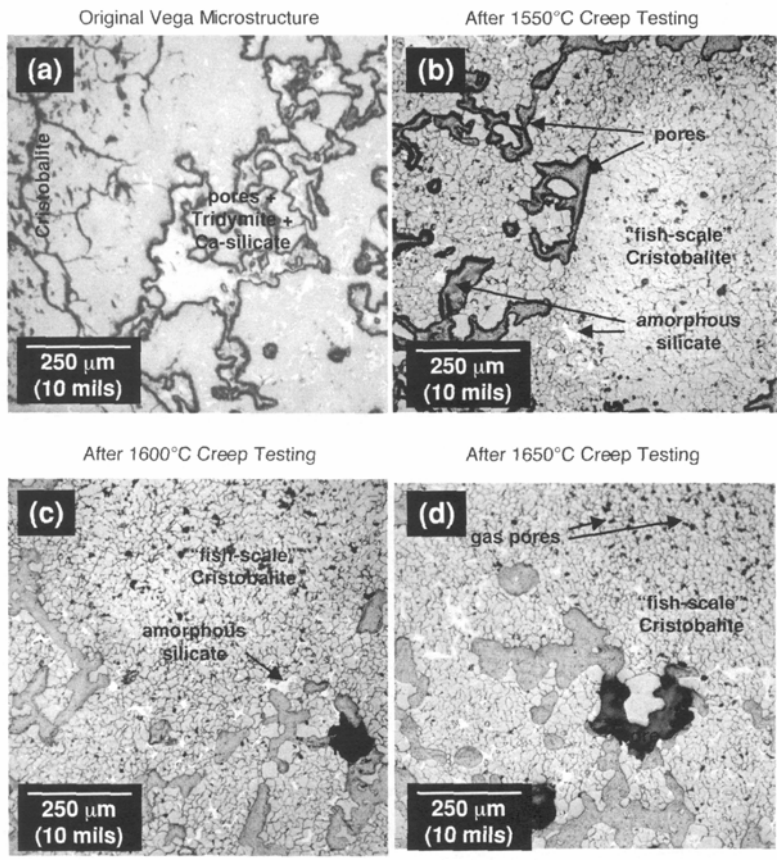

Fig. 17. Vega's microstructural changes as a function of temperature as revealed by reflected-light microscopy.

In the case of the corrosion testing, a portion of the silica refractory lid was dissolved by the sodium carbonate vapor, forming a liquid phase at temperature. After the test, the maximum amount of recession was measured and summarized (Fig. 19). In general, there was only a slight variation in the amount of attack among the six silicas, and it may be concluded that their corrosion resistances were statistically equivalent. The amount of recession showed an almost linear relationship with temperature, as shown in Fig. 20. Because a vapor attack is expected, this effect seems reasonable. Varying the amount of sodium carbonate by 50% more (18.75 g) and by 50% less (6.25 g) from the standard 12.5 g had very little effect. Apparently, the sodium carbonate is not fully consumed during the test, and the lowest amount does not limit the extent of attack.

5.2 Mullite Refractories

The crystalline phases present in each of the ten mullite refractories varied from material to material, but some trends or similarities existed among the brands (see Table 10). The ten brands could be broadly categorized as either fused-grained or non-fused-grained (see Table 4). The non-fused-grained materials all contained mullite grains derived from andalusite or kyanite while the fused-grained mullite was made by fusion (melting) of alumina and silica. All the refractories were composed of variously sized mullite grains floating in a matrix of secondary mullite with various levels of glass and porosity present in the matrix. The DURITAL S75, HF 17, and ZED FMC brands all contained very little glassy phase. All the others possessed significant quantities of glassy phase. The HF 17, UFALA UCR, and ZED FMC brands were all found to possess high levels of matrix porosity when examined by optical microscopy and SEM; the rest showed little or no matrix porosity.

Room-temperature thermal conductivity testing resulted in the average values shown in Fig. 21. Frimul F showed the highest thermal conductivity at just under 3.5 W/mK. It was followed by Durital S75, GEM, MU75AF, and ZED FMC, which all had a thermal conductivity of approximately 3.0 W/mK. BP mullite and HF 17 both had similar thermal conductivity values of 2.7 to 2.8 W/mK, followed by ZED FM with a value of just over 2.5 W/mK. The two brands with the lowest thermal conductivity values were SL75AF and UFALA UCR, which had values of approximately 2.5 W/mK.

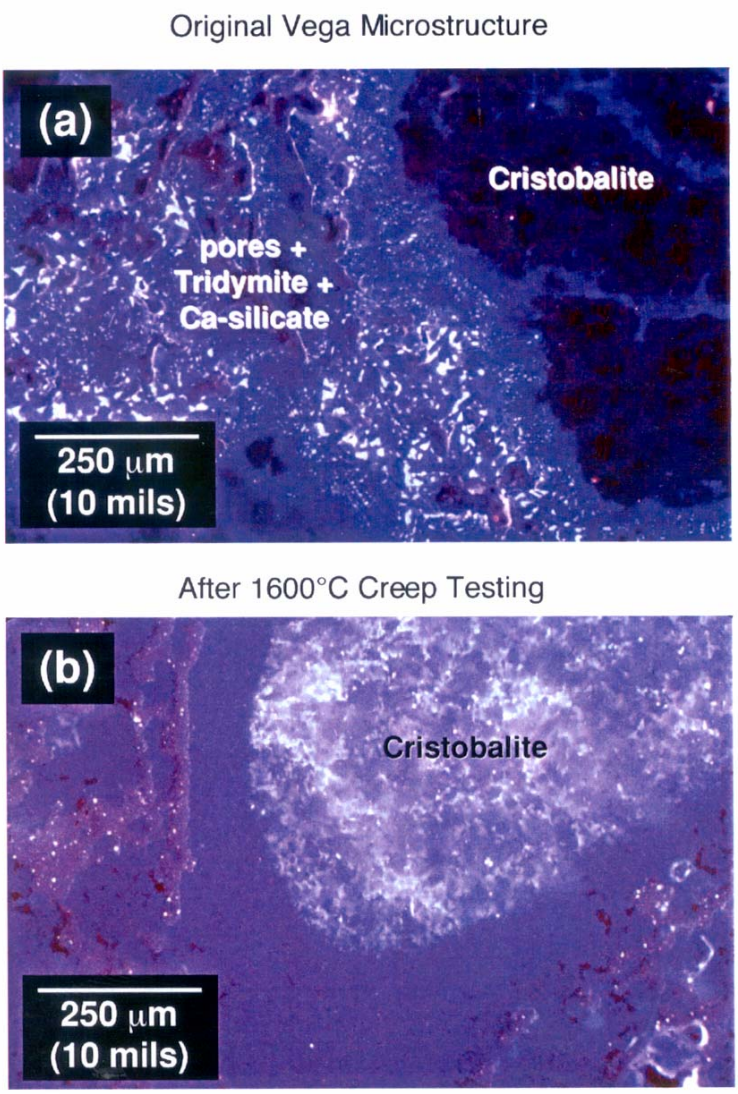

Fig. 18. Vega's microstructural changes as a function of temperature as revealed by cathodoluminescence imaging.

These values were all higher than those given in the manufacturers' literature, which ranged from 2.0 to 2.4 W/mK.

The results from creep testing at an applied stress of 0.5 MPa are shown in Fig. 22. The amount of compressive creep for the various refractories fell into three levels. BP mullite, HF 17, and Frimul F all showed low amounts of creep at temperatures between 1300 and 1450°C (2370 to 2640°F). Although the creep rate for the MU75AF at 1450°C was also quite low, it exhibited anomalous behavior in that the creep rate increased as the temperature was lowered to 1375°C. Slightly greater amounts of creep were seen in the GEM, DURITAL S75, and ZED FM brands at temperatures between 1300 and 1450°C (2370 to 2640°F). Creep rates for these refractories were found to be on the order of 10^{-10} s^{-1} at the lower test temperature and 10^{-9} s^{-1} at the higher test temperature. The SL75AD, UFALA UCR, and ZED FMC brands all showed significant amounts of creep at temperatures between 1375 and 1450°C (2500 to 2640°F). Their creep rates were on the order of 10^{-9} s^{-1} at the lower test temperature and 10^{-8} s^{-1} at the higher test temperature. Because only one specimen per condition was tested, the authors were unable to statistically conclude that any one of the refractories in each group had superior creep resistance to the others. If differences exist within a grouping, they are believed to be insignificant.

The activation energy in the Norton-Bailey creep equation was found for each brand by equating the respective slope in Fig. 22 to the quantity $-Q/R$. Although the values of the stress exponents could have also been determined from the experimental data, that procedure was not implemented because the uncertainties were high in the resulting estimates. Specifically, because n is typically very close 1, an increase in stress from 0.2 to 0.6 would only increase the creep rate by a factor of 3. Replicate creep tests of other structural ceramics have shown that the minimum creep rate value can vary by an order of magnitude or more. Consequently, the stress range used in the present investigation was probably not sufficient to generate a significant increase in creep rate with increasing stress. Therefore, the value of A in Eq. (1) was calculated by assuming $n = 1$. The effect of specimen

elongation or contraction in the absence of a stress was ignored in the calculations. The resulting expressions were then derived for the creep rate of the mullite refractories:

- BP mullite $d\varepsilon/dt_{min}$ (1/s) = 4.2×10^{-1} σ exp[−73 (kcal/mole)/RT]
- DURITAL S75 $d\varepsilon/dt_{min}$ (1/s) = 1.5×10^{5} σ exp[−110 (kcal/mole)/RT]
- Frimul F $d\varepsilon/dt_{min}$ (1/s) = 3.3×10^{7} σ exp[−130 (kcal/mole)/RT]
- GEM $d\varepsilon/dt_{min}$ (1/s) = 7.4×10^{1} σ exp[−80 (kcal/mole)/RT]
- HF 17 $d\varepsilon/dt_{min}$ (1/s) = 6.6×10^{16} σ exp[−200 (kcal/mole)/RT]
- MU75AF [Could not be determined]
- SL75AD $d\varepsilon/dt_{min}$ (1/s) = 6.0×10^{-2} σ exp[−50 (kcal/mole)/RT]
- SL75AD $d\varepsilon/dt_{min}$ (1/s) = 2.4×10^{4} σ exp[−90 (kcal/mole)/RT]
- ZED FMC $d\varepsilon/dt_{min}$ (1/s) = 1.1×10^{12} σ exp[−150 (kcal/mole)/RT]
- ZED FM $d\varepsilon/dt_{min}$ (1/s) = 5.1×10^{8} σ exp[−130 (kcal/mole)/RT]

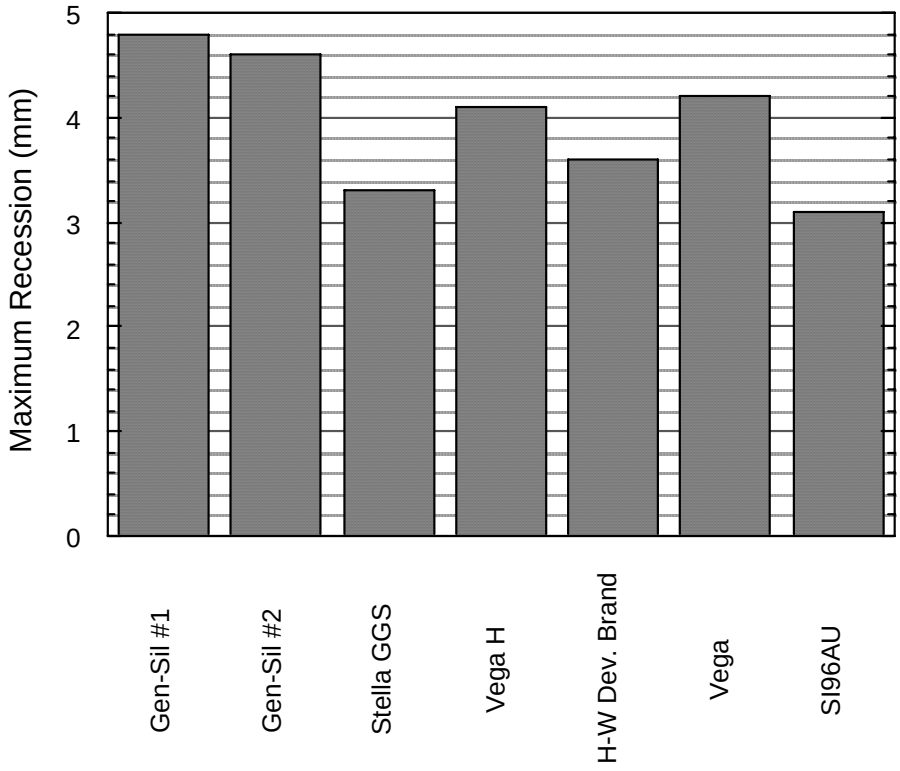

Fig. 19. Amount of refractory recession when exposed to sodium carbonate at 1400°C for 24 h.

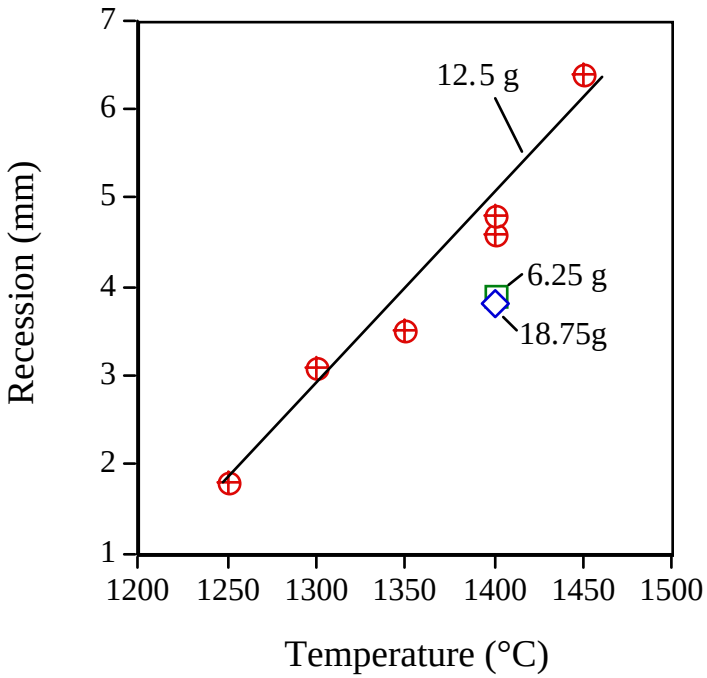

Fig. 20. Amount of recession as a function of temperature and sodium carbonate addition for Gen-Sil silica.

Table 10. Summary of microstructural observation for the mullite refractories before and after creep testing

Brand name	Starting microstructure	Microstructure after creep
BP mullite	RL&CL: large and small fused mullite grains dense matrix of secondary mullite and glass XRD: mullite and alumina SEM/EDS: mullite is stoichiometric while the glassy phase contains K_2O, Na_2O, and CaO	No change
DURITAL S75	RL&CL: non-fused mullite grains derived from and alusite along with tabular and fused alumina grains floating in a matrix of secondary mullite, little detectable glass XRD: mullite and alumina SEM/EDS: mullite is stoichiometric	No change
Frimul F	RL&CL: fused mullite aggregates floating in a very glassy matrix of secondary mullite, small mullite grains present in the glassy matrix XRD: mullite and traces of alumina SEM/EDS: mullite is stoichiometric while glassy phase contains K_2O, CaO, and TiO_2	No change
GEM	RL&CL: large and medium sized fused mullite grains in a secondary mullite matrix containing amorphous phase XRD: crystalline mullite; SEM/EDS: large mullite crystals and smaller (3–5 μm) secondary mullite crystals in an amorphous matrix, glassy matrix has a similar composition to the mullite crystals with small amounts of Na_2O, CaO, and TiO_2	No change

Table 10. continued

Brand name	Starting microstructure	Microstructure after creep
HF 17	RL&CL: large fused mullite grains in a highly porous matrix of fine fused mullite grains plus very tiny alumina crystals XRD: mullite and alumina SEM/EDS: secondary mullite crystals present as observed as agglomerates devoid of glassy bonding phase	Microstructure appeared denser
MU75AF	RL&CL: large fused mullite grains or aggregates with round morphology in a fine "granular" mullite and glassy matrix XRD: mullite plus trace alumina SEM/EDS: the glassy phase contains K_2O and Na_2O along with trace amounts of TiO_2 and CaO	No change
SL75AD	RL&CL: andalusite grains partially converted to mullite along with alumina grains and fine fused grain mullite; secondary mullite matrix formed around and between partially mullitized andalusite grains, large fused alumina grains, and fine fused mullite grains; andalusite grains contain free quartz that is converted to cristobalite during firing XRD: andalusite, mullite, alumina, and cristobalite SEM/EDS: glassy matrix contains Na_2O, MgO, CaO, K_2O, and TiO_2	Andalusite grains are converted to mullite aggregates and the amount of glassy phase has increased
UFALA UCR	RL&CL: finely crystalline mullite aggregates formed through the calcination of andalucite or kyanite in a fine crystalline mullite matrix, which contains a large number of micro-fissures and fine pores along with a large amount of glassy phase XRD: mullite SEM/EDS: skeletonized mullite containing elliptical and spherical pores characteristic of mullite derived from andalucite; mullite present in the matrix has a prismatic morphology and a variable crystal size with most crystals being small and needle-like but some crystals having a large rectangular shape due to crystal growth, the prismatic mullite crystals contain TiO_2 impurities and the glassy phase contains K_2O, CaO, and TiO_2	Reduction in porosity, elimination of the micro-fissures, and appearance of cristobalite
ZED FMC	RL&CL: large, medium and fine fused mullite grains; the matrix between the large grains contains poorly-sintered fine fused mullite particles as well as large amounts of micro-fissures along with small amounts of alumina and zirconia XRD: mullite plus trace alumina SEM/EDS: very small amounts of silica glass formation (with CaO imourities) along with secondary 1- to 2-μm mullite crystal	No change
ZED FM	RL&CL: primarily fused mullite grains similar to the ZED FMC and trace amounts of alumina and zirconia particles; good particle to particle bonding XRD: mullite plus trace alumina SEM/EDS: strong mullite and glassy bonding, glass contains CaO	No change

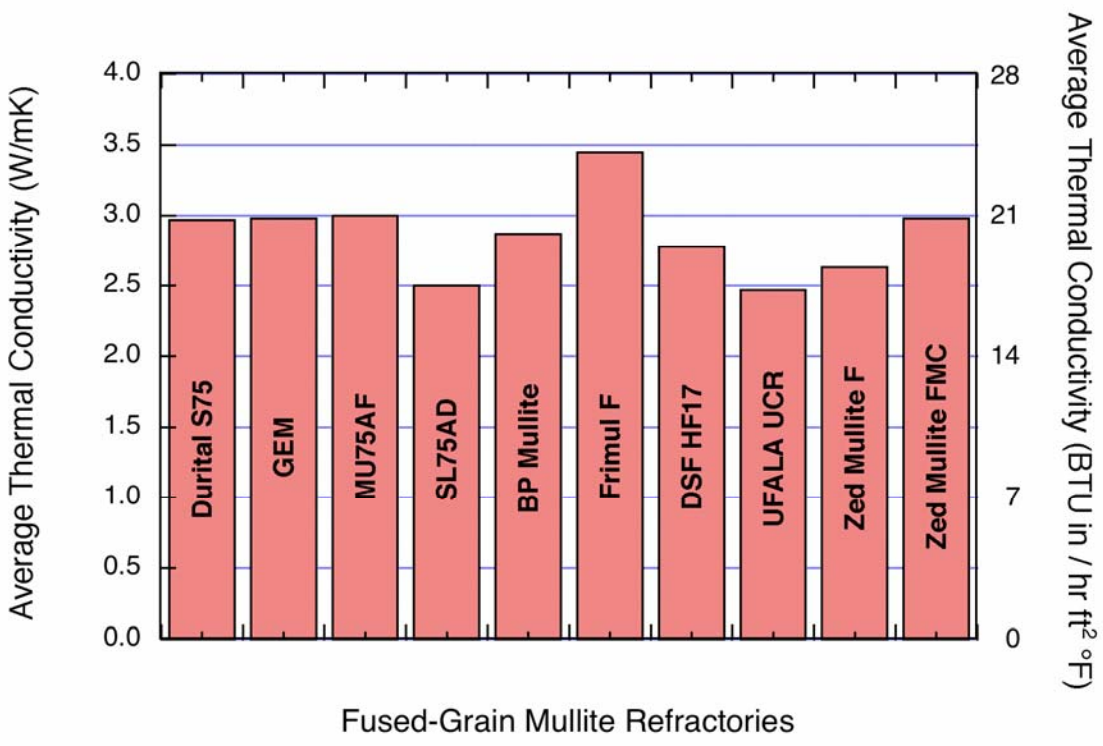

Fig. 21. Thermal conductivity of mullite refractories as measured by the "hot-disk" method.

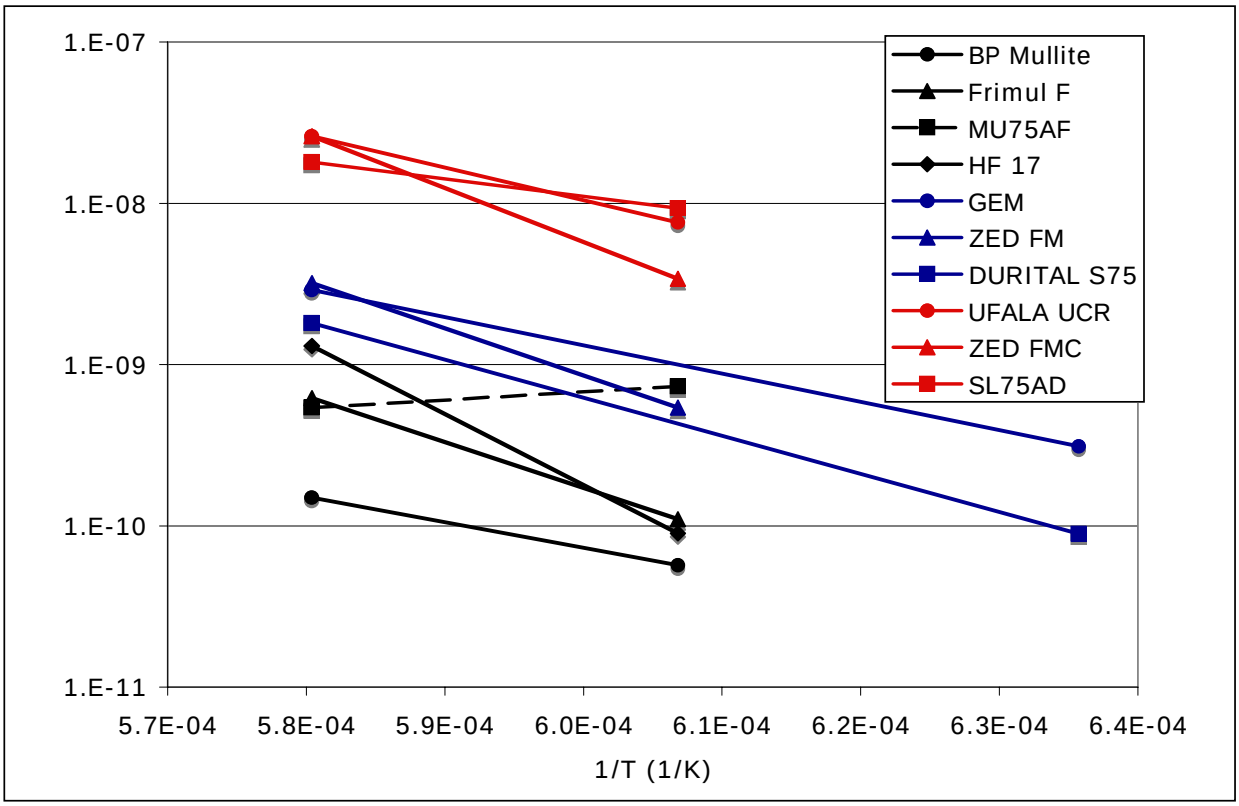

Fig. 22. Creep rate measured at 0.6 MPa as a function of reciprocal temperature.

Activation energies for the various refractory brands ranged from 50 to 200 kcal/mol. Although no direct correlation between the magnitude of the activation energy and the amount of creep exhibited by a particular brand could be drawn from the data, it is known that materials possessing a high activation energy have greater sensitivity to temperature than those possessing a lower activation energy. The values for three of the calculated activation energies correspond to the activation energy of vitreous silica, which falls in the range of 120 to 170 kcal/mol [20, 21]. This would indicate that the glassy phases in these brands affect the overall creep behavior of the material.

As indicated in Table 10, all of the refractories except the SL75AD, UFALA UCR, and HF 17 brands exhibited no major changes after creep testing. The microstructure of the HF 17 appeared to be slightly denser. In the case of the SL75AD brand, the andalusite grains were converted to mullite aggregates, and the amount of glassy phase increased in the crept specimens. The crept samples of the UFALA UCR refractory exhibited a reduction in porosity, the elimination of the microfissures, and the appearance of cristobalite. Additional details are provided in Ref. [11].

In subsequent aging tests, eight of the ten refractory specimens exhibited similar behavior, with the ZED FMC and ZED FM showing extraneous amounts of change (≈8.5%) in mass and volume due to thermal exposure. The other eight brands showed less than 0.2% change in mass and less than 0.6% change in volume. The changes in volume resulted in less than a 0.5% change in overall density for all samples, including the ZED FM and FMC brands. The two Minteq brands along with the Frimul F brand all exhibit activation energies associated with vitreous silica. They also exhibit the largest changes in mass, which may indicate that the silica plays some role in the temperature-induced mass changes.

Results from the ASTM lid test showed that only minimal amounts of recession occurred for the mullite refractories under the testing conditions set forth by the standard. Also, the mass change data were found to be ambiguous; some of the specimens had deposits on their surfaces and actually gained weight while others lost a small amount of mass. Therefore, those data are not reported here. Figure 23 shows the small amounts of refractory recession occurring on the various refractory samples. It can be seen that the nonfused grained refractories (Durital S75, SL75AD, and UFALA UCR) show a minimal amount of recession and some discoloring while the fused grained materials show practically no recession at all.

5.3 Fusion-Cast Alumina Refractories

The density profiles (Fig. 24) for the Corhart and Monofrax bulk blocks based on the *x* and *y* cores (see Fig. 7 for sectioning details) showed a mean bulk density on the order of 3.4 to 3.5 g/cm^3 (212.3 to 218.5 lb/ft^3) at their surface. This density is fairly constant for the entire *x*3 core and for the *y* core up to about 5 in. into the block for both cases. At the *y* core 5-in. mark the densities of both blocks begin to fall off due to porosity encountered in the header zones of the blocks. The *x*7 cores for both blocks also showed similar behavior with a fairly constant density in both cases up to around 3.5 in. and then a decline in density to around 3.3 g/cm^3 (206.0 lb/ft^3) for the Corhart block and to around 3.1 g/cm^3 (193.5 lb/ft^3) for the Monofrax block. Similar trends were seen in the porosity. If the columnar regions of the blocks are considered to exist in the outer 1 in. of the samples with the remainder of the block exhibiting bulk structure, then average columnar and bulk densities and porosities can be determined for each brand based on the previously described measurements. This determination

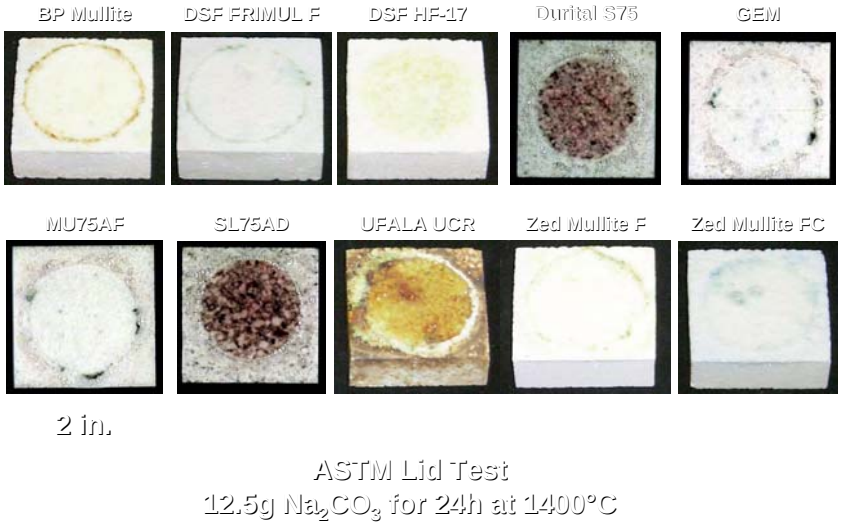

Fig. 23. Refractory recession when exposed to sodium carbonate at 1400°C for 24 h (according to ASTM C98).

would result in average columnar density values of 3.45 ± 0.05 g/cm^3 and 3.38 ± 0.02 g/cm^3 and average bulk density values of 3.45 ± 0.08 g/cm^3 and 3.37 ± 0.14 g/cm^3 for the Corhart and Monofrax brands, respectively. Average porosity values were found to be 1.38 ± 0.15% and 1.44 ± 0.19% for the Corhart columnar and bulk regions, respectively, and 2.64 ± 0.55% and 1.78 ± 0.92% for the Monofrax columnar and bulk regions, respectively. These values are close to those published by the manufacturers, although the density and porosity values obtained experimentally are a little lower for both brands (Corhart bulk density = 3.54 g/cm^3 and porosity = 2.0%, Monofrax bulk density = 3.40 g/cm^3 and porosity = 1.9%).

Density measurements were made on ten bulk Monofrax creep samples, ten bulk Corhart creep samples, two longitudinal columnar Monofrax creep samples, and two transverse columnar Monofrax creep samples. Porosity measurements were only made on five of each brand of bulk specimens and on representative samples for each type of columnar specimens. For the Monofrax bulk material, an average apparent density of 3.44 ± 0.02 g/cm^3 (214.76 ± 1.25 lb/ft^3), and bulk density of 3.44 ± 0.01 g/cm^3 (214.60 ± 0.89 lb/ft^3) was found with an average porosity value of 1.82 ± 0.31%. An average apparent density of 3.48 ± 0.01 g/cm^3 (217.26 ± 0.69 lb/ft^3) and average bulk density of 3.48 ± 0.01 g/cm^3 (217.19 ± 0.75 lb/ft^3) with an average porosity of 1.47 ± 0.59% was found for the Corhart bulk material. These values are in line with those supplied by the manufacturers, but the experimental density value is slightly higher and the experimental porosity value is slightly lower for the Monofrax material while both the experimental density and porosity levels are slightly lower for the Corhart material (Monofrax bulk density = 3.40 g/cm^3 and porosity = 1.9%, Corhart bulk density = 3.54 g/cm^3 and porosity = 2.0%). The longitudinal columnar Monofrax material showed an average apparent density of 3.42 ± 0.01 g/cm^3 (213.51 ± 0.69 lb/ft^3), an average bulk density of 3.42 ± 0.01 g/cm^3 (213.35 ± 0.50 lb/ft^3), and an average porosity of 1.06 ± 0.01%. The transverse columnar Monofrax material showed an average apparent density of 3.41 ± 0.01 g/cm^3 (212.89 ± 0.50 lb/ft^3), an average bulk density of 3.42 ± 0.01 g/cm^3 (213.29 ± 0.33 lb/ft^3), and an average porosity of 1.09 ± 0.21%.

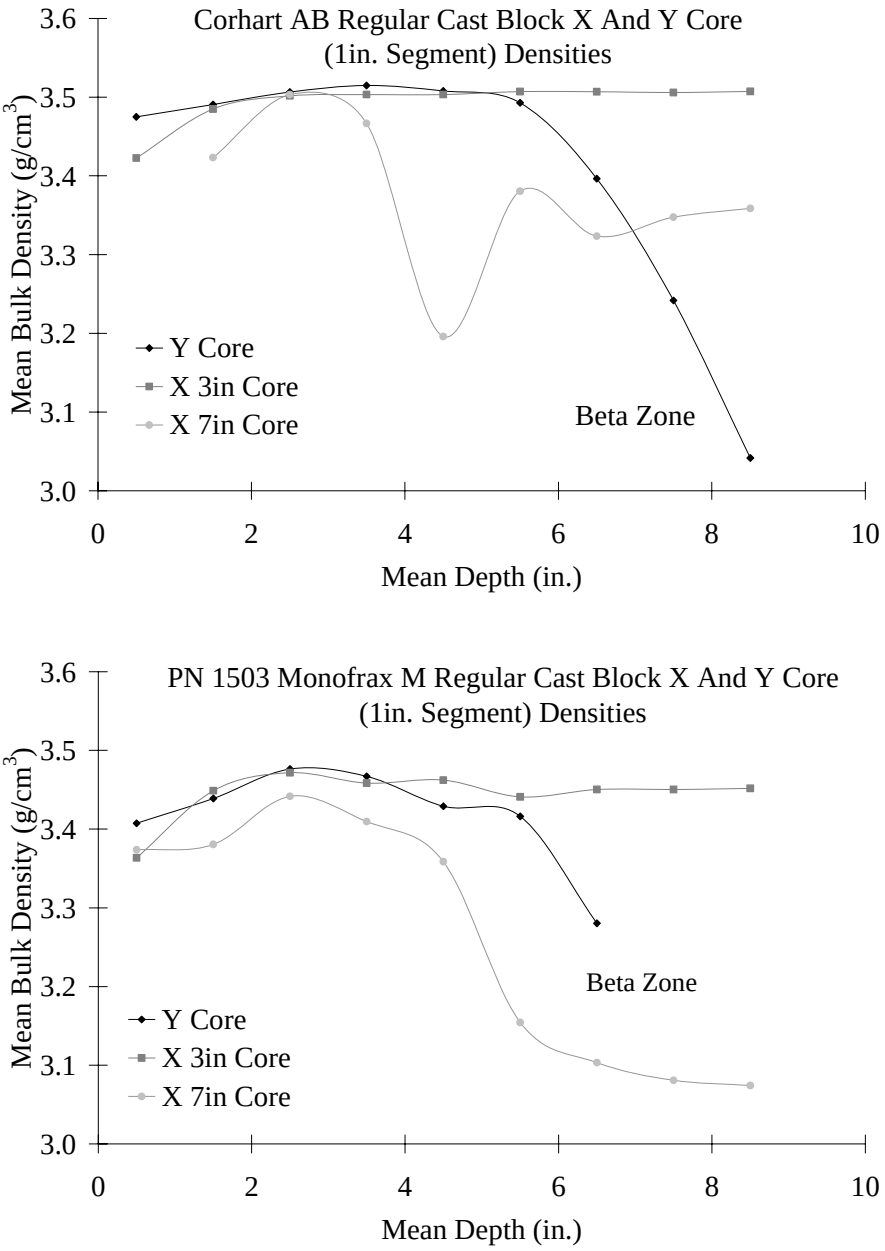

Fig. 24. *x*3-, *x*7-, and *y*-core density profiles for the (a) Corhart refractory and (b) Monofrax refractory.

The phase profiles of both refractories were measured by X-ray fluorescence (XRF) and XRD. For the *x*-direction profiles, the Corhart block showed large amounts of β-alumina (much greater than the mean pour stream chemistry of the melt) present in the outer 1 to 2 in. of the block and a lower (below the mean pour stream of the melt), more consistent, β-alumina content through the remainder of the block. In the case of the *y* core, there was an extremely large amount of β-alumina at the bottom block surface and a fairly consistent level of β-alumina in line with what was seen in the interior *x*-cores from ≈ 0.5 to 6.5 in. Beyond the 6.5-in. mark, the header of the block was encountered, and the β-alumina content increased to the original high level. The Monofrax block showed levels of β-alumina similar to the mean pour stream chemistry of the melt for all three cores up to ≈ 1.5 in. Beyond that point, the three cores all showed a lower β-alumina content, similar to what was seen in the Corhart block. This low level of β-alumina was sustained for the *x*3 core but showed an increase at ≈ 4.5 in. for the *x*7 core and at ≈ 6.5 in. for the *y* core. It is expected that the increase in β-alumina content was due to the cores entering the β-alumina-rich header region of the block, as seen in the Corhart block.

Patterns for bulk and columnar regions of Corhart M and Monofrax M could be matched to known peaks for corundum (α-alumina) (PDF# 10-0173) and sodium aluminum oxide (β-alumina) (PDF# 31-1263). Initially, optical microscopy was used to characterize the various components present in the microstructure of the fusion-cast alumina blocks. It was found that both the Corhart and Monofrax as-cast blocks displayed a similar variable microstructure. As shown in Fig. 25, the bulk region of the blocks was composed of blocky α-alumina grains embedded in a continuous matrix of β-alumina while the columnar exterior regions were composed of longer, more slender α-alumina grains embedded in the continuous
β-alumina matrix.

Grain size analysis was performed on characteristic regions (bulk and columnar) of the two regular-cast block brands. In-house LabView™ software that relates the pixels contained in the area of each grain to a calculated average grain diameter in microns was used. For the Corhart columnar regions, 133 grains were analyzed, yielding an average grain size of 82 μm (3.2 mils) ± 43 μm (1.7 mils). The Monofrax columnar region had a similar average grain size of 79 μm (3.1 mils) ± 46 μm (1.8 mils) based on the analysis of 164 grains. The bulk regions of the Corhart and Monofrax as-cast blocks exhibited a larger average grain size and showed more variation between the two brands. Analysis was carried out on 225 grains in various Corhart bulk regions, giving an average grain size of 172 μm

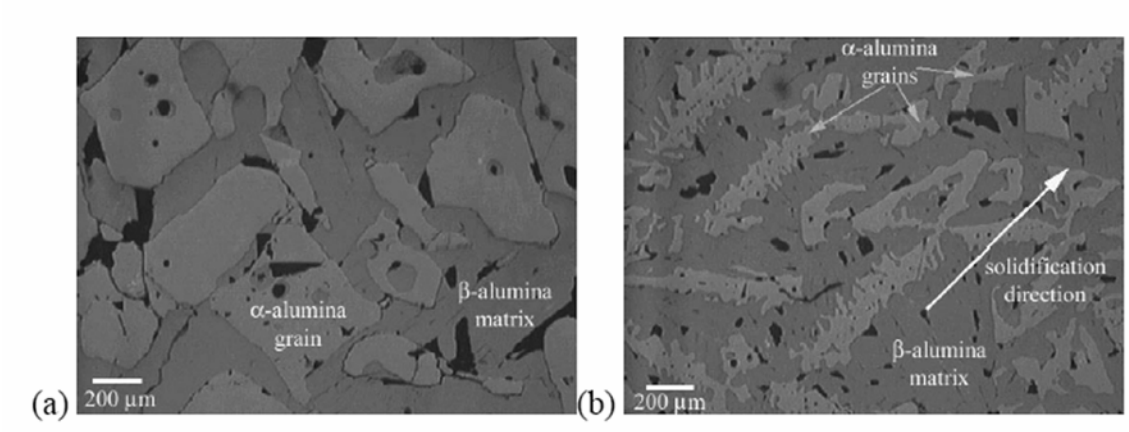

Fig. 25. Optical microscopy of characteristic grain structures for (a) bulk structure, and (b) columnar structure.

(6.8 mils) ± 20 μm (0.8 mils). For the Monofrax bulk regions, 179 grains were evaluated, yielding an average grain size of 231μm (9.1 mils) ± 47μm (1.9 mils).

It was originally hypothesized that the *c*-axes of the hexagonal α-alumina crystals in the columnar microstructural zone would all be aligned along the direction of rapid cooling, as indicated by the long dimension of the columnar crystals. This is in fact not the case, (i.e., Fig. 26). Through analysis of optical micrographs it was found that incomplete α-alumina grains in the microstructure actually have their *c*-axis aligned perpendicular to the cooling direction. The skeletal columnar grains were found to be polycrystalline (not single crystals) and to have their *c*-axes randomly oriented as additionally seen in the random habit of the α-alumina phase. The shape of these grains was found to therefore be due more to the cooling behavior than the crystallographic direction.

Other optical images were taken showing the nephelitic (calcium-aluminosilicate) grain boundary phase present between the α- and β-alumina phases and in isolated areas of the β-alumina phase. These areas appear as grayish, angular features between grains and isolated in the β-alumina phase, as shown in Fig. 27.

Elastic modulus measurements were generated by cyclic compression. Supplemental values were generated for comparison by using a nanoindentation technique. At room temperature, an average value of 72 ± 4 GPa (10.4 ± 0.6 × 106 psi) was found for the Monofrax bulk material, while the Corhart bulk material showed an average value of 109 ± 7 GPa (15.8 ± 0.9 × 106 psi). The longitudinal columnar Monofrax samples gave an average value of 112 ± 12 GPa (16.2 ± 1.7 × 106 psi), while the transverse columnar yielded a value of 113 GPa (16.4 × 106 psi) based solely on specimen AG18. High-temperature testing was carried out on a sample from each of the above categories. Results from the high-temperature testing are shown in Fig. 28. As expected, in general the modulus decreased with increasing temperature. Unexpectedly, the modulus of the Monofrax bulk at 900°C (1652°F) was higher than that measured at room temperature. This may suggest that the room-temperature modulus of the Monofrax bulk material should be higher (on the order of 140 GPa, 20.3 × 106 psi).

Nanoindentation measurements were made in each of the three phases (α-alumina, β-alumina, and nephelitic grain boundary phase) for both the Corhart and Monofrax bulk materials at room temperature. Three analyses were run in α-alumina grains (one Corhart and two Monofrax) and three in β-alumina grains (one Corhart and two Monofrax). Six analyses were run in nephelitic grain boundary regions (four Corhart and two Monofrax). All results are shown in Table 11. The modulus values obtained through nanoindentation of the alumina phases (214 – 442 GPa, 31.0 × 106 – 64.1 × 106 psi) were higher than those previously found for the bulk material by static and measurements (62 – 117 GPa, 4.6 × 106 – 17.0 × 106 psi). This may partly be due to the fact that in the nanoindentation measurements α - and β-alumina grains are individually sampled where in the other measurements, a composite of the bulk material was sampled. Also, it is documented that values found through nanoindentation are higher than those found through other methods simply due to the technique itself [22]. Regardless, the values are fairly consistent between the different brands of material for each sample type and provide a means of comparison between the different components of the bulk structure. The α-alumina grains were found to have a much higher modulus than the β-alumina grains. The Corhart grain boundary samples also possessed a high modulus on the order of those values measured for the β-alumina grains (≈ 260 GPa, 37.7 × 106 psi), but the Monofrax boundary specimens had a modulus value more in line with the values measured previously for bulk materials with the static techniques (≈ 95 GPa, 13.8 × 106 psi).

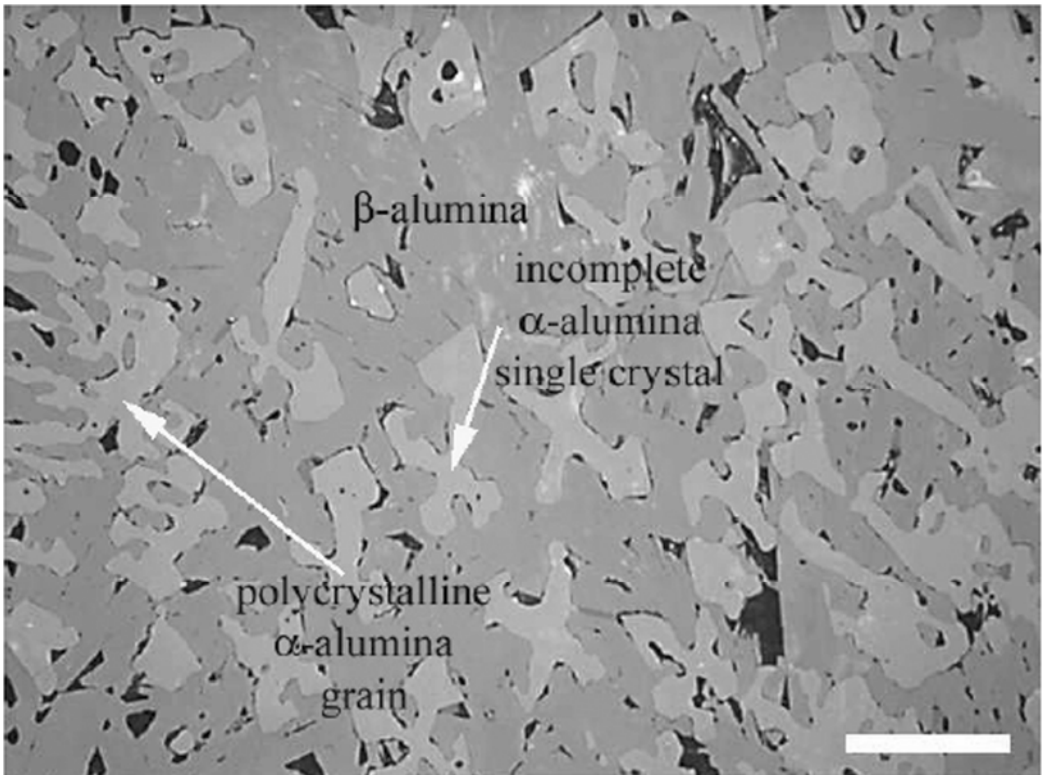

Fig. 26. Optical microscopy of columnar region (micron bar = 200 μm).

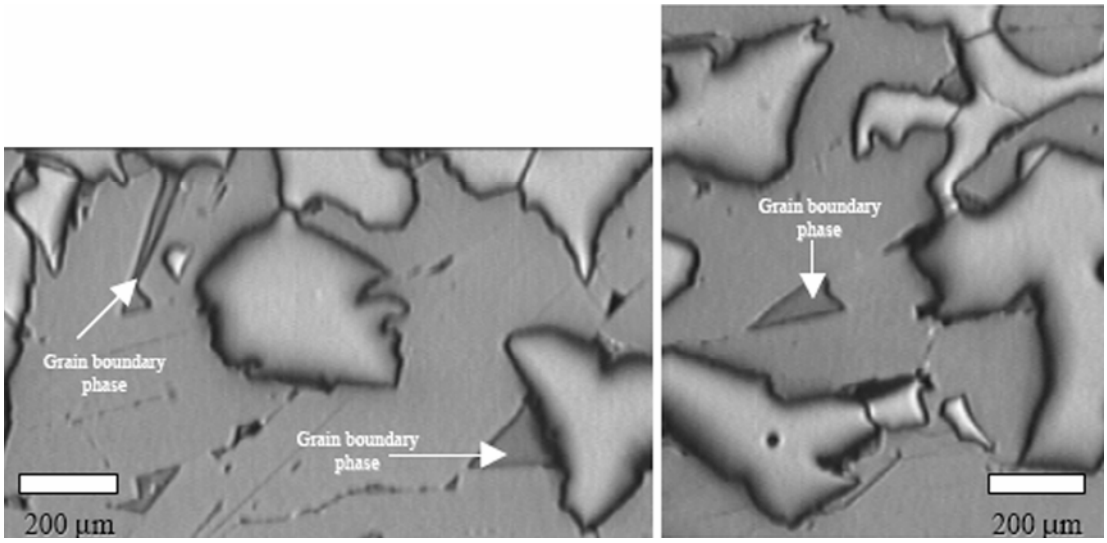

Fig. 27. Optical microscopy of nephelitic grain boundary phases.

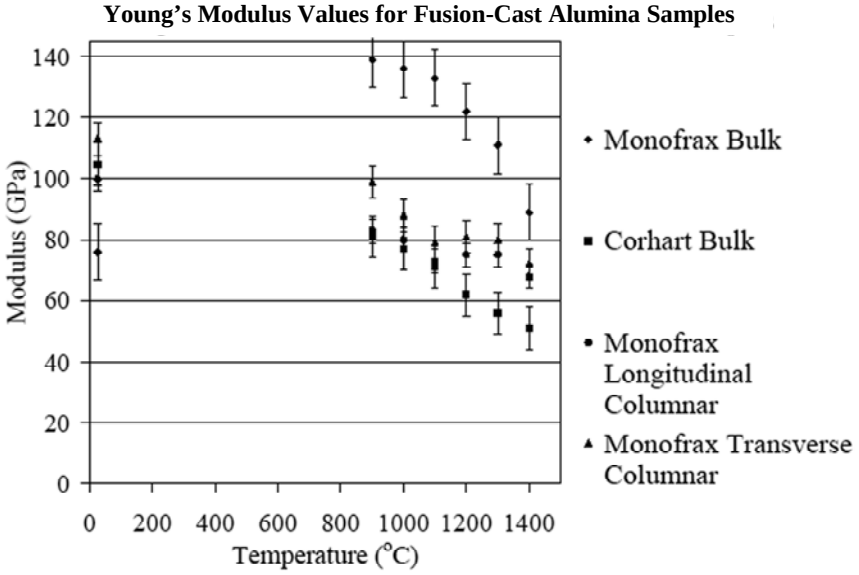

Fig. 28. Static Young's modulus values for fusion-cast alumina sample types.

Table 11. Fusion-cast alumina nanoindentation results

Grain	Young's modulus (GPa)
Corhart α-alumina	407 ± 15
Monofrax α-alumina	442 ± 13
Monofrax α-alumina	424 ± 14
Corhart β-alumina	237 ± 5
Monofrax β-alumina	214 ± 6
Monofrax β-alumina	231 ± 5
Corhart grain boundary	296 ± 13
Corhart grain boundary	269 ± 11
Corhart grain boundary	249 ± 11
Corhart grain boundary	240 ± 10
Monofrax grain boundary	97 ± 5
Monofrax grain boundary	92 ± 6

Initial thermal expansion measurements were made from room temperature up to 900°C on high-purity (99.4%) alumina (theoretical coefficient of thermal expansion and temperature range = 8.2×10^{-6}/°C) using the dual rod dilatometry technique to verify its calibration. Three measurements were made, yielding an average value of 8.7×10^{-6}/°C. This was deemed sufficiently close to the theoretical value for experimental testing to continue.

Testing on Corhart and Monofrax M bulk material was initially carried out on specimens at 1450°C (2642°F) under the following schedule. Cylindrical samples were heated to temperature in a 4-h period and then held at temperature for 100 h. Following the soak period, the samples were cooled to room temperature through natural cooling. Three tests were run on each commercial brand with the Corhart material, yielding an average value of 7.8×10^{-6}/°C, and on the Monofrax bulk, yielding an average value of 8.4×10^{-6}/°C. The values published by the manufacturers for Corhart M and Monofrax M are 11.1 x 10^{-6}/°C and 7.9×10^{-6}/°C respectively. Theoretically, α-alumina is anisotropic due to its hexagonal crystal structure and possesses thermal expansion values of 8.3×10^{-6}/°C perpendicular to its c-axis and 9.0×10^{-6}/°C parallel to its *c*-axis. β-alumina has an isotropic thermal expansion value of 6.4×10^{-6}/C.

Monitoring of the overall linear sample dimensions during the thermal expansion testing resulted in evidence of unrecoverable expansion of the specimens during exposure to temperature. Exposure for 100 h at 1450°C (2642°F) resulted in a 0.194% change in length for Corhart M specimens and a 0.131% change in length for Monofrax M specimens. Supplemental testing was performed at 1550°C (2822°F) and 1650°C (3002°F) to evaluate the unrecoverable expansion at those temperatures. Again, cylindrical specimens were heated to temperature in a 4-h-period and then held at temperature for over 100 h before being allowed to return to room temperature through natural cooling. Testing revealed that exposure for 100 h at 1550°C (2822°F) resulted in a 0.2151% change in length for Corhart M specimens and a 0.357% change in length for Monofrax M specimens. Exposure for 100 h at 1650°C (3002°F) resulted in a 0.268% change in length for Corhart M specimens and a 0.396% change in length for the Monofrax M specimens. The results for the bulk Corhart and bulk Monofrax refractories are summarized in Figs. 29(a) and 29(b), respectively.

The transient technique was used to make thermal conductivity measurements on both cylindrical creep specimens and on sectioned pieces of the original as-cast blocks. Two bulk creep cylinders and one sectioned piece with both cut surfaces and original surfaces were sampled for each brand. Results from original surfaces are thought to give measurements representative of the columnar structure with a parallel orientation to the direction of measurement (longitudinal columnar). Results from the center of the cut surfaces are representative of the bulk structure, and measurements on the edges of the cut surfaces yield values indicative of the columnar structure with a perpendicular orientation to the direction of measurement (transverse columnar). For the creep cylinders, measurements were taken on each sample by the single-sided method and between both samples by the standard method.

Sets of three single-sided measurements on the two bulk creep cylinders (B1 and B2) yielded average thermal conductivity values of 5.91 ± 0.10 and 5.97 ± 0.04 W/mK, respectively. The three standard measurements taken between the two cylinders gave an average value of 6.00 ± 0.11 W/mK. These values agree well with the sectioned block measurements of 6.04 to 6.21 W/mK. Measurements on the longitudinal and transverse columnar microstructures yielded average values of 7.10 and 5.82 W/mK, respectively. The differences in thermal conductivity values between the two columnar microstructures and the bulk structure are thought to be due to the varying contributions and orientations of the α- and β-alumina grains in the three different cases.

The piece sectioned from the Corhart block was analyzed along two vertical lines on the cut surface. One was taken along the edge of the surface and the other 3 in. in from the edge. Measurements taken along the edge of the cut surface (line along surface) correspond to the columnar microstructure with a perpendicular orientation to the direction of measurement (transverse columnar). Measurements taken along the 3-in. line are representative of the bulk microstructure except for material in about the first inch. Measurements along that region contain transverse columnar structure due to interaction with surface OS1 (Fig. 30), and the measurements made above 7.0 in. are in the header microstructure. The results indicate that the transverse columnar microstructure had an average thermal conductivity ranging anywhere from 5.04 to 7.46 W/mK. The lower values occurred at the top of the block, in the vicinity of the header region and were due to the increased porosity in this region and therefore are not considered representative of the actual thermal conductivity of the transverse columnar structure. Thus the average thermal conductivity values are in the range of 6.50 to 7.50 W/mK. If it is hypothesized that the α-alumina columnar structure controls the conductivity in these regions to varying degrees, then these higher values would make sense because the α-alumina grains will possess a higher thermal conductivity than the β-alumina matrix, thus raising the overall thermal conductivity of the material. The same phenomenon is seen in the sectioned Monofrax block for the longitudinal columnar microstructure. For cut block surfaces, this is considered to be the case because the harder α-alumina grains protrude slightly from the block surface (as seen by the intensity differences in optical microscopy). The slight protrusion would then cause the α-alumina grains to

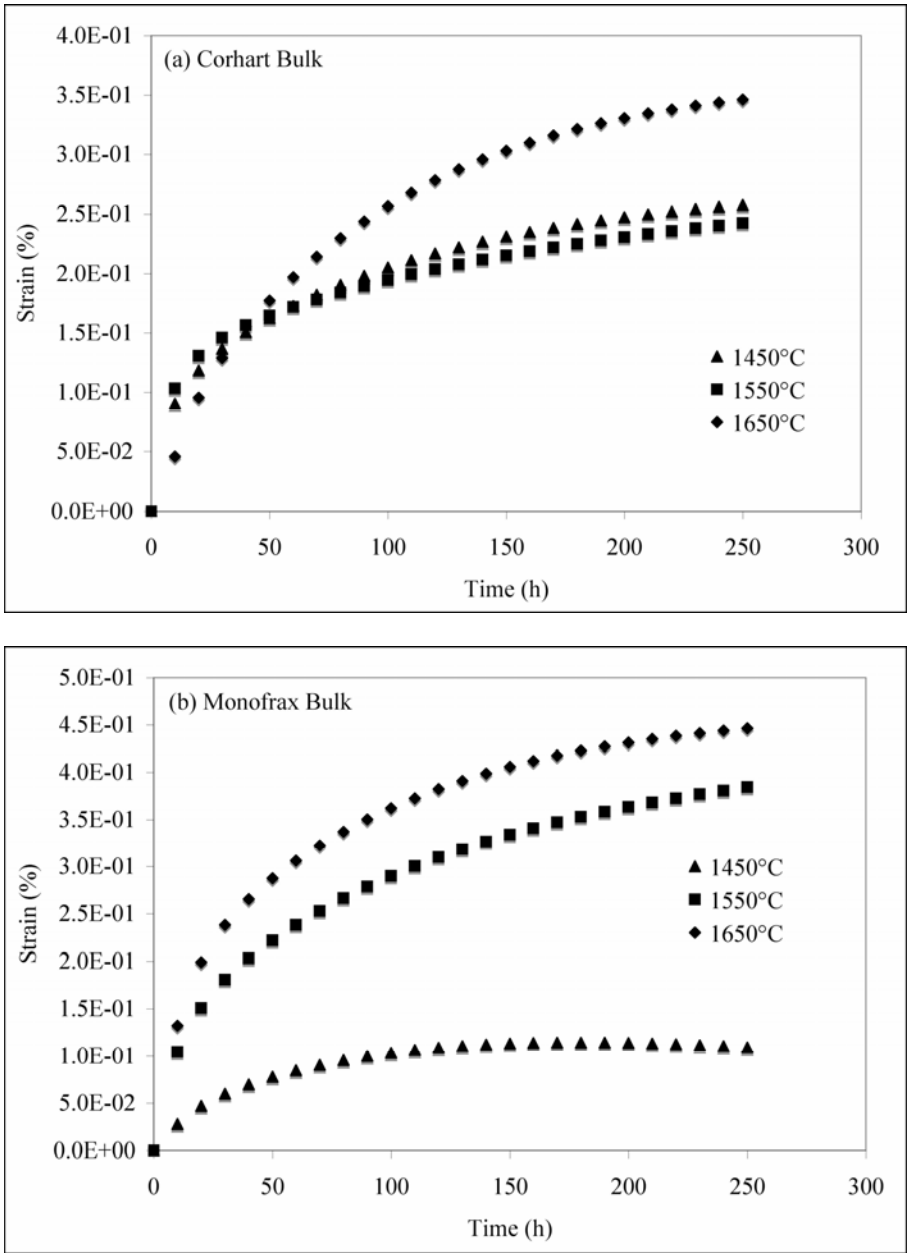

Fig. 29. Specimen elongation as a function of time for (a) the bulk Corhart and (b) the bulk Monofrax refractories. The curves represent mathematical fits to the experimental data as described in J. G. Hemrick, "Creep Behavior and Physical Characterization of Fusion-Cast Alumina Refractories," Ph.D. dissertation, University of Missouri-Rolla, 2001.

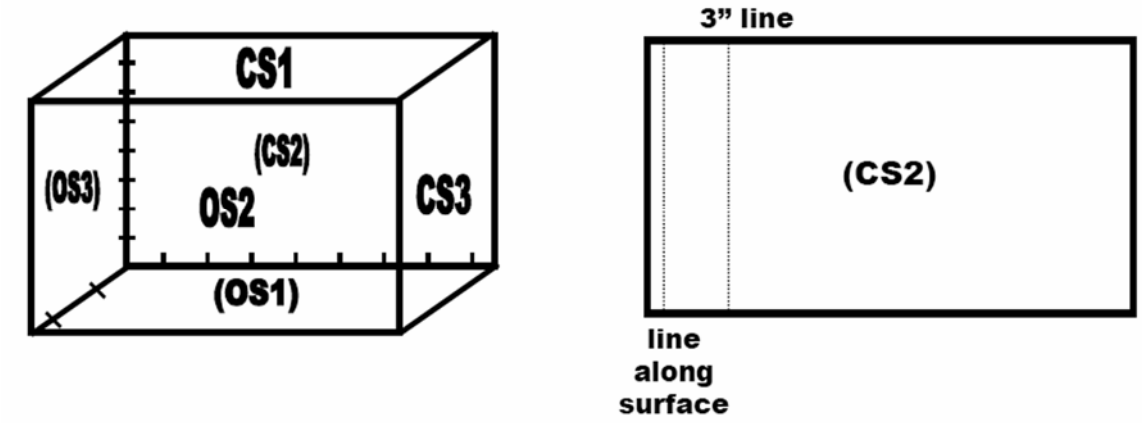

Fig. 30. Monofrax thermal conductivity block section denoting test surfaces. Parentheses denote hidden surface. Dotted lines designate positions of line scans (os = original surface; cs = cut surface).

dominate the thermal conductivity measurements made on these surfaces and would cause the "composite reading" to be higher than expected.

In the case of the 3-in. line, the bulk microstructure of the Corhart material had an average thermal conductivity on the order of 6.25 to 7.10 W/mK with a mean value of 6.78 W/mK. The higher values in the bulk region may be due to direct measurements of the α-alumina grains as opposed to measurements for areas containing both α- and β-alumina grains. Therefore, it is thought that the actual bulk thermal conductivity of the bulk Corhart material is on the order of 6.61 W/mK because the continuous β-alumina phase should dominate the conductivity behavior. Due to the high void content, the thermal conductivity in the header region fell from approximately 5.00 W/mK down to approximately 0.25 W/mK.

The laser flash method yielded thermal diffusivity/conductivity values from room temperature up to 1400°C for both the Corhart and Monofrax bulk as-cast materials. Two measurements were taken at each temperature value on separate samples with 15 temperatures being measured. Specific heat measurements were also made from room temperature up to 1400°C using a calorimeter method. Plots of the change in thermal conductivity with temperature are shown for the Corhart and Monofrax materials in Fig. 31. The thermal conductivity of the Corhart material at room temperature was higher than that measured by the transient method (9.0 W/mK as opposed to 6.6 W/mK). This value then decreased to just above 4.0 W/mK at 600°C (1112°F) and then slowly increased to about 7.0 W/mK at 1400°C (2552°F). The thermal conductivity of the Monofrax material was much more consistent. The room-temperature value, measured to be on the order of 6.0 W/mK was similar to that determined from the transient method. The value for the Monofrax sample dropped slightly to around 4.0 W/mK, as it did for the Corhart material, but at a lower temperature, only 100°C (212°F). The thermal conductivity was relatively constant until 900°C (1652°F), at which point the value began to increase to around 6.0 W/mK at 1400°C (2552°F).

The compressive creep curves for the Corhart bulk specimens at 1450°C exhibited a period of rapid strain accumulation followed by a leveling off of the accumulated strain. The total accumulated strain and the associated length of time over which the rapid strain accumulation occurs was expected to be related to the applied stress state. This was not always found to be the case. For example, the creep response at 0.8 MPa was significantly lower than the response at 0.6 MPa. In the case of the curves obtained at 1550°C, the strain accumulation also exhibited a leveling off with time. However, for a given time, the amount accumulated strain increased with increasing stress, predicted by the creep equation. The creep curves generated at 1650°C were different from those obtained at the lower

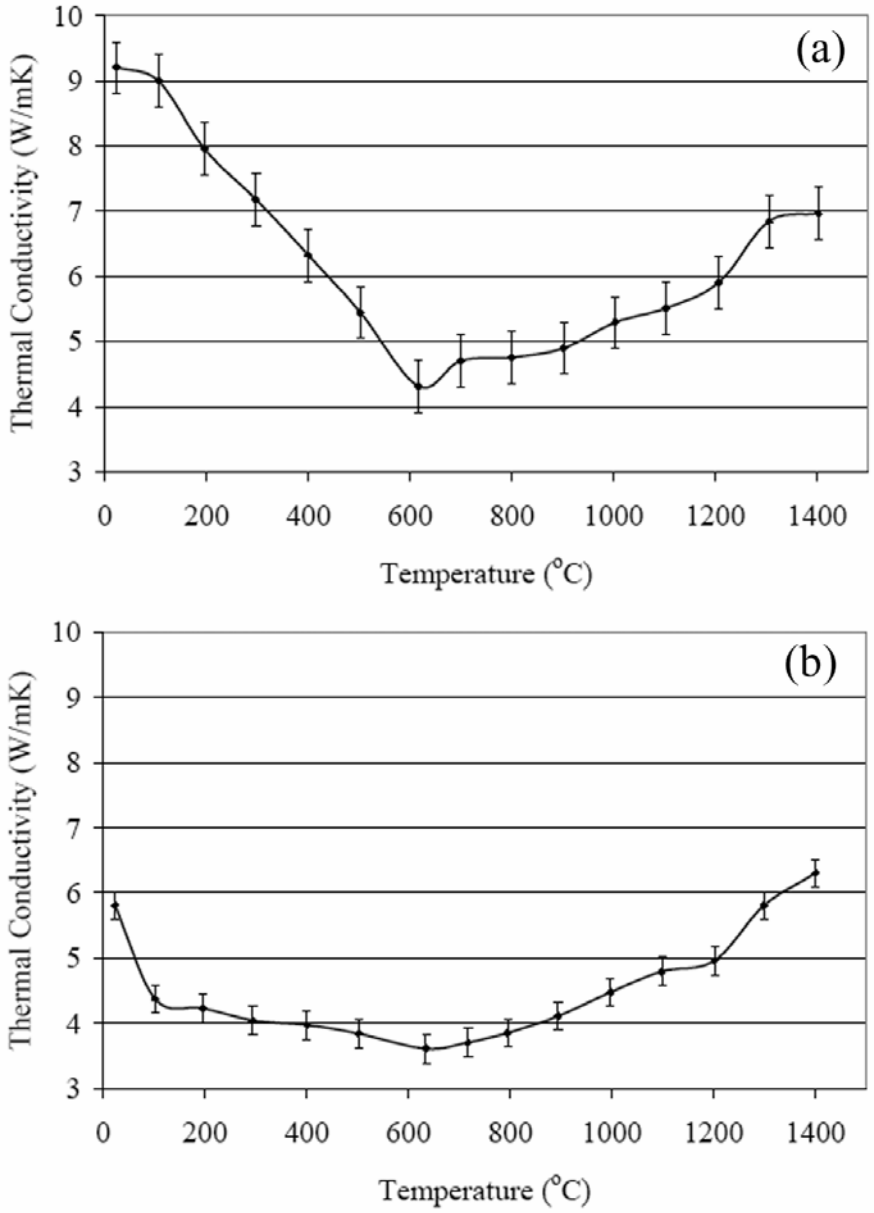

Fig. 31. Average laser flash thermal conductivity for as-cast bulk refractories: (a) Corhart and (b) Monofrax.

temperatures. Both the 0.6-MPa and 0.8-MPa curves exhibited similar behavior, initially showing large amounts of accumulated strain followed by a leveling off at 100 and 150 h, respectively. In both cases a larger amount of total accumulated strain was seen under these stresses than at either 1450°C or 1550°C. The 1.0-MPa curve showed an increase in accumulated strain followed by a region of constant negative slope. This was the first test in which traditional creep behavior was exhibited. Similar trends were observed for the bulk Monofrax specimens.

In the case of the Monofrax refractory, creep curves were obtained for longitudinal and transverse columnar samples at both the low (1450°C, 6 MPa) and high (1650°C, 1.0 MPa) extreme matrix conditions, with an additional transverse columnar sample being tested at 1450°C and 1.096 MPa. For

the curves at 1450°C, both the transverse and longitudinal columnar samples showed similar behavior at 0.6 MPa with a small amount of accumulated strain being followed by a leveling off of accumulation after ≈ 150 h. The total amount of accumulated strain was about half as much as that for both the Corhart and Monofrax bulk samples under similar conditions. The plot of the transverse columnar specimen at 1.0 MPa showed an increase in accumulated strain over that seen at 0.6 MPa and a sharp leveling off of the strain accumulation at an earlier point (≈ 50 h). The total accumulated strain in this sample (≈ 0.05%) was much lower than that seen in both Corhart and Monofrax bulk samples under similar conditions (0.09 and 0.13%, respectively). At 1650°C both 1.0-MPa curves showed similar behavior to that seen in the Corhart and Monofrax samples under similar conditions, although the rate of accumulated strain was lower in the columnar cases, resulting in lower total accumulated strains. This behavior included an increase in accumulated strain followed by a region of accumulated strain characterized by a constant slope and traditional creep behavior.

Based on the above observations, it is clear that nontraditional creep behavior was exhibited by fusion-cast alumina under most test conditions (those below 1650°C/1.0 MPa). This behavior was thought to be due to the unrecoverable expansion phenomenon shown in Fig. 29. Based on those premises, plots were constructed incorporating both the expansion effects and creep effects seen by each material under the various test conditions and the composite effect resulting from the combination of these two concurrent mechanisms. Such plots are shown below for both Corhart (Fig. 32) and Monofrax (Fig. 33) bulk specimens. These plots were constructed by subtracting a similar exponential fit of the measured expansion curve as determined by dilatometry at each test temperature from the modeled creep curves at each stress of the representative same temperature.

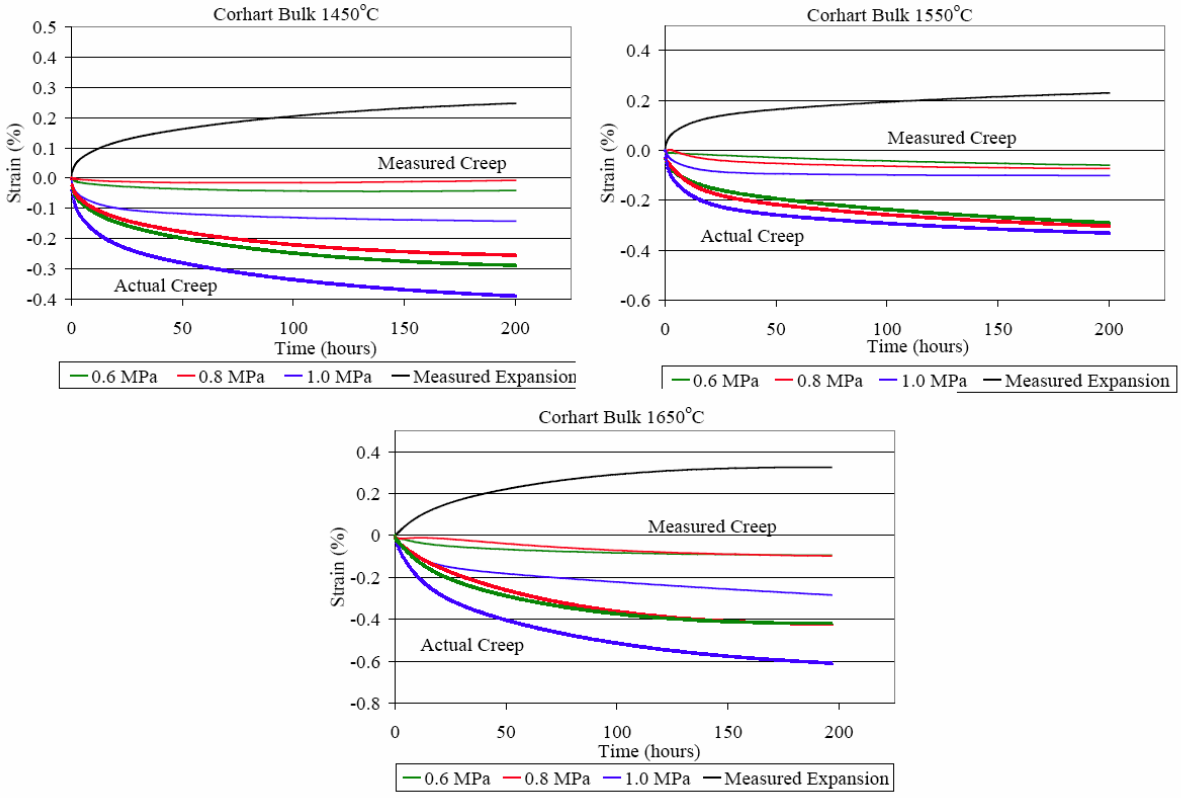

Fig. 32. Combined plots of expansion and creep effects in Corhart bulk samples.

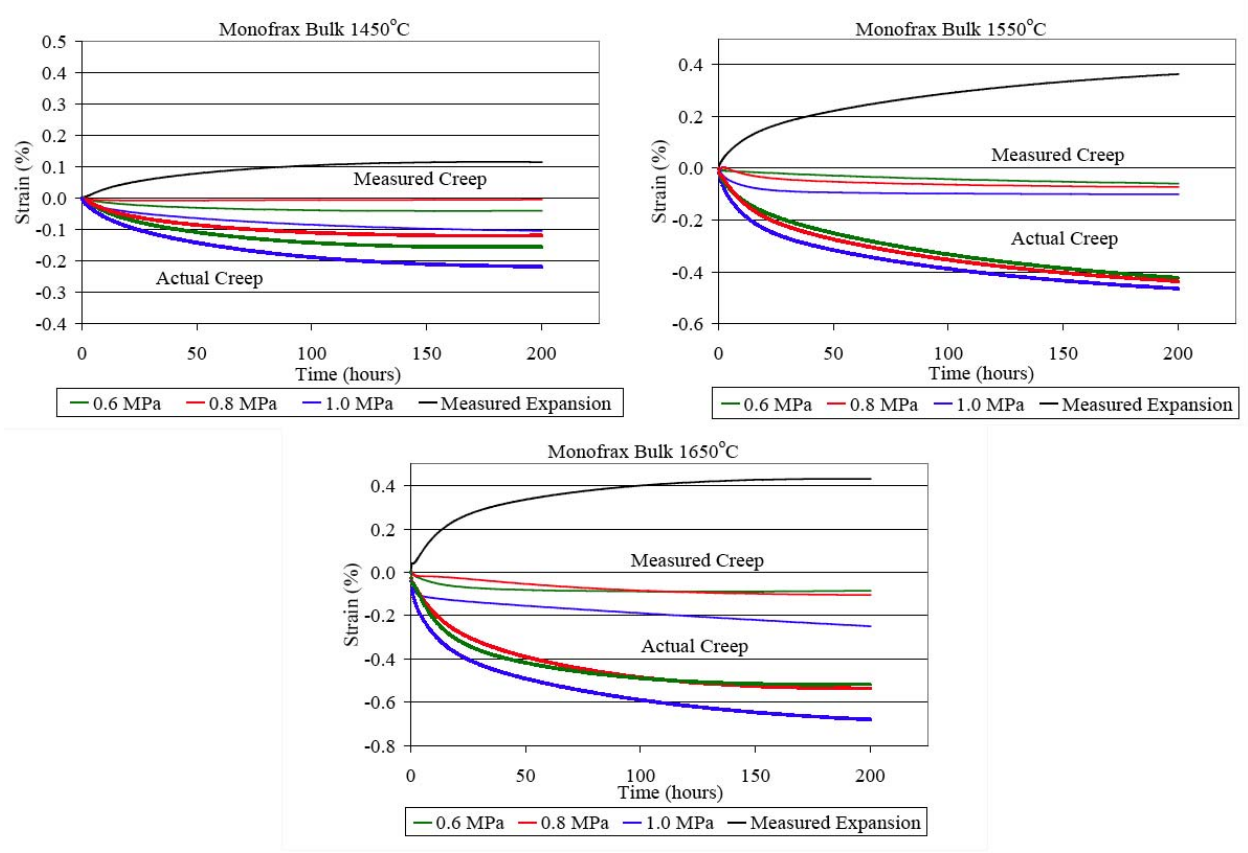

Fig. 33. Combined plots of expansion and creep effects in Monofrax bulk samples.

The new curves predict a greater creep resistance in the Monofrax bulk material at 1450°C (better by ≈ 0.20%), but a greater creep resistance in the Corhart bulk material at 1550°C (better by ≈ 0.15%) and at 1650°C (better by ≈ 0.10%). However, this may not be an accurate portrayal of the creep behavior exhibited by these materials. It must be remembered that the behavior exhibited by these materials in service would still be represented by the measured creep curves. Therefore, by performing the analysis in this fashion, it may be possible to produce creep curves that possess a steady-state, non-zero creep regime from which a model can be conceived by using a traditional method such as the NBA equation. Doing so will not capture the actual behavior exhibited by this material, however, because any model must incorporate the effect of the expansion along with the creep. A model is needed that can handle the high degree of nonlinearity seen in the measured creep curves generated for fusion-cast alumina while also being sensitive to the transient nature of the data because no equilibrium state is in effect.

Several samples were analyzed after being crept, and results were compared with those previously obtained from virgin samples. Analysis included thermal conductivity, optical microscopy, and SEM/EDS chemical analysis. The thermal conductivity values for the Monofrax post-creep cores were similar to those obtained earlier from the virgin cores, which had thermal conductivities in the range of 5.9 W/mK. The value obtained from the Corhart post-creep core was significantly lower than the average value of 6.61 W/mK found earlier for the Corhart bulk material.

Initial optical microscopy and SEM/EDS analyses were performed on Corhart and Monofrax bulk samples exposed to 1550°C and 1.0 MPa. This work was conducted to determine whether any

changes in the microstructure or chemistry could be detected at that intermediate condition. SEM/EDS analysis was then used to determine whether analysis needed to be performed on samples at the lower temperatures and stresses. No discernible deformation and only slight chemical changes were seen in the samples.

Subsequent optical microscopy and SEM/EDS analyses were performed on Corhart and Monofrax bulk samples exposed to the extreme conditions of 1650°C and 1.0 MPa. The structure of the Corhart sample was found to resemble the virgin structure, while the Monofrax crept structure displayed a smaller
α-alumina grain size and a tighter α-alumina grain structure with more equiaxed angular grains than previously observed in the virgin structure. More severe chemical changes were also seen between the virgin and crept samples.

5.4 Fusion-Cast Spinel Refractories

Engineering creep data for selected refractory materials was generated to a temperature of 1650°C in ambient air. Tests for the fusion cast material at 1650°C and 3.0 MPa. One test was run on bulk material and one was run on columnar (with the structure running parallel to the loading direction). There is some initial movement due to the application of the load [the samples were heated to temperature under low load (30–50 lb) and were allowed to dwell for 24 h before the main load (768.909lb) was applied], then very little creep over the time of testing. The test frame was refitted with a larger air cylinder and load cell to enable testing at higher loads in an attempt to get this material to creep. Also examined was the effect of using smaller samples to obtain higher loads.

The behavior exhibited by the transverse columnar structure was not as expected (Fig. 34). It was expected to be similar to the behavior of the longitudinal columnar sample with perhaps even less accumulated strain. Instead, the behavior is more similar to that of the bulk structure with about the same amount of total accumulated strain but a slower initial rate of strain accumulation. Curves from two separate samples both show the same initial strain accumulation, showing that the results are repeatable. Rather than analyzing the final 100 h of the test, all the data available past 100 h of testing were analyzed (Table 12). This analysis provided a better representation of the apparent “steady-state” creep rates exhibited by these materials. There was a plot of this analysis included as well. The conclusion was that the fusion-cast material does not creep (even at 8.5 MPa). There was more initial strain due to application of the load (~ 3% more, which corresponds with the increase from 3 to 8.5 MPa), but there was not a change in steady-state creep rate with the increased load. The creep rate for the longitudinal columnar structure was lower, but the transverse columnar structure showed a creep rate similar to that of the bulk structure. The bonded material showed significant creep and was far inferior to the fusion-cast material, as shown in Figs. 35, 36, and 37.

Thermal diffusivity measurements were made by the laser flash method. Density and thermal diffusivity are required as input into the calculation of thermal conductivity. The density of the fused cast spinel was measured as 3.47 g/cc with a porosity of 2.3%. The density of the columnar structure and bulk structure were 3.47 g/cc and 3.5 g/cc with porosities of 2.1% and 2.5%, respectively. The density of the bonded spinel was measured as 3.04 g/cc with a porosity of 14.2%. The calculated thermal conductivity results are shown in Fig. 38.

Table 12. Calculated strain rates

Material	Temperature (°C)	Stress (MPa)	Strain rate
Fused spinel longitudinal Columnar	1650	3.0	1.27×10^{-6}/h
Fused spinel transverse columnar	1650	3.0	4.27×10^{-6}/h
Fused spinel bulk	1650	3.0	5.66×10^{-6}/h
Fused spinel bulk	1650	8.5	5.00×10^{-6}/h
Bonded spinel bulk	1650	0.07	48.0×10^{-6}/h
Bonded spinel bulk	1550	0.06	8.89×10^{-6}/h
Bonded spinel bulk	1550	0.3	23.8×10^{-6}/h

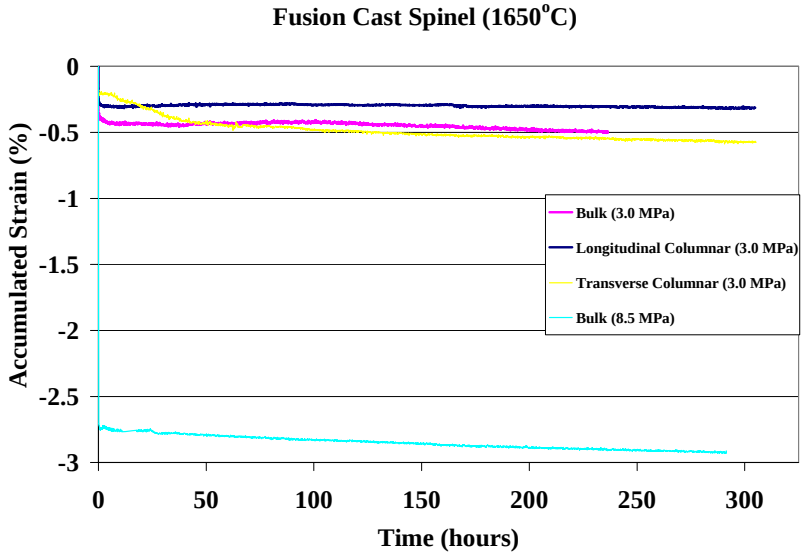

Fig. 34. Fused spinel accumulated strain curves.

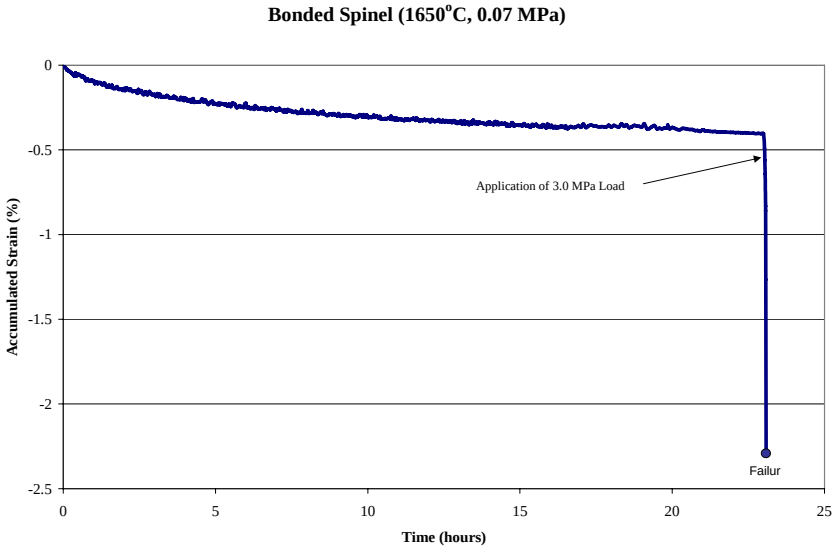

Fig. 35. Bonded spinel accumulated strain curve at 1650°C.

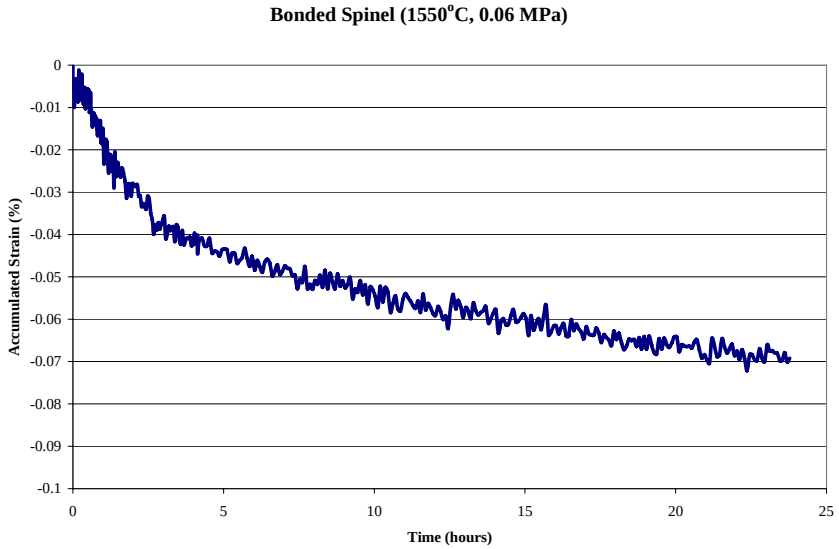

Fig. 36. Bonded spinel accumulated strain curve at 1550°C.

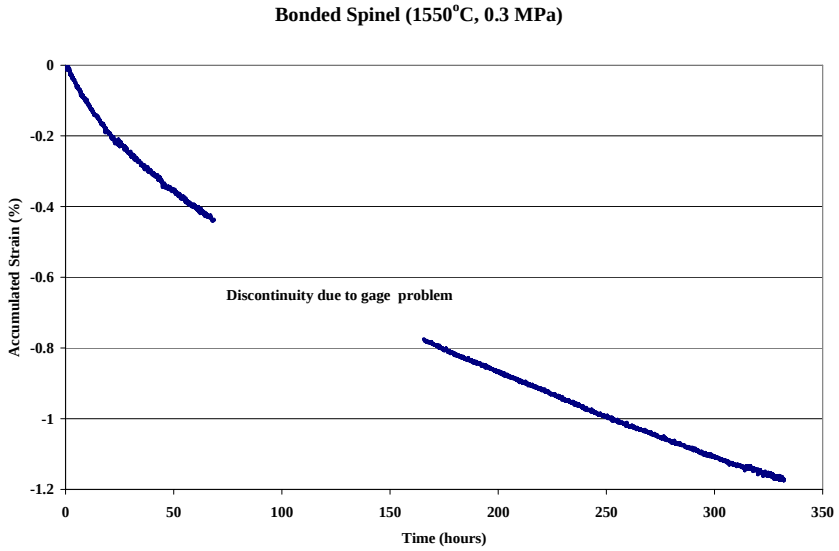

Fig. 37. Bonded spinel accumulated strain curve at 1550°C.

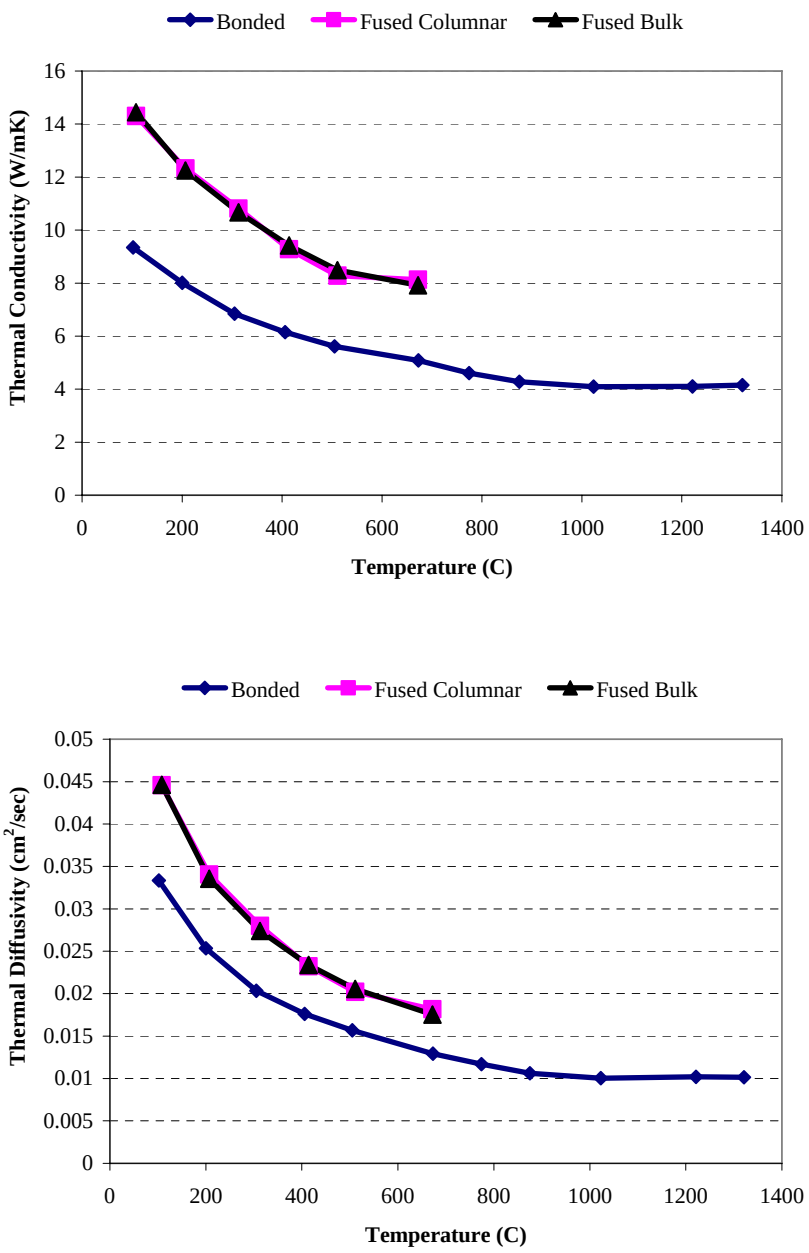

Fig. 38. Thermal diffusivity of fused and bonded spinel.

The creep specimens were subjected to detailed microstructural and phase analysis. One objective of this task was to better understand how creep and corrosion behavior relates to microstructure and microchemistry. X-ray diffraction data showed little differences in the patterns between the “as supplied” and “exposed” samples. The spinel peaks were slightly shifted due to heat treatment and stress relief. There were no additional phases found after exposure.

The sintered spinel brick was made from high-purity large fused spinel grains. The matrix contained 16% to 18% porosity but was well sintered. No impurity phase (forsterite, monticellite, merwinite or melilite) was identified/recognized at the magnification scale of RL/CL microscope used. This does

not, however, exclude the presence of small amounts of glassy or ternary phases, which would coat the smaller spinel grains in the matrix. In general, the fused spinel block consisted of spinel and magnesia. The presence of free magnesia or magnesia inclusions suggests that the liquid was rich in MgO. The composition of spinel was also expected to be rich in MgO. Due to the rapid cooling or crystallization columns of spinel skeletons were formed and the magnesia was segregated as tiny inclusions within these skeletal spinel columns. Such rapid crystallization appeared as linear or locally oriented features in the fused block. The orientation of these skeletal spinel columns was, in general, also random. In a single section both transversal or longitudinal microstructures were observed. For example, Fig. 39 shows a diagonal (NW to SE) crystallization feature. Although spinel (green CL) crystals still exhibit random orientation, overall there is a diagonal (in these micrographs) feature developed during crystallization of spinel liquid. These micrographs illustrate the microstructure of rapidly crystallized spinel columns sectioned perpendicularly along the axis of the column.

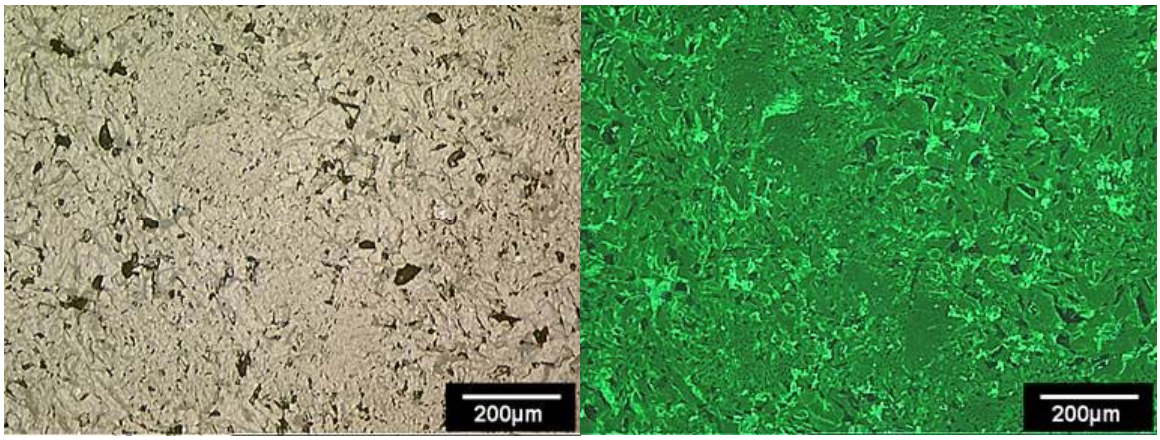

Fig. 39. RL (left) and CL (right) images of fused spinel.

6. Accomplishments

6.1 Research-Based Accomplishments

This study led to significant improvements in the resolution of the techniques commonly used to measure thermal expansion and creep of refractories. For example, the "Standard Test Method for Load Testing Refractory Brick at High Temperatures" involves loading a refractory brick for a prescribed duration and temperature and then determining the material's resistance to deformation by comparing its before- and after-test axial dimensions. A shortcoming of this test is the introduction of error in the analysis if the refractory brick's ends "bed-down." The procedures and equipment recommended in the "Standard Test Method of Measuring the Thermal Expansion and Creep of Refractories Under Load" are similar to those used in the present study. A shortcoming of this procedure involves the recommended measurement of dimensional change in the creep specimen. The use of LVDTs to measure the contraction of the specimen ends is advocated but can be problematic for reasons described previously. The extensometry system described in Fig. 2 of ASTM C832 closely matches the extensometry system used in the present study; however, in the present study a capacitance gage is used while in the standard the use of an LVDT for the measurement is shown. The load that activates an LVDT can be enough to affect the intimacy of the extensometer contact with the specimen and thus can yield a misleading creep measurement if there is insufficient horizontal load applied to the specimen. Because of its differing operating principle, the capacitance gage on the extensometry systems used in the present study requires no load for activation and does not introduce uncertainties associated with the horizontal load and the use of an LVDT.

This study also identified new mechanisms responsible for deformation of fusion-cast alumina and silica refractories in the absence of an applied stress. For both refractories these mechanisms led to expansion of the test specimens in the absence of an applied stress.

6.2 Technology Transfer

The results of this project have established hardware and a test methodology that can be used by the refractories community to evaluate the creep and aging behaviors of most refractory materials. Of particular merit is the development of specialized extensometry, which offers extremely high resolution required for the measurement of small deformations. The project staff made presentations at national meetings and published results in industry technical journals.

6.3 Publications and Patents

[1] A. A. Wereszczak, T. P. Kirkland, G. A. Pecoraro, and R. A. New, "Compressive Creep Behavior of Fusion-Cast Alumina Refractories," pp. 401–406 in *Ceramic Transactions, Vol. 82, Advances in Fusion and Processing of Glass II*, ed. A. G. Clare and L. E. Jones, American Ceramic Society, Westerville, Ohio (1998).

[2] A. A. Wereszczak, T. P. Kirkland, and W. F. Curtis, "Compressive Creep Resistance of MgO Refractories at Temperatures ≥ 1400°C (2550°F),"pp. 407–412 in *Ceramic Transactions, Vol. 82, Advances in Fusion and Processing of Glass II*, ed. A. G. Clare and L. E. Jones, American Ceramic Society, Westerville, Ohio (1998).

[3] A. A. Wereszczak, T. P. Kirkland, and W. F. Curtis, "Creep of CaO/SiO_2 - Fluxed MgO Refractories," *J. Mater. Sci* (1998) in press.

[4] A. A. Wereszczak, M. Karakus, K. C. Liu, B. A. Pint, T. P. Kirkland, and R. E. Moore, *Compressive Creep Performance and High Temperature Dimensional Stability of Conventional Silica Refractories*, ORNL/TM-13757, Oak Ridge National Laboratory (1999).

[5] J. G. Hemrick, A. A. Wereszczak, M. Karakus, K. C. Liu, H. Wang, B. A. Pint, T. P. Kirkland, and R. E. Moore, *Compressive Creep and Thermophysical Performance of mullite Refractories*, ORNL/TM-2002/84, Oak Ridge National Laboratory (2002).

[6] J. G. Hemrick and A. A. Wereszczak, "Compressive Creep of Fusion-Cast Alumina as a Function of Microstructure," *Glass Industry* (November 1999).

[7] J. G. Hemrick, "Creep Behavior And Physical Characterization Of Fusion-Cast Alumina Refractories," a Dissertation Presented to the Faculty of the Graduate School of the University of Missouri-Rolla in Partial Fulfillment of the Requirements for the Degree of Doctor of Philosophy in Ceramic Engineering (2001).

6.4 Commercialization

The data generated in this project were provided to participating refractory manufacturers and are available from those manufacturers to any users of these types of refractories. It has been confirmed with industrial partners involved in this project that creep data and other thermomechanical property information generated as part of this project was used in analysis of glass furnaces currently in service and for the planning and design of refractory systems for future furnace constructions. The data has not only been used by glass companies in their analysis and planning of furnace systems, but by refractory companies and industrial consultants as well. The information generated was said to be "invaluable" by one industrial participant and more data of similar scope is felt to be of general interest to the industry as a whole.

7. Summary and Conclusions

7.1 Silica

The creep and corrosion performances of the six refractories were examined. The bulk characteristics of the refractories were then characterized before and after their creep testing in an attempt to correlate their changes to the measured creep responses. Bulk density, phase content, microstructure, and secondary phase composition were examined, and their changes as a function of test temperature were analyzed. Lastly, the effect of temperature on the dimensional stability of these refractories was examined. Specimens were aged at the same temperatures that the creep tests were performed. The procedures used and the results generated are discussed.

- The amount of compressive creep of Gen-Sil, Stella GGS, Vega, Vega H, and Harbison-Walker's new developmental brand (flux factors less than 0.5% or "Type A" for all five of these brands) conventional silica was negligible at temperatures between 1550 and 1650°C (2820–3000°F) and at compressive stresses from 0.2 to 0.6 MPa (29–57 psi). Only one specimen per condition was tested, so the authors were unable to statistically conclude that any one of the five brands had superior creep resistance to the others; however, if differences do indeed exist, then they are believed to be insignificant.
- The compressive creep of SI96AU (flux factor greater than 0.5% or "Type B") conventional silica was negligible at 1550°C. However, SI96AU deformed (contracted) by more than 20% at 1600°C at stresses between 0.2 and 0.6 MPa. This behavior was inferior to that of the other five tested brands. SI96AU was not creep tested at 1650°C; however, its creep deformation was expected to still be inferior to the other five silica brands.
- The compressive creep rates of all six brands were not able to be represented as a function of temperature and compressive stress by the conventionally used NBA creep equation (i.e., the Arrhenius power-law creep model). Concurrently active mechanisms other than creep, resulted in larger or oppositely anticipated dimensional changes than those produced by creep; this effect limited the ability to identify or interpret the lesser-active creep mechanism in these silica refractories. Models other than NBA (or equivalent "creep" models that represent creep rate as a function of temperature and stress) should be used to represent or predict the long-term dimensional stability of conventional silica superstructures that are subjected to compressive stresses less than 0.6 MPa and temperatures between 1550 and 1650°C.
- The change in dimensions of the compressively crept specimens indicated that their size (both diameter and length) had actually increased as a consequence of the creep test conditions. The relatively large amount of expansion of the specimen diameters could not have been a sole consequence of "compressive creep barreling" because some specimens did not contract at all, and those that did not contract enough to cause a Poisson effect. All six brands showed this expansion effect. The increases in diameter and length of the creep specimens were between 0.35 and 1.0%. Only a fraction of the expansion was detected during the compressive creep testing. This indicates that most of the permanent expansion exhibited by the silica specimens occurred during their heating from ambient to the creep-testing temperature or during the cooling from test temperature to ambient.
- The secondary phase constituents remained in all brands when they were tested at 1550°C (cumulative time at temperature approximately 250 h). A fraction of these phases visibly evolved from the specimens at 1600°C (slight glass bubbling on the specimen and fixturing). This phenomenon was quite severe at 1650°C. The density changes in the crept specimens (a net effect of the volume expansion and loss in secondary phase mass) ranged from a decrease of 1.6 to

3.9% with a subtle trend of greater density decreases at higher test temperatures. The density decreases among the six brands were statistically equivalent within the data scatter.

- The cause of the volume expansion was not identified; however, because of the absence of quartz it can be concluded that the expansion was not due to quartz (a relatively high-density phase) converting to tridymite or cristobalite (lower-density phases). The authors speculate that the volume expansion is due to the high-temperature process of the conversion of tridymite to cristobalite and the consequential growth of the residual pores and the original cristobalite aggregates.
- Unstressed or "aged" silica refractory specimens from all six materials also exhibited a loss of mass, dimensional increases, and density decreases between 1550 and 1650°C.
    - The mass losses of the six brands at 1550 and 1600°C were equivalent; however, some silica brands lost more mass than others at 1650°C: Harbison-Walker's developmental brand lost approximately 0.1% of its mass; SI96AU lost ≈ 0.2%, Vega H lost ≈ 0.3%, Gen-Sil lost ≈ 0.5%, Vega lost ≈ 1.0%, and Stella GGS lost ≈ 1.5%. Most of the mass loss for all six brands occurred in less than 25 h.
    - The dimensional increases of the silica specimens were a function of temperature. Additionally, some brands expanded more than others. The ranges of expansion were ≈ 1–2.5% at 1550°C, ≈ 2.25–3.75% at 1600°C, and ≈ 3.5–6% at 1650°C. Harbison-Walker's developmental brand expanded the least amount at all three temperatures, followed by Gen-Sil. The ascending order of expansion for the other four brands varied with temperature. Stella GGS expanded the most at 1550°C (≈ 2.5%), SI96AU expanded the most at 1600°C (≈ 3.75%), and Vega expanded the most at 1650°C (≈ 6%). Dimensional increases were greater than axial expansion of the crept silica specimens at the same temperatures, indicating that the axially applied compressive load during creep testing resulted in some specimen contraction.
    - The density decreases of the silica specimens were a function of temperature. Additionally, some brands became less dense than others. The changes in density are a consequence of the above-described changes in mass and volume. The ranges of density decreases were
      ≈ 1–2.75% at 1550°C, ≈ 2.25–4.0% at 1600°C, and ≈ 3.5–7.0% at 1650°C. The density of Harbison-Walker's developmental brand changed the least of the six brands at all three temperatures. The ascending order of density for the other five brands varied with temperature. The density of Stella GGS decreased the most at 1550°C (≈ 2.75%), that for SI96AU decreased the most at 1600°C (≈ 4%), and that for Vega decreased the most at 1650°C (≈ 7%).

- The corrosion resistances of the six silicas were statistically equivalent when they were exposed to sodium carbonate at 1400°C (2550°F) for 24 h. The amount of recession increased linearly with temperature between 1250 and 1450°C for the Gen-Sil silica.

7.2 Mullite

Compressive creep testing of ten commercially available mullite refractories was performed at 1300 to 1450°C and at static stresses between 0.2 and 0.6 MPa. The mullite refractories were examined because they are used in borosilicate glass furnace crowns and superstructures as well as in sidewall applications. Additionally, despite their high cost (≈\$500/ft^3), they are cheaper than other refractories such as chrome alumina (≈ \$3000/ft^3) or fusion-cast alumina (≈\$900/ft^3), which are used as replacements for traditional silica refractories in harsh oxy-fuel environments. Corrosion resistance was also evaluated. In addition, measurements were made that tracked their dimensional stability, phase content, microstructure, and composition as a function of temperature and time. The techniques used for these characterizations and their respective analyses are described.

An intent of this study was to provide objective and factual results whose interpretations were left to the reader. The salient observations and conclusions are as follows.

- The amount of compressive creep for the BP mullite, Durital S75, and Frimul F brands was found to be low at temperatures between 1300 and 1450°C (2370 to 2640°F) and at compressive stresses between 0.2 and 0.6 MPa (29 to 87 psi). Creep rates were on the order of 10^{-11} s^{-1} at the lower test temperature and on the order of 10^{-10} s^{-1} at the higher test temperature. Only one specimen per condition was tested, so the authors were unable to statistically conclude that any one of the three brands had superior creep resistance to the others; however, if differences do indeed exist, then they are believed to be insignificant.
- The amount of compressive creep for the GEM, HF 17, MU75AF, and ZED FM brands was found to be slightly higher than that for the three refractories listed above, but still low at 1300 to 1450°C and 0.2 to 0.6 MPa . Creep rates were on the order of 10^{-10} s^{-1} at the lower test temperature and on the order of 10^{-9} s^{-1} at the higher test temperature. The GEM brand specimen showed higher amounts of creep than the other three brands in this group and a low stress exponent (0.4). This places its behavior closer to that described next for the brands exhibiting significant amounts of creep. Again, only one specimen per condition was tested so the authors were unable to statistically conclude that any one of the other three brands had superior creep resistance to the others; however, if differences do indeed exist, then they are believed to be insignificant.
- The amount of compressive creep for the SL75AD, UFALA UCR, and ZED FMC brands was found to be significant at 1375 to 1450°C and at 0.4 and 0.6 MPa. Creep rates were on the order of 10^{-9} s^{-1} at the lower test temperature and on the order of 10^{-8} s^{-1} at the higher test temperature. All three of these brands exhibited low stress exponents (< 0.5) and changes in chemistry or microstructure due to the creep testing conditions. Only one specimen per condition was tested, so the authors were unable to statistically conclude that any one of the three brands had superior or inferior creep resistance to the others; however, if differences do indeed exist, then they are believed to be insignificant.
- Durital S75 was found to have a stress exponent of 2.4, indicating that the rate-controlling mechanism may be grain boundary creep. This is opposed to diffusion-controlled or Coble creep, which is expected to be the rate-controlling mechanism in the brands that exhibited a stress exponent of approximately unity (Frimul F, HF 17, and MU75AF).
- It is believed that the low-stress exponents seen for the BP mullite, GEM, SL75AD, UFALA UCR, ZED FMC, and ZED FM brands are due to a non-steady-state condition existing during the entire extent of testing. This condition is a consequence of contraction or time-hardening effects occurring during testing and of the samples never reaching a state of equilibrium. The result is measurement of creep due to the applied compressive stress coupled with contraction of the sample due to time-hardening effects. Therefore, the assumption of a single deformation mechanism being active at all temperatures and stresses is not valid, and multilinear regression falsely yields extremely low stress exponent values.
- The brands that possessed high levels of matrix porosity (HF 17, UFALA UCR, and ZED FMC) all showed compaction of the microstructure due to creep testing. This is believed to be the reason for the poor creep resistance of the UFALA UCR and ZED FMC brands. In addition, the UFALA UCR sample was found to possess a fine grain size, which could have contributed to the increased creep rate.
- SL75AD was found to be composed of andalusite grains containing free quartz, which was converted to cristobalite during firing. Further, the andalusite grains are fully converted to mullite during creep testing, and the amount of glassy phase increased. These events in combination may lead to the brand's poor creep resistance.

- Activation energies for the various refractory brands ranged from 50 to 223 kcal/mol. Although no direct correlation between the magnitude of the activation energy and the amount of creep exhibited by a particular brand could be drawn from the data, it is known that materials possessing a high activation energy have greater sensitivity to temperature than those possessing a lower activation energy. Also, the values for many of the calculated activation energies correspond to the activation energy of vitreous silica. This indicates that the glassy phases in these brands affect the overall creep behavior of the material.
- The distinction of a brand being fused-grained or non-fused-grained mullite did not appear to have a bearing on the creep resistance of the individual brands.
- Room-temperature thermal conductivity values were similar for all ten brands of mullite with the average being on the order of 3.1 W/mK [21.5 (Btu*in.)/(h*ft^2*°F)]. Frimul F was found to have the highest thermal conductivity at just below 3.5 W/mK [24.3 (Btu*in.)/(hr.*ft^2*°F)]. SL75AD, UFALA UCR, and ZED FM were found to have the lowest thermal conductivities at around 2.5 W/mK [17.4 (Btu*in.)/(hr.*ft^2*°F)].
- Eight of the ten refractory brands showed less than 0.2% change in mass and less than 0.6% change in volume due thermal aging in the absence of an applied load. The two exceptions, ZED FM and ZED FMC, exhibited extraneous amounts of change (≈8.5%) in both mass and volume due to thermal exposure. All samples showed a less than 0.5% change in bulk density.
- The corrosion rates of the ten mullite brands could not be determined through the use of ASTM C987, but it was determined visually that only minimal amounts of recession occurred due to exposure as defined by the ASTM lid test.

7.3 Fusion-Cast Alumina

The creep and corrosion performances of the two brands of M-type fusion-cast alumina refractories (Corhart Refractories of Louisville, Kentucky, and Monofrax, Inc., of Falconer, NewYork) were examined. All specimens were fabricated from regular fusion-cast alumina blocks of approximate dimensions 0.60 × 0.50 × 0.30 m (24 × 20 × 12 in.). Key findings are summarized below.

- As expected, both the density and porosity of the as-cast refractory blocks were highly consistent. The phase profiles for the α- to β-alumina ratios also showed similar trends to those seen in the density/porosity profiles. XRD showed that both brands consisted of only peaks identifiable as corundum (PDF# 10-0173) or sodium aluminum oxide (PDF# 31-1263). Closer examination of the XRD patterns showed that there were some differences in ratios of α- to β-alumina between the two brands and between the bulk and columnar microstructures. The microstructures of the two brands of refractory were also comparable with a columnar region existing in the outer 1½ in. of the blocks and then transitioning to a more equiaxed structure of α-alumina grains floating in a β-alumina matrix as sampling moves into the center of the block. Average grain sizes were found to be on the order of 172 μm and 82 μm for the Corhart bulk and columnar regions, respectively. Average grain sizes were found to be on the order of 231 and 79 μm for the Monofrax bulk and columnar regions, respectively.
- With exception of the Monofrax bulk material, all of the elastic modulus values obtained by static testing (cyclic compression) at room temperature were similar, ranging from 109 to 113 GPa. Contrary to this, the Monofrax bulk material showed a significantly lower modulus at room temperature (72 GPa). These values are substantiated by dynamic values obtained by resonant ultrasound spectroscopy. Although the room-temperature value is vastly different and the magnitude of the modulus values at elevated temperatures for the bulk Monofrax is higher, the general trend of decreasing modulus with increasing temperature holds as it does in the other microstructures. Furthermore, the modulus value of the bulk Monofrax at 1400°C is approaching that of the other sample types, indicating that at even higher temperatures (like those experienced

by these materials in service), the modulus values for the four microstructures may be virtually the same.

- Thermal expansion values obtained for the two brands of fusion-cast alumina by the dual-rod dilatometry technique were found to be different from those published in the manufacturers' literature, but both materials showed similar values of expansion. The Corhart material was found to have lower expansion (by ≈ 30%) than published; while the Monofrax material was found to have higher expansion (by ≈ 6%) than published. Based on the published values and the experimental results, it would seem that both materials have an experimental thermal expansion of around8.0×10^{-6}/°C over the 500 to 1200°C temperature range.
- Room-temperature thermal conductivity measurements produced by the transient plane source ("hot disk") technique show the Monofrax bulk material to possess a lower thermal conductivity (on the order of 6.00 to 6.25 W/mK) than the Corhart bulk material (mean value of 6.78 W/mK). The columnar structures in the Corhart block show a range of thermal conductivities between 6.50 and 7.50 W/mK. This is similar to the values obtained for the longitudinal columnar measurements made on the Monofrax block (average = 7.10 W/mK). Values on the transverse columnar structure of the Monofrax block (average = 5.82 W/mK) were lower than those of the two bulk microstructures and lower than those of the Corhart columnar and Monofrax longitudinal columnar microstructures. These results indicate that the columnar structure is not as well oriented in the Corhart blocks as in the Monofrax blocks.
- Laser-flash thermal diffusivity/conductivity values show a gradual trend moving from the low- to elevated-temperature data. A change in thermal conductivity from decreasing to increasing slope was seen, as is common in materials where the mechanism controlling thermal conductivity changes with temperature. It is expected that the mechanism controlling the sign of the curves' slope changes from conduction to radiation. Further, this behavior is characteristic of a material that contains microcracking. The presence of microcracks initially lowers the thermal conductivity of the material, but as the material is exposed to elevated temperatures, the "healing" of the microcracks will cause thermal conductivity values to increase.
- The Monofrax material was found to be slightly more creep-resistant than the Corhart material at 1450°C and 0.6 and 1.0 MPa. The advantage in creep resistance is only slight (0.03% strain at the most extreme) and can be considered negligible in relation to the magnitude of deformation it would cause in a furnace crown. Behavior of the 0.8-MPa samples is similar with both brands of material, showing an initial period of increased strain accumulation followed by a sustained period of decreasing strain accumulation. The final amount of accumulated strain for both brands is also similar, causing the overall trend of the 0.8-MPa curves to show considerably less total accumulated strain than both the 0.6- and 1.0-MPa curves.
- Similar behavior occurs at 1550°C, where the Corhart material initially accumulates strain at a more rapid rate but the total accumulated strains for both materials are nearly identical, further negating any advantage the Monofrax material may hold over the Corhart material.
- At 1650°C, the behavior of both brands is nearly identical for both 0.6- and 0.8-MPa stresses; all of the curves overlap one another, and neither material shows even a slight advantage. All three of the 1.0-MPa curves display traditional creep behavior, which is not seen in any of the other bulk test conditions.
- Both columnar orientations show much less accumulated strain than the bulk samples under similar stresses. This is due to the elongated needle-like grains, which are oriented perpendicular to the direction of the applied compressive load, acting to inhibit creep in the transverse columnar samples. In the longitudinal columnar case, it is expected that the unrecoverable expansion effect plays a role in the reduced strain accumulation. The columnar samples at 1650°C show less accumulated strain than the bulk sample under similar stress, but the behavior between the bulk and columnar samples is more similar. Both microstructures show traditional creep behavior under 1.0 MPa of stress and much larger amounts of accumulated strain than the bulk samples at 0.6 and 0.8 MPa.

- The three bulk 1650°C/1.0-MPa samples all have a similar creep rate; the rate for the Corhart material is on the order of 5×10^{-6} h^{-1}, and that for the Monofrax material is on the order of 6×10^{-6} h^{-1}. The columnar structures at 1650°C/1.0 MPa have a lower creep rate, on the order of 4.25 to 4.50×10^{-6} h^{-1}. Creep rates for the other samples were not obtainable because nontraditional creep behavior occurred. Stress exponents and activation energies could not be calculated from this data because steady-state creep rates were only obtained at one stress and temperature.
- The combined expansion/creep plots predict a greater creep resistance in the Monofrax bulk material at 1450°C (better by ≈ 0.20%), but a greater creep resistance in the Corhart bulk material at 1550°C (better by ≈ 0.15%) and at 1650°C (better by ≈ 0.10%). These predictions may not be an accurate portrayal of the creep behavior exhibited by these materials. Behavior exhibited in service would still be represented by the measured creep curves.
- Unrecoverable expansion was seen in all materials, and is thought to be connected to the nontraditional creep behavior seen in the compressive creep testing at temperatures up to 1650°C and loads up to 0.8 MPa. As the temperature increases, the amount of unrecoverable expansion also increases such that when samples are heated and immediately cooled with no hold time at temperature, no unrecoverable expansion occurs. The mechanism causing the unrecoverable expansion effect occurs during the prolonged exposure of the sample to high temperatures and therefore would be of great importance during creep testing and during service of a brick in a furnace campaign. The occurrence of this unrecoverable expansion is thought to be caused by thermal expansion hysteresis due to microstresses or microcracking.
- The data generated in this work for fusion-cast alumina refractories are unique in that very little data of that kind has been generated. The behavior exhibited by this material is highly transient due to the non-steady-state nature of the material (it fails to reach equilibrium). Consequently, the generated creep curves could not be represented by the empirical NBA creep equation. Instead, an empirical fit utilizing an exponential expansion series with multiple time constants was used to represent the behavior exhibited by the fusion-cast alumina refractories. The same exponential fit used to model the raw creep curves was also utilized to describe this composite behavior.
- Several samples were analyzed after being crept, and results were compared with those previously obtained from virgin samples. Analysis included thermal conductivity, optical microscopy, and SEM/EDS chemical analysis. The thermal conductivity values for the Monofrax post-creep cores were similar to those obtained earlier from the virgin cores, which had thermal conductivities in the range of 5.9 W/mK. The value obtained from the Corhart post-creep core was significantly lower than the average value of 6.61 W/mK found earlier for the Corhart bulk material. Initial optical microscopy and SEM/EDS analyses were performed on Corhart and Monofrax bulk samples exposed to 1550°C and 1.0 MPa. This work was conducted to determine whether any changes in the microstructure or chemistry could be detected at that intermediate condition. This analysis was then used to determine whether analysis needed to be performed on samples at the lower temperatures and stresses. No discernible deformation and only slight chemical changes were seen. Subsequent optical microscopy and SEM/EDS analyses were performed on Corhart and Monofrax bulk samples exposed to the extreme conditions of 1650°C and 1.0 MPa. The structure of the Corhart sample was found to resemble the virgin structure, but the crept Monofrax structure displayed a smaller α-alumina grain size and a tighter α-alumina grain structure with more equiaxed angular grains than previously observed in the virgin structure. More severe chemical changes were also seen between the virgin and crept samples.
- Considering that the behavior of fusion-cast alumina in service would be represented by the measured creep curves, any model that is used to capture its true behavior must incorporate both the effect of the expansion and the effect of creep. This means that a model is needed that can handle the high degree of nonlinearity seen in the measured creep curves generated for fusion-cast alumina while also being sensitive to the transient nature of the data due to the lack of an equilibrium state.

7.4 Fused Spinel

The fused spinel materials had negligible creep rates up to 1650°C at 8.5MPa of stress. The bonded spinel, surprisingly, crept substantially compared to the fused material. However, these findings must be compared with other common crown materials, the total creep of the bonded material is less than 0.5% over 100 h at 1550°C and 0.3 MPa, which are fairly standard temperature and pressure for testing refractory materials The creep of silica materials is approximately 0.4% over 100 h at 1450°C and 0.3 MPa. The spinel materials did not react with soda in the exposure tests. There was some limited reaction with silica and calcia from the gasifier atmosphere. Thermal conductivity was determined by laser flash and was found to decrease as temperature increases from 14 (100°C) to 8 (700°C) W/mK for the fused spinel and 9.5 (100°C) to 4 (1300°C) for the bonded spinel. A model of the glass tank crown was developed, which takes into account nonlinear changes in the refractory material due to time, temperature, and corrosion.

8. Recommendations

- To truly model the deformation behaviors of fusion-cast alumina and silica refractories as a function of temperature, time, and stress, the composite effects of unrecoverable expansion (aging behavior) and creep response must be known. Given that these processes may be highly nonlinear, the traditional equations, which assume that steady-state deformation rates are dominant, are not appropriate. New models must be derived from basic theoretical principles that can describe the nonlinear, transient, nonsteady equilibrium behavior observed in this work.
- Creep testing needs to include simultaneous measurement of specimen elongation/contraction occurring in the absence of an applied stress. Such testing could be conducted using a system consisting of furnace of sufficient size to accommodate multiple mechanical load trains. During testing one load train would be used to monitor elongation/contraction in the absence of any appreciable stress. The stress range employed with the other load stations must be large enough to promote significant and measurable changes in the deformation response. It is recommended that the stress range cover at least one order of magnitude (e.g., 5 to 50 MPa). Testing times must also be much longer (>1000 h) to ensure that representative deformation data are generated. A second approach for distinguishing creep from aging effects is to use the stress relaxation technique [23] for measuring creep response. Because this method is able to generate an entire creep-rate vs stress curve in a matter of a few hours, one could use it to measure creep behavior at periodic intervals during a standard aging test. Thus a single sample could be used to assess both aging and creep behavior.
- To facilitate model development, the microstructural changes responsible for elongation/contraction in the absence of an applied stress must be identified.
- Creep testing and physical characterization of salvaged fusion-cast alumina refractory bricks from oxy-fuel furnaces should be carried out. Results from such work could be compared with results generated in this work and would be useful in validating any finite-element models generated from the data collected in this work.
- Work needs to be pursued in the area of nonlinear finite element analysis of furnace crowns. This kind of analysis would provide a better prediction of furnace life and long-term refractory behavior.
- Technical efforts should be undertaken to measure and model the composite effects of unrecoverable expansion (aging behavior) and creep response. Given that these processes may be highly nonlinear, the traditional equations, which assume that steady-state deformation rates are dominant, are not appropriate. New models must be derived from basic theoretical principles that can describe the nonlinear, transient, nonsteady equilibrium behavior observed in this work. Creep testing needs to include simultaneous measurement of specimen elongation/contraction occurring in the absence of an applied stress. Such testing could be conducted using a system consisting of a furnace of sufficient size to accommodate multiple mechanical load trains. During testing one load train would be used to monitor elongation/contraction in the absence of any appreciable stress. The stress range employed with the other load stations must be large enough to promote significant and measurable changes in the deformation response. It is recommended that the stress range cover at least one order of magnitude (e.g., 5 to 50 MPa). Testing times must also be much longer (> 1000 h) to ensure that representative deformation data are generated. A second approach for distinguishing creep from aging effects is to use the stress relaxation technique for measuring creep response. Because this method is able to generate an entire creep-rate vs stress curve in a matter of a few hours, one could use it to measure creep behavior at periodic intervals during a standard aging test. Thus a single sample could be used to assess both aging and creep behavior.

- To facilitate technology transfer and commercialization, software tools should be developed that allow users to readily link the key properties to finite element codes used in furnace construction. This software would allow one to quickly assess the effects of specific materials upon long-term thermal and structural reliability. It should also include a routine that allows the user to optimize performance of a given material by changing the material properties; these altered properties would serve as new targets for those involved in materials development.
- Any follow-on effort must also address new materials.

9. References

[1] Crown Refractories for Glass Manufacturing with Oxy-Fuel Combustion, Teltech Research Services, Minneapolis, Minnesota (1996).

[2] M. Gridley, "Philosophy, Design, and Performance of Oxy-Fuel Furnaces," Ceram. Eng. Sci. Proc., **18** 1–14 (1997).

[3] R. W. Schroeder, "Development of Oxy-Fuel Technology in the Glass Industry," The Glass Researcher **8** (1), 1–4 (1998).

[4] A. A. Wereszczak, T. P. Kirkland, G. A. Pecoraro, and R. A. New, "Compressive Creep Behavior of Fusion-Cast Alumina Refractories," pp. 401–406 in Ceramic Transactions, Vol. 82, Advances in Fusion and Processing of Glass II, ed. A. G. Clare and L. E. Jones, American Ceramic Society, Westerville, Ohio (1998).

[5] A. A. Wereszczak, T. P. Kirkland, and W. F. Curtis, "Compressive Creep Resistance of MgO Refractories at Temperatures ≥ 1400°C (2550°F),"pp. 407–412 in Ceramic Transactions, Vol. 82, Advances in Fusion and Processing of Glass II, ed. A. G. Clare and L. E. Jones, American Ceramic Society, Westerville, Ohio (1998).

[6] A. A. Wereszczak, T. P. Kirkland, and W. F. Curtis, "Creep of CaO/SiO_2 - Fluxed MgO Refractories," J. Mater. Sci (1998) in press.

[7] Glass: A Clear Vision for a Bright Future, U.S. Dept. of Energy, Office of Industrial Technologies, Advanced Industrial Materials Program (January 1996).

[8] Refractories for Industrial Processing: Opportunities for Improved Energy Efficiency, U.S. Dept. of Energy, www.eere.energy.gov/industry/ imf/pdfs/**refractories**reportfinal.pdf.

[9] "Standard Practice for Vapor Attack on Refractories for Furnace Superstructures," ASTM C987, Vol. 15.01, American Society for Testing and Materials, West Conshohocken, Pa. (1998).

[10] A. A. Wereszczak, M. Karakus, K. C. Liu, B. A. Pint, T. P. Kirkland, and R. E. Moore, *Compressive Creep Performance and High Temperature Dimensional Stability of Conventional Silica Refractories*, ORNL/TM-13757, Oak Ridge National Laboratory (1999).

[11] J. G. Hemrick, A. A. Wereszczak, M. Karakus, K. C. Liu, H. Wang, B. A. Pint, T. P. Kirkland, and R. E. Moore, *Compressive Creep and Thermophysical Performance of Mullite Refractories*, ORNL/TM-2002/84, Oak Ridge National Laboratory (2002).

[12] J. G. Hemrick and A. A. Wereszczak, "Compressive Creep of Fusion-Cast Alumina as a Function of Microstructure," *Glass Industry* (November 1999).

[13] J. G. Hemrick, "Creep Behavior And Physical Characterization Of Fusion-Cast Alumina Refractories," a Dissertation Presented to the Faculty of the Graduate School of the University of Missouri-Rolla in Partial Fulfillment of the Requirements for the Degree of Doctor of Philosophy in Ceramic Engineering (2001).

[14] "Standard Classification of Silica Refractory Brick," ASTM C416, Vol. 15.01, American Society for Testing and Materials, West Conshohocken, Pa. (1998).

[15] S. Shin and O. Buyukozturk, *Material Property Development for Refractories*, US DOE Report ORNL/Sub/79-07862/02 (1990).

[16] F. H. Norton, *The Creep of Steel at High Temperature*, McGraw Hill, New York (1929).

[17] M. Karakus and R. E. Moore, “CLM—A New Technique for Refractories,” *Ceramic Bulletin* **77** 55–61 (1998).

[18] S.E. Gustafsson, “Transient Plane Source Techniques for Thermal Conductivity and Thermal Diffusivity Measurements of Solid Materials,” *Review of Scientific Instruments*. **62** (3), 797–804 (1991).

[19] “Standard Test Method for Thermal Diffusivity of Solids by the Flash Method,” ASTM E1461-92, Vol. 15.01, American Society for Testing and Materials, West Conshohocken, Pa. (2000).

[20] G. Hetherington, J. H. Jack, and J .C. Kennedy, “The Viscosity of Vitreous Silica,” *Physics and Chemistry of Glasses* **5,** 130–136 (1964).

[21] F. E. Wagstaff, “Crystallization and Melting Kinetics of Cristobalite,” *Journal of the American Ceramic Society* **52,** 650–654 (1969).

[22] M. F. Doerner and W. D. Nix, “A Method for Interpreting Data from Depth-Sensing Indentation Instruments,” *Journal of the Materials Research Society* **1** (4) (1986).

[23] M. G. Jenkins and M. K. Ferber, “Determination of High-Temperature Creep Parameters in Structural Ceramics From Constant-Displacement, Stress-Relaxation Tests,” pp. 94–101 in *Proceedings of the 1991 SEM Spring Conference on Experimental Mechanics*, Milwaukee, Wisconsin, June 9–13, 1991, Society of Experimental Mechanics, Bethel, Connecticut (1991).

Appendix: Publications

A. A. Wereszczak, J. Heide, and T. P. Kirkland, "High Temperature Deformation of an AZS Refractory," *Advances in Fusion and Processing of Glass II*, 379–384.

A. A. Wereszczak, T. P. Kirkland, and W. F. Curtis, "Creep of CaO/SiO_2–Containing MgO Refractories," *Journal of Materials Science* 34 (1999): 215– 227.

A. Wereszczak, H. Wang, M. Karakus, W. Curtis, V. Aume, and D. VerDow, "Postmortem Analyses of Salvaged Conventional Silica Bricks from Glass Production Furnaces," *Glastech. Ber. Glass Sci. Technol.* 73 (2000), No. 6: 165–174.

J. G. Hemrick, C. W. Kistler Jr., A. A. Wereszczak, and M. K. Ferber, "Thermal Conductivity of Alumina Measured with Three Techniques," 1–13.